VOLUME 83 NO. EM3
JULY 1957

JOURNAL OF THE

Engineering Mechanics Division

PROCEEDINGS
AMERICAN SOCIETY
OF CIVIL ENGINEERS

BASIC REQUIREMENTS FOR MANUSCRIPTS

This Journal represents an effort by the Society to disseminate information to the [illegible] the greatest possible speed. To this end the material herein has [illegible] the usual editing requirements of more formal publications.

Original papers and discussions of current papers should be submitted to the [illegible] of Technical Publications, ASCE. The final date on which a discussion [illegible] through the Society is given as a footnote with each paper. Those who are [illegible] this material will expedite the review and publication procedures [illegible] the following basic requirements:

1. Titles should have a length not exceeding 50 characters and spaces.
2. A 50-word [illegible] should accompany the paper.
3. The manuscript (original copy and two copies) should be double spaced [illegible] 8½-in. [illegible] papers. Papers that were originally prepared for [illegible] presentation must be rewritten into the third person before being submitted.
4. The [illegible] full name, membership grade, and footnote reference [illegible] should appear on the first page of the paper.
5. [illegible] directly from the copy that is submitted. [illegible] necessary that capital letters be drawn, in black ink, 3/16-in. [illegible] of all subscripts and characters in the proportions dictated by [illegible] and that no line of mathematics be longer than 6½-in. [illegible] typewriter equations may be used but they will be proportionately [illegible] the printed version.
6. [illegible] (two copies) on one side of 8½-in. by 11-in. [illegible] frame. Small tables should be grouped [illegible] explanation should be made in the text [illegible]
7. [illegible] in black ink on one side of 8½-in. by 11-in. [illegible] 6½-in. by 10½-in.; the caption [illegible] the same. Because illustrations will be reduced [illegible] the capital letters should be 3/16-in. high. Photographs [illegible] glossy prints not less than 6½-in. by 10½-in. [illegible] with the text for each illustration.
8. [illegible] 3,000 to 5,000 words in length and should be no [illegible] 18 double-spaced pages. For [illegible] each full page of typed text, [illegible] the equivalent of 250 words.

[illegible] the preparation of technical papers is con- [illegible] Handbook" which can be obtained from [illegible]

[illegible] may be made on condition that the full title of [illegible] reference (or paper number), and date of [illegible] given. The Society is not responsible for any [illegible] publications.

[illegible] by the American Society of Civil [illegible] 20 South State Street, Ann Arbor, Michigan. [illegible] are: 33 West 39 Street, New York 18, New York. [illegible] subscription to this Journal: Second-class [illegible] at Ann Arbor, Michigan.

EM,SM

Journal of the
ENGINEERING MECHANICS DIVISION
Proceedings of the American Society of Civil Engineers

CONTENTS

July, 1957

Papers

Journal of the
ENGINEERING MECHANICS DIVISION
Proceedings of the American Society of Civil Engineers

DEFLECTIONS OF STRUCTURES IN THE INELASTIC RANGE

Kurt H. Gerstle,[1] J.M. ASCE
(Proc. Paper 1290)

SYNOPSIS

An approach to the problem of finding deflections of structures of perfectly plastic material in the inelastic range is developed. Charts relating loads and deformations of rectangular beams are furnished, and may be used to analyze indeterminate structures composed of members of such cross sections in the inelastic range.

INTRODUCTION

Two basic approaches to the problem of finding deformations of structures in the inelastic range have been taken in the past. On one hand, certain convenient approximate methods[2] are available, which, due to the simplifying assumptions involved, are of questionable accuracy for certain cases. On the other hand, rigorous methods have been devised, which, however, are of such complexity as to make them unsuitable for many applications.

This paper attempts to simplify the determination of deformations and the analysis of moments of indeterminate structures in the inelastic range while subjecting itself to the same assumptions as the rigorous approach mentioned above.

The integration of unit angle changes results in expressions for total angle change and tangential deviation which may be written as dimensionless coefficients dependent on the loading condition, to be multiplied by a factor dependent only on the properties of the member. The coefficients are plotted for different loading conditions of members of rectangular cross section. Using

Note: Discussion open until December 1, 1957. Paper 1290 is part of the copyrighted Journal of the Engineering Mechanics Division of the American Society of Civil Engineers, Vol. 83, No. EM 3, July, 1957.

1. Instr. of Civ. Eng., Univ. of Colorado, Boulder, Colo.

2. A summary of various methods of inelastic deflection calculations is contained in Progress Report No. 9, "Plastic Strength and Deflections of Continuous Beams," by K. E. Knudsen, C. H. Yang, Bruce G. Johnston, and Lynn S. Beedle, Fritz Engineering Laboratory Reprint No. 86.

the graphs, the deformations of a structure due to a given moment diagram may be determined.

Statically indeterminate structures may be analyzed in the inelastic range by assuming a statically compatible moment diagram and performing a check upon the conditions of geometry, utilizing the furnished graphs.

The application of the proposed method to the analysis of structures composed of members of I-section is discussed.

Assumptions

1. Idealized flat-topped stress-strain diagram. Strain hardening is neglected. Equal properties in tension and compression.
2. Plane sections remain plane after bending in both elastic and inelastic ranges.
3. Small deflections.
4. Internal shear, axial forces, and possibility of buckling are neglected.
5. Effects of residual stresses, stress reversal, and sequence of loading are neglected.

Since the neglect of strain hardening results in error on the side of safety, whereas the assumptions stated in items 3, 4, and 5 give results on the unsafe side, therefore the errors will tend to compensate.

Inelastic Bending of Rectangular Beams

It is desired to find a relationship between the rotation of adjoining sections of a beam, and the applied moment. In the elastic range, such a relationship is furnished by the well known expression

$$\phi = \frac{M}{EI} \qquad 1.$$

In the inelastic range, considerations of statics and geometry help to establish a similar relationship. Equating external and internal moments on any section of the rectangular beam,

$$M = S_{YP}\, t\,(c^2 - 3y^2) .$$

From geometric relationships,

$$\phi = \frac{\epsilon_{Extr.}}{c} = \frac{\epsilon_{YP}}{y} = \frac{S_{YP}}{Ey} .$$

Solving the two conditions simultaneously, the required relation is seen to be

$$\phi = \frac{M_{YP}}{EI} \frac{1}{\sqrt{2}\sqrt{3/2 - M/M_{YP}}} \qquad 2.$$

in the inelastic range.

Angle changes and tangential deviations of flexural members may be determined by direct integration of the unit angle changes:

$$\theta_{AB} = \int_A^B \phi\, dx = \frac{M_{YP}L}{EI}\left[\int_{El.Req.} \frac{M}{M_{YP}}\, d\left(\frac{x}{L}\right) + \int_{Inel.Req.} \frac{d\left(\frac{x}{L}\right)}{\sqrt{2}\sqrt{3/2 - M/M_{YP}}}\right] \qquad 3.$$

$$\delta_{AB} = \int_A^B \phi x\, dx = \frac{M_{YP}L^2}{EI}\left[\int_{El.Req.} \frac{M}{M_{YP}} \frac{x}{L} d\left(\frac{x}{L}\right) + \int_{Inel.Req.} \frac{\frac{x}{L}\, d\left(\frac{x}{L}\right)}{\sqrt{2}\sqrt{3/2 - M/M_{YP}}}\right], \qquad 4.$$

where θ_{AB} is the total angle change between Points A and B, and δ_{AB} is the tangential deviation of Point A from a tangent from Point B, if x is measured from A. The results of these integrations may be written in form of a dimensionless coefficient C dependent only on the ratio of moment to the yield point moment M_{yp}, to be multiplied by a factor involving only the properties of the member:

$C_1 \dfrac{M_{yp} L^2}{EI}$ for tangential deviations,

and $C_2 \dfrac{M_{yp} L}{EI}$ for angle changes.

Since the relationship between load and resulting deformation is non-linear in the inelastic range, the coefficients C_1 and C_2 must be determined separately not only for different types of load and points of application, but also for different magnitudes of inelastic loads.

Deformation of Beams Subject to End Moments

In this section are presented procedures and results for evaluating the coefficients C_1 and C_2 for members subjected only to end moments. Such cases occur in structures whenever an unloaded member helps carry a load imposed on an adjoining member; unloaded spans of continuous beams and legs of rigid frames may be cited as examples. Furthermore, the results of this section will be used in the evaluation of deformations of beams subjected to concentrated loads.

The moment variation in such beams, according to Fig. 1 b, is

$$M = \left(h - \frac{h-k}{L} x\right) M_{YP} \quad ;$$

therefore, according to Eq. 3, the total angle change is given by

$$\theta_{AB} = \frac{M_{YP}L}{EI}\left\{\int_{El.Req.}\left[h-(h-k)\frac{x}{L}\right]d\left(\frac{x}{L}\right) + \frac{1}{12}\int_{Inel.Req.}\frac{d\left(\frac{x}{L}\right)}{\sqrt{\left(\frac{3}{12}-h\right)+(h-k)\frac{x}{L}}}\right\} \quad 5.$$

and the tangential deviation, according to Eq. 4, is given by

$$\delta_{AB} = \frac{M_{YP}L^2}{EI}\left\{\int_{El.Req.}\left[h\left(\frac{x}{L}\right)-(h-k)\left(\frac{x}{L}\right)^2\right]d\left(\frac{x}{L}\right) + \frac{1}{12}\int_{Inel.Req.}\frac{\frac{x}{L}\,d\left(\frac{x}{L}\right)}{\sqrt{\left(\frac{3}{12}-h\right)+(h-k)\frac{x}{L}}}\right\} \quad 6.$$

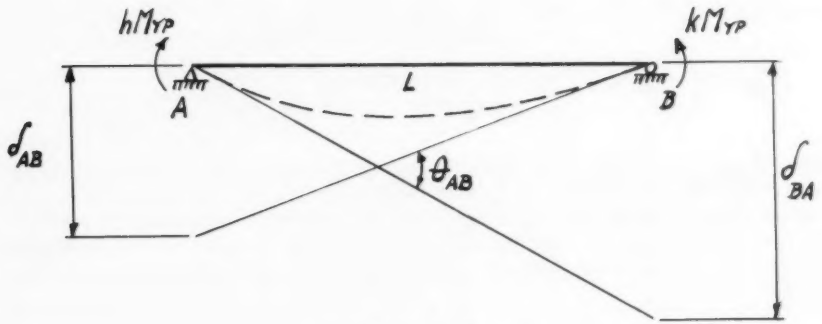

a, Deflected Shape

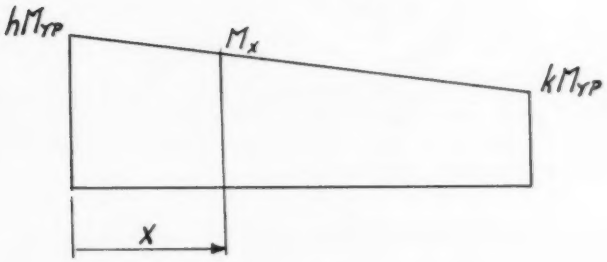

b, Moment Diagram

Fig. 1. Beam subject to End Moments.

The coefficients C_1 and C_2 are given by the results of the integrations in Eq. 5 and 6. Figures 2 and 3 furnish the values of these coefficients for all combinations of end moments hM_{yp} and kM_{yp}. Tangential deviation δ_{BA} is easily determined from the previous two quantities by the geometry apparent in Fig. 1 a:

$$\delta_{BA} = \theta_{AB} \cdot L - \delta_{AB} \quad . \quad 7.$$

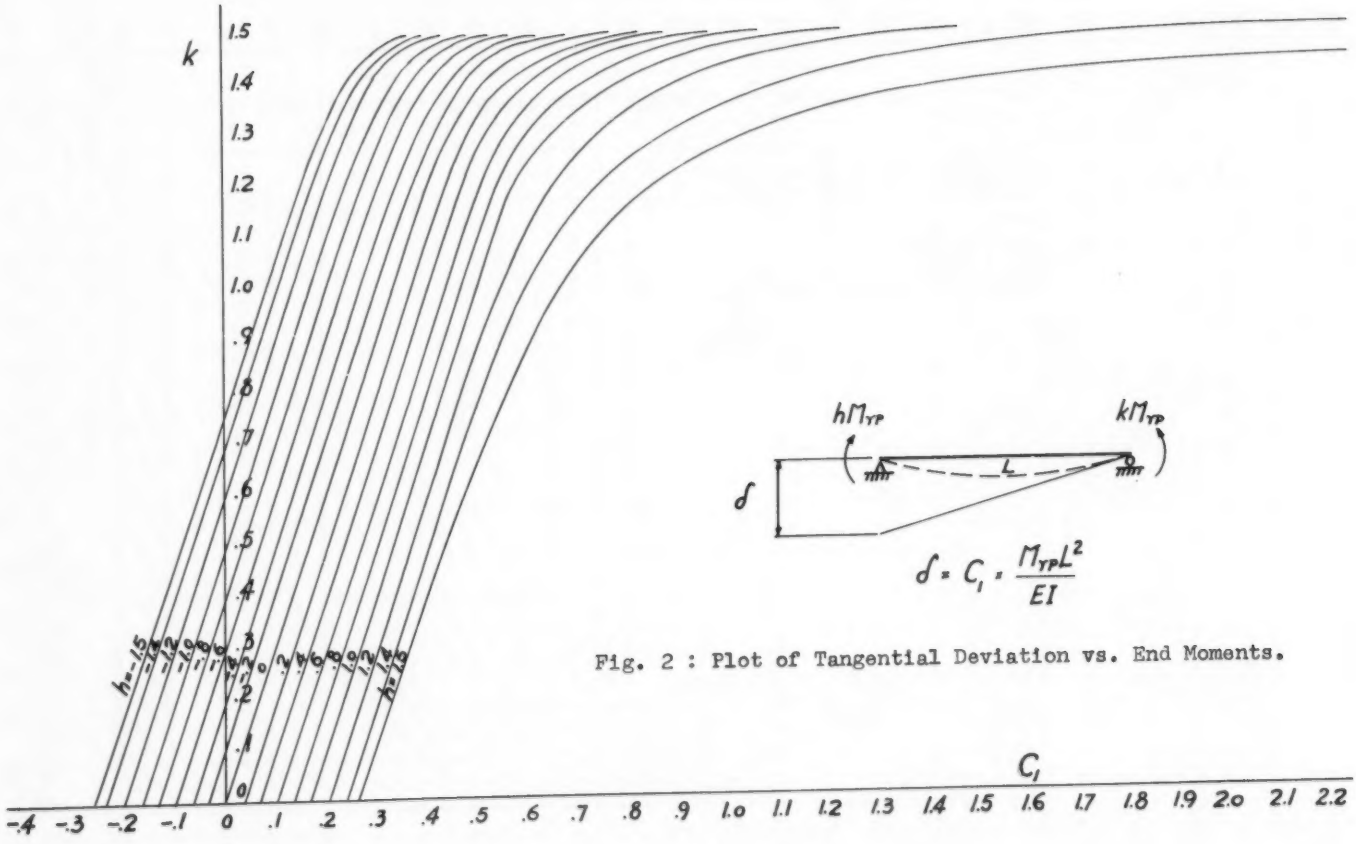

Fig. 2 : Plot of Tangential Deviation vs. End Moments.

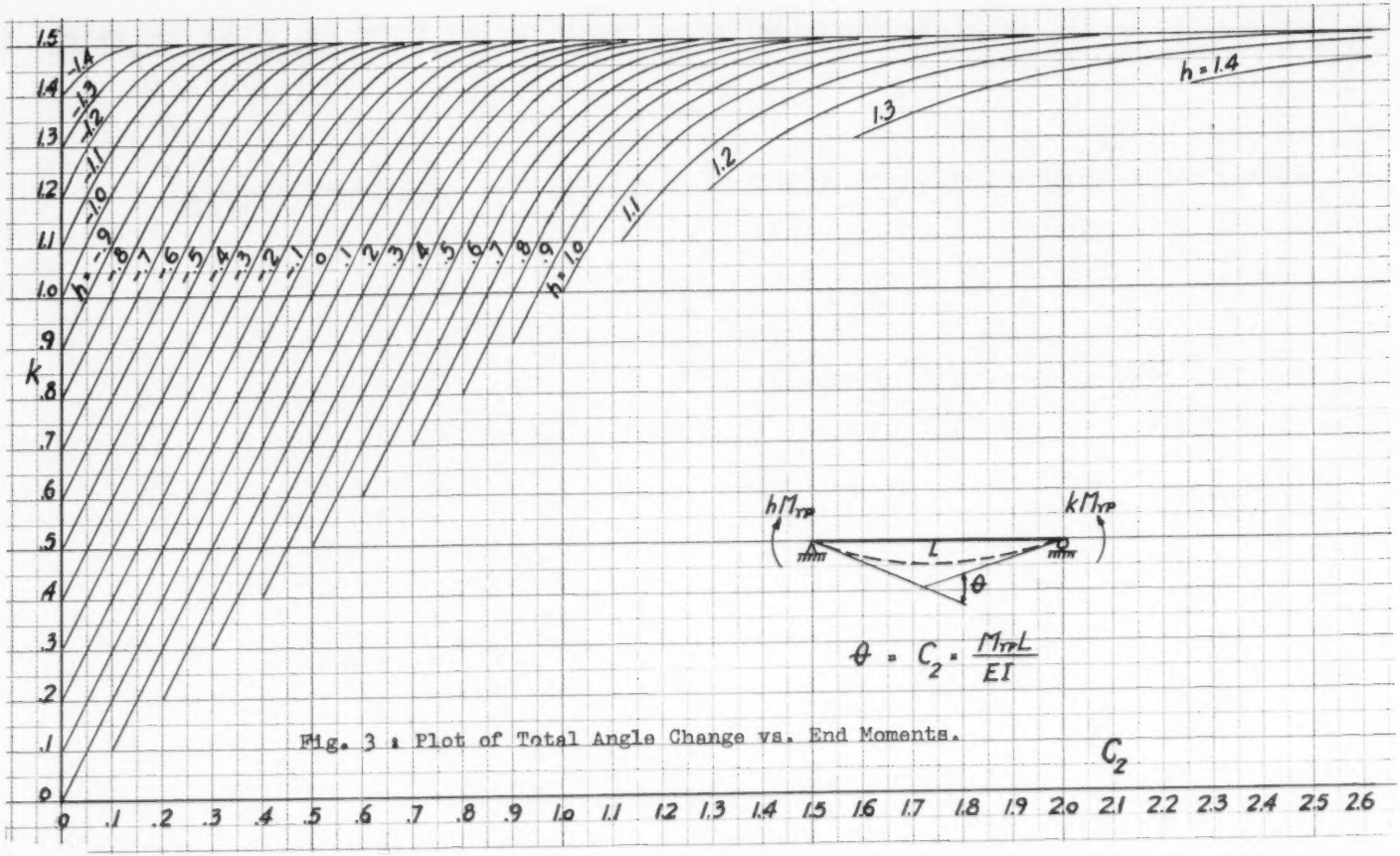

Fig. 3 : Plot of Total Angle Change vs. End Moments.

Deformation of Beams Subject to Concentrated Loads and End Moments

For purposes of finding deflections of beams subjected to concentrated loads, as well as to satisfy conditions of geometry for continuous beams and frames, it is necessary to determine the end slopes of such members. In this section a method for doing this will be set forth, making use of the coefficients for angle change and tangential deviation found in the preceding section. The method presented is restricted to the case of one concentrated load on any one span. It could easily be expanded to include the case of any number of loads at any location, but it should be remembered that each combination requires an entirely new set of calculations, since the superposition of effects of individual loads is not admissible in the inelastic range.

Since information for beam segments with straight line moment diagrams has been obtained in the preceding section, it is convenient to treat the two parts of the beam, shown in Fig. 4, AC, of length aL, and BC, of length bL, separately, each one as a beam with cranked-in end moments, $k_A M_{yp}$ and hM_{yp}, and $k_B M_{yp}$ and hM_{yp}, respectively. Given the end moments $k_A M_{yp}$ and

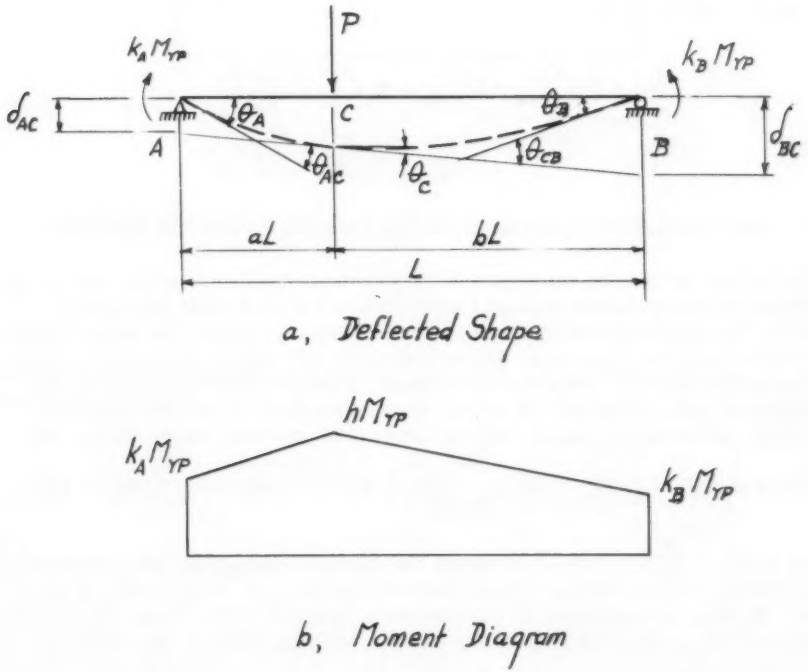

Fig. 4. Beam subject to Conc. Load and End Moments.

$k_B M_{yp}$, the magnitude, and the location of the load P, the moment at the point of load application may be found by statics:

$$hM_{YP} = \left(bk_A + a k_B + \frac{PabL}{M_{YP}}\right) M_{YP} . \qquad 8.$$

A study of the deflected curve of Beam AB in Fig. 4 a will lead to the following useful relationships:

$$\theta_A = \frac{\delta_{AC} - \delta_{BC}}{L} + \theta_{CA} \quad ,$$

and

$$\theta_B = \frac{\delta_{AC} - \delta_{BC}}{L} + \theta_{CB} \quad . \qquad 9.$$

The end slopes are now given in terms of the tangential deviation and total angle change of the individual beam segments AC and BC, the values of which may be determined by means of the coefficients given in Figures 2 and 3. Denoting the coefficients pertaining to segment AC by the subscript a, and those pertaining to segment BC by subscript b, at the same time adhering to the previous subscripts 1 and 2 to denote tangential deviation, and angle change, respectively, there result the general formulas for the end slopes of the type of beam considered here:

$$\left.\begin{aligned} \theta_A &= \left(a^2 C_{1a} - b^2 C_{1b} - a\, C_{2a}\right) \frac{M_{YP} L}{EI} \\ \text{and} \quad \theta_B &= \left(a^2 C_{1a} - b^2 C_{1b} + b\, C_{2b}\right) \frac{M_{YP} L}{EI} \quad . \end{aligned}\right\} \qquad 10.$$

Deformation of Beams Subject to Uniform Loads and End Moments

The same principles employed in the previous sections may be used to determine the deformation of beams subjected to uniform loads and end moments. To avoid extremely long and cumbersome formulas, the beam will be separated into two segments. These segments will extend from each end of the beam to the point of maximum moment, at which point the origin of the variable of integration will be taken. One segment AC of the beam as described, and shown in Fig. 5, will be considered; the total angle change between A and C, θ_{AC}, given by $C_2 \frac{M_{yp} L}{EI}$, and the tangential deviation δ_{CA}, given by $C_1 \frac{M_{yp} L^2}{EI}$, are to be found; the moments kM_{yp} and hM_{yp} and the load intensity w are known. These three values are not independent of each other, if hM_{yp}, as assumed, is the maximum moment of the Beam AB. Given kM_{yp} and hM_{yp}, the load intensity w may be found by statics, according to Fig. 5 a:

$$\frac{wL^2}{M_{YP}} = 2(h-k) \quad . \qquad 11.$$

The moment variation in terms of x measured as shown is then

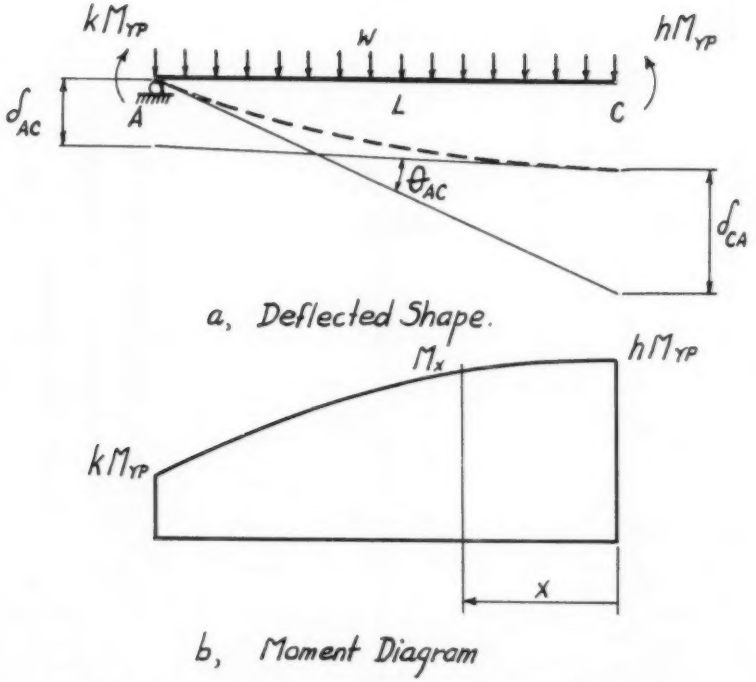

Fig. 5. Beam Segment under Uniform Load and Moments.

$$M = \left[h - (h-k)\left(\frac{x}{L}\right)^2 \right] M_{YP} . \qquad 12.$$

From previously presented theory, the total angle change between ends of the segment is given by

$$\theta_{AC} = \frac{M_{YP} L}{EI} \left\{ \int_{El.Reg.} \left[h - (h-k)\left(\frac{x}{L}\right)^2 \right] d\left(\frac{x}{L}\right) + \frac{1}{\sqrt{2}} \int_{Inel.Reg.} \frac{d\left(\frac{x}{L}\right)}{\sqrt{\left(\frac{3}{2}-h\right) + (h-k)\left(\frac{x}{L}\right)^2}} \right\} \qquad 13.$$

and the tangential deviations are

$$\delta_{CA} = \frac{M_{YP} L^2}{EI} \left\{ \int_{El.Reg.} \left[h\left(\frac{x}{L}\right) - (h-k)\left(\frac{x}{L}\right)^3 \right] d\left(\frac{x}{L}\right) + \frac{1}{\sqrt{2}} \int_{Inel.Reg.} \frac{\left(\frac{x}{L}\right) d\left(\frac{x}{L}\right)}{\sqrt{\left(\frac{3}{2}-h\right) + (h-k)\left(\frac{x}{L}\right)^2}} \right\} \qquad 14.$$

and

$$\delta_{AC} = \theta_{AC} L - \delta_{CA} .$$

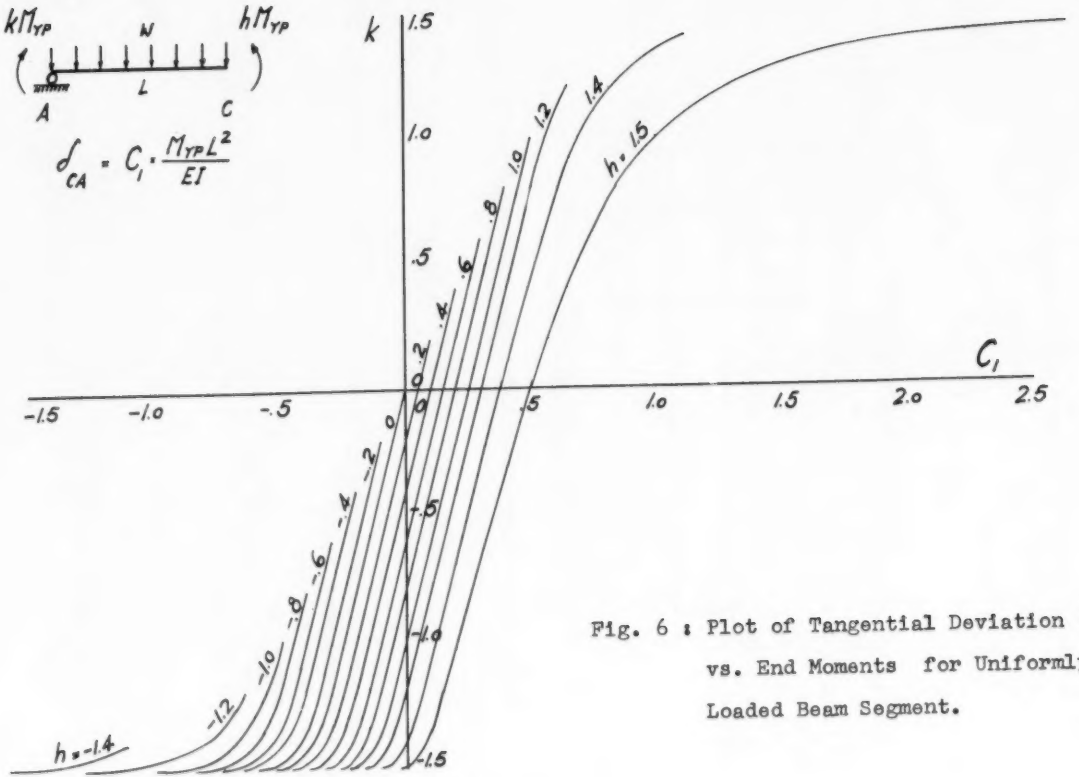

Fig. 6 : Plot of Tangential Deviation δ_{CA} vs. End Moments for Uniformly Loaded Beam Segment.

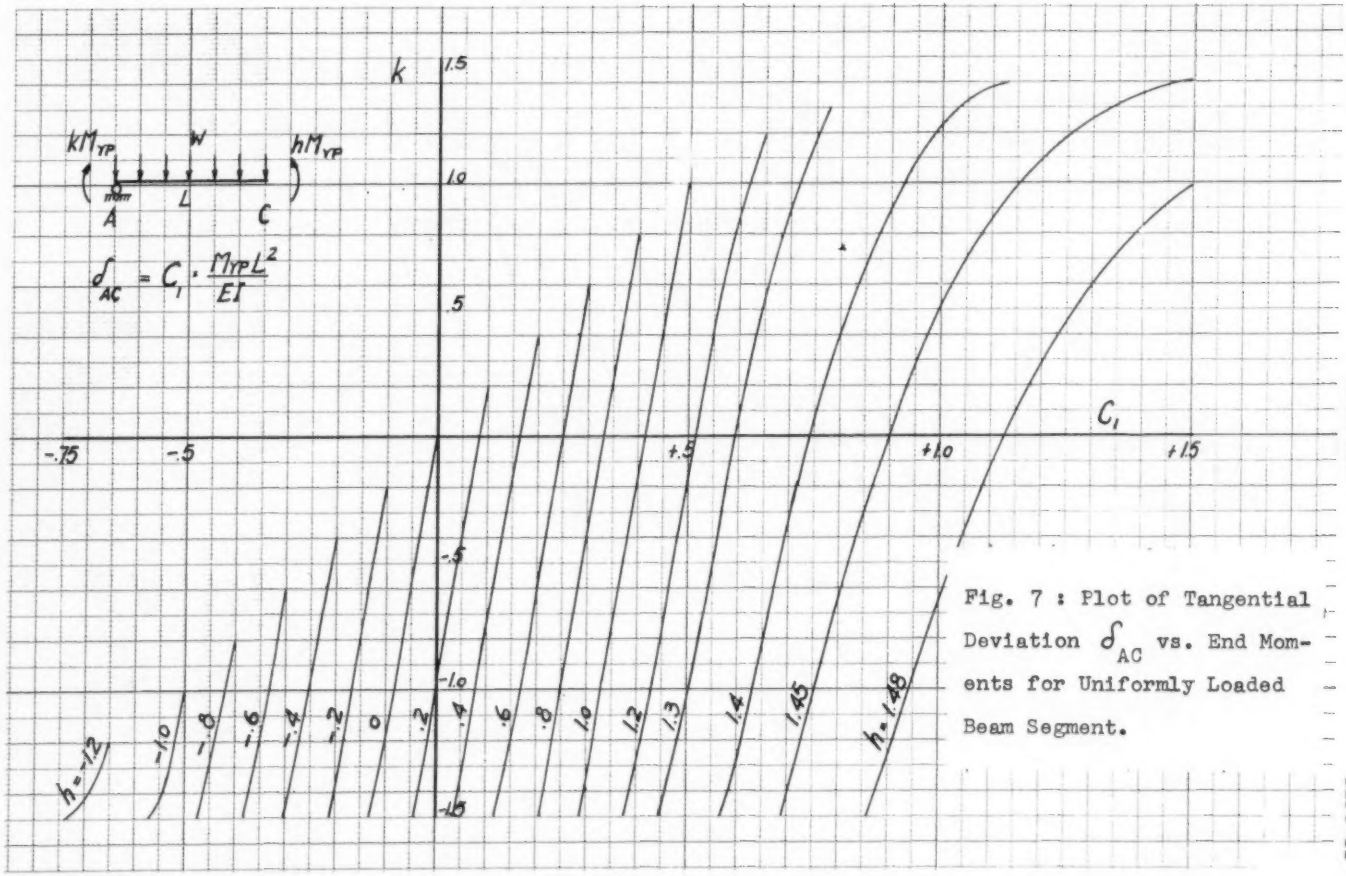

Fig. 7 : Plot of Tangential Deviation δ_{AC} vs. End Moments for Uniformly Loaded Beam Segment.

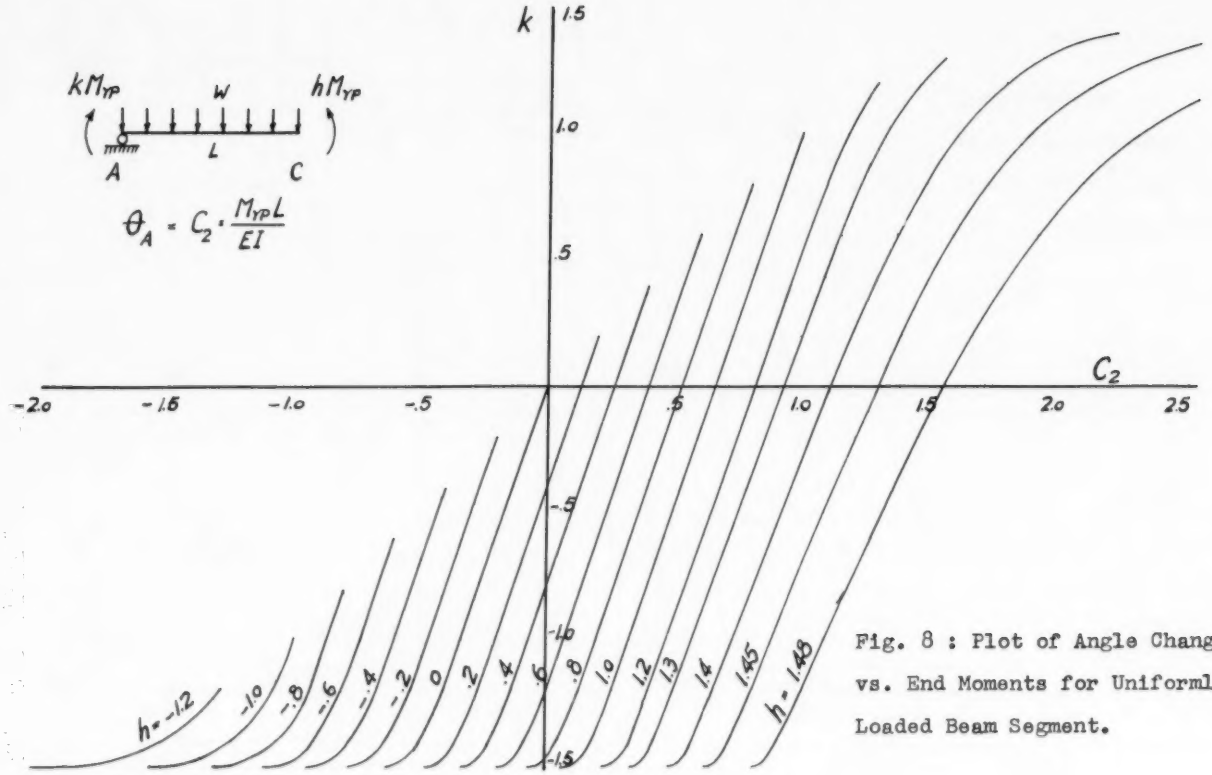

Fig. 8 : Plot of Angle Change vs. End Moments for Uniformly Loaded Beam Segment.

In these expressions the integrand has been arranged in non-dimensional form, so that integration results in the dimensionless coefficients C_1 and C_2, to be multiplied by the familiar factors $\frac{M_{yp} L^2}{EI}$, and $\frac{M_{yp} L}{EI}$, respectively.

Before the indicated integrations can be performed, it is necessary to locate the limits of the elastic and inelastic portions of the beam segment. This may be done by setting the moment expression equal to $\pm M_{yp}$ and solving for x:

$$x_{\pm M_{yp}} = \sqrt{\frac{2M_{yp}}{wL^2}\left(h \mp 1\right)} \cdot L$$

All the information is now assembled to evaluate the desired angle changes and deviations for the beam segment. Values of coefficients C_1 and C_2 are presented in Figures 6, 7, and 8 for all possible combinations of the end moments kM_{yp} and hM_{yp}.

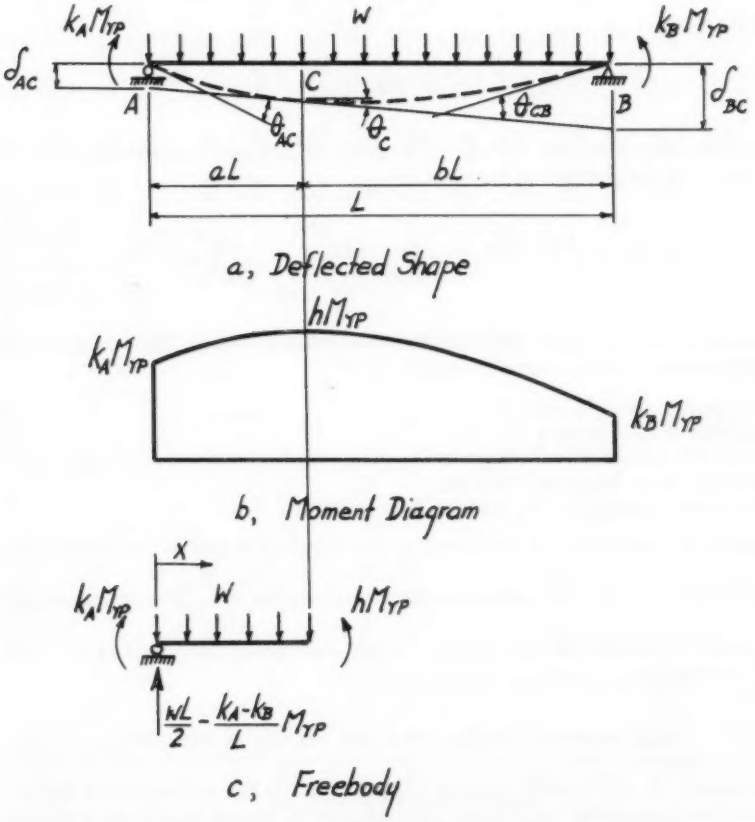

Fig. 9. Beam subject to Uniform Load and End Moments.

Having evaluated the deformations of each of the two beam segments AC and BC, of the beam AB shown in Fig. 9, individually, they may be combined to arrive at the required end slopes of the beam. Fig. 9 a shows the relationships of the deformed shape of the beam; these will be recognized as being identical with those of Fig. 4 a, and are therefore given by Equations 10.

If for any beam the end moments $k_A M_{yp}$ and $k_B M_{yp}$, and the load intensity w are given, there remain two items to be evaluated before the above Equations 10 can be solved: the maximum moment hM_{yp} and its location. Both of these can be found by statics. Referring to the free body shown in Fig. 9 c, the general expression for the moment in terms of the variable x measured from End A of the beam is written:

$$M = \left(\frac{wL}{2} - \frac{k_A - k_B}{L} M_{yp} \right) x + k_A M_{yp} - \frac{wx^2}{2} .$$

Differentiating with respect to x and setting the result equal to zero allows a solution for the distance aL of the point of maximum moment from End A:

and therefore

$$\left.\begin{aligned} aL &= \left[\frac{1}{2} - (k_A - k_B) \frac{M_{yp}}{wL^2} \right] L \\ bL &= \left[\frac{1}{2} + (k_A - k_B) \frac{M_{yp}}{wL^2} \right] L \end{aligned}\right\} \qquad 16.$$

Resubstituting the value for aL in the general moment expression furnishes the value of the maximum moment hM_{yp}:

$$hM_{yp} = \left[\frac{k_A + k_B}{2} + \frac{(k_A - k_B)^2}{2\, wL^2/M_{yp}} + \frac{wL^2}{8 M_{yp}} \right] M_{yp} \qquad 17.$$

To summarize the steps taken in the evaluation of end slopes for uniformly loaded beams in their correct order:

1. Calculate a and b, Eq. 16.
2. Calculate h, Equation 17.
3. Find the values of coefficients C_{1a}, C_{1b}, C_{2a}, C_{2b} for beam segments AC and BC from Figures 7 and 8.
4. Evaluate end slopes θ_A and θ_B, Equation 10.

If extensive computations involving uniformly loaded beams are required, it is convenient to plot the dimensionless coefficients of $\frac{M_{yp} L}{EI}$ in Equations 10 for direct evaluation of end slopes. A different graph is required for each load intensity.

Application of the Method to the Finding of Deflections

Graphs 2, 3, 6, 7 and 8 furnish information for the evaluation of angle changes and tangential deviations for portions of beams and frames subject to

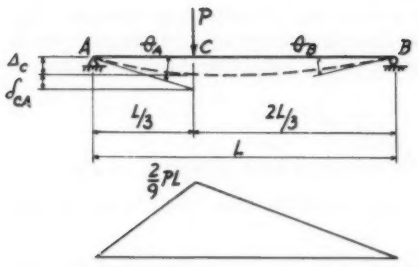

Fig. 10 : Example Problem 1. Simply Supported Beam under Concentrated Load. Deflected Shape and Moment Diagram.

$\frac{PL}{M_{TP}}$	$\frac{M_c}{M_{TP}}$	C_{1a}	C_{1b}	C_{2a}	C_{2b}	$\frac{1}{9}C_{1a}$	$\frac{4}{9}C_{1b}$	$\frac{1}{3}C_{2a}$	θ_A^*	$\frac{2}{3}C_{2b}$	θ_B^*	C_{1a}'	$\frac{1}{3}C_{1a}'$	Δ_c^{**}
4.5	1	.33	.33	.50	.50	.037	.147	.167	-.277	.333	+.223	.17	.057	.073
5.0	1.11	.37	.37	.56	.56	.041	.164	.187	-.310	.374	+.251	.19	.063	.082
5.5	1.22	.41	.41	.62	.62	.046	.182	.207	-.345	.414	+.276	.21	.070	.091
6.0	1.33	.47	.47	.70	.70	.052	.209	.233	-.390	.466	+.309	.23	.077	.104
6.5	1.45	.57	.57	.82	.82	.063	.254	.273	-.464	.546	+.355	.25	.083	.127
6.75	1.50								∞		∞			∞

* multiply by $\frac{M_{TP}L}{EI}$; ** multiply by $\frac{M_{TP}L^2}{EI}$.

Table 1 : Computations for Prob.1.

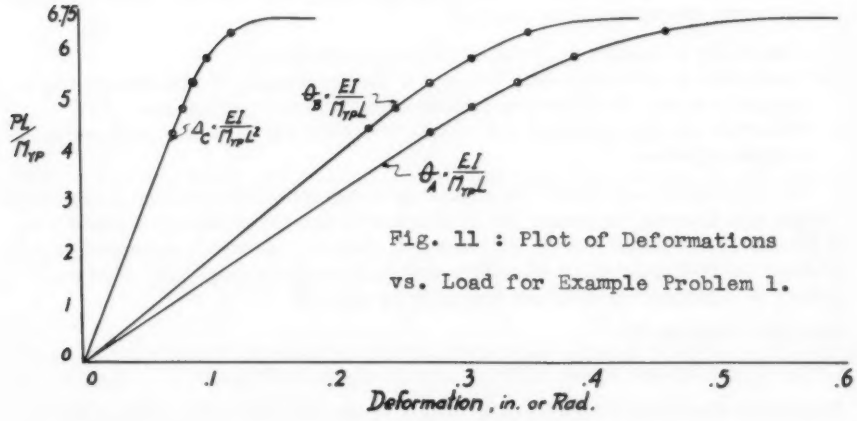

Fig. 11 : Plot of Deformations vs. Load for Example Problem 1.

either concentrated or uniform loads. Anyone familiar with the calculation of elastic deflections by means of the well known moment area method should have little trouble in using these charts to find any desired deformation. As in the moment area method, it is essential to draw a picture of the deformed shape of the structure, indicating the geometrical relationships needed for the calculation.

Example Problem 1:

Given: Simply supported beam under concentrated load as shown in Fig. 10.

Required: Curves of End Slopes θ_A and θ_B and Deflection under load Δ_C vs. load up to collapse.

To find the end slopes θ_A and θ_B, Equations 10 are used, which for the particular position of load are written as

$$\theta_A = \left(\frac{1}{9} C_{1a} - \frac{4}{9} C_{1b} - \frac{1}{3} C_{2a}\right) \frac{M_{TPL} L}{EI},$$

and

$$\theta_B = \left(\frac{1}{9} C_{1a} - \frac{4}{9} C_{1b} + \frac{2}{3} C_{2b}\right) \frac{M_{TPL} L}{EI}.$$

Coefficients C_{1a} and C_{1b} are found from Fig. 2, and Coefficients C_{2a} and C_{2b} from Fig. 3. To find the Deflection Δ_C, relations obtained from the deflected structure of Fig. 10 are used:

$$\Delta_C = \theta_A \cdot \frac{L}{3} - \delta_{CA} = \frac{1}{3}\left(\theta_A \cdot L - \frac{1}{3} C'_{1a} \cdot \frac{M_{TPL} L^2}{EI}\right).$$

C'_{1a} refers to the deviation of Point C from the tangent through Point A and is obtained from Fig. 2.

Application of the Method to the Inelastic Analysis of Indeterminate Structures

In regard to the analysis of indeterminate structures in the inelastic range, these points are to be borne in mind:

1. Conditions of statics apply under all circumstances.
2. Conditions of geometry may be used if the deformations are obtained in a manner similar to the one described in the preceding sections.
3. Principle of superposition is invalid. The total effect of all loads must be lumped together.

The procedure used here for analyzing structures is to assume a statically compatible moment diagram, and to check whether the prescribed conditions of geometry are satisfied. If they are not, then the assumed moments must be revised till both conditions of statics and geometry are fulfilled. This procedure is explained in detail in Example Problem 2.

Example Problem 2:

Given: Rigid Frame under vertical load as shown in Fig. 12.

Required: Vertical deflection under the load Δ_E and side sway deflection Δ_C up to collapse.

The frame shown in Fig. 12 and 13 is estimated simultaneously, such that two conditions of geometry are satisfied; using the convention that clockwise rotations, or deflections connected with clockwise rotation of chord, are called positive, these conditions may be written, referring to the deformed structure shown in Fig. 13, as

$$\theta_{BA} = \theta_{BC}$$

and $\Delta_B = \Delta_C$, or $\delta_{BA} = \theta_C L_3 + \delta_{DC}$.

Moments M_A and M_B are guessed at, the other moments are calculated by statics, and a check is performed whether the above conditions are fulfilled. This work is shown in Table 2. An elastic analysis was first performed to get an idea of the relative magnitudes of moments, and for further work it was recalled that the smaller moments always tend to catch up with the larger ones.

A plastic hinge forms under the load when it reaches a value of approximately $10 \frac{M_{yp}}{L}$. After this instant, the structure becomes indeterminate to the first degree, and only the second of the above mentioned conditions of geometry must be satisfied. At this time, two requirements should be observed:

1. The graphs may not be used to determine angle changes through a yield hinge.
2. No line tangent to the deflected beam at a point where a yield hinge is located may be used, since the inclination of such a tangent is indeterminate.

To find the value of θ_C for the above condition of geometry without violating these rules, the fact may be utilized that the vertical deflection of the plastic hinge under the load must have the same value whether measured from the right or from the left. Thus,

$$-\left(\theta_B \cdot \frac{L_2}{2} + \delta_{EB}\right) = \theta_C \cdot \frac{L_2}{2} + \delta_{EC}$$

or

$$\theta_C = -\theta_B - \frac{2}{L_2}\left(\delta_{EB} + \delta_{EC}\right) .$$

Substituting this value of θ_C in the above condition of geometry, it will take the form

$$\delta_{BA} = -\left[\theta_B + \frac{2}{L_2}\left(\delta_{EB} + \delta_{EC}\right)\right] L_3 + \delta_{DC} .$$

All quantities in this expression may be calculated without violating the stated two rules.

Table 2 shows all calculations connected with this work. The required results may be taken directly from this table.

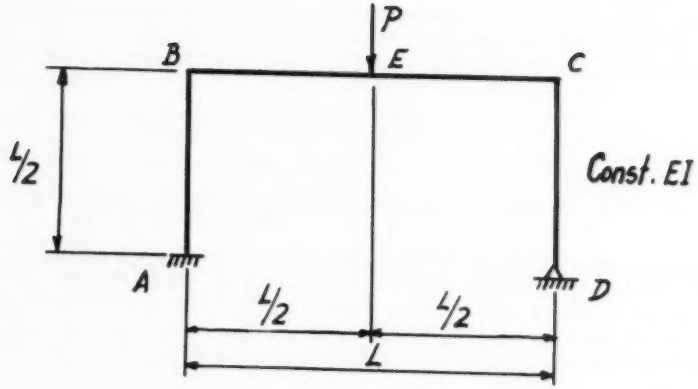

Fig. 12 : Example Problem 2.

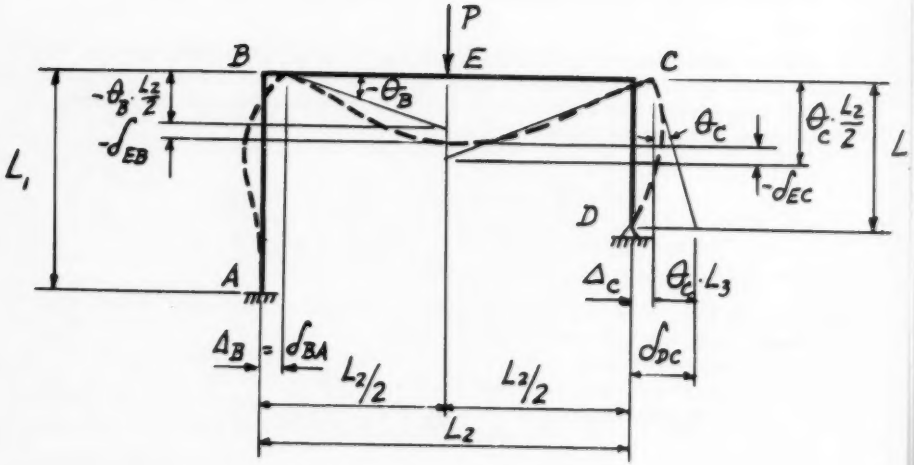

Fig. 13 : Deflected Shape of Frame.

Pl/M_{TP}	M_A/M_{TP}	M_B/M_{TP}	M_C/M_{TP}	M_E/M_{TP}	C_{1a}	C_{1b}	$\frac{1}{4}(C_{1a}-C_{1b})$	C_{2a}	θ^*_{BC}	θ^*_{BA}	δ^{**}_{BA}	C_{2b}	θ^*_C	δ^{**}_{DC}	Δ^{**}_C	δ^{**}_{EB}	δ^{**}_{EC}	Δ^*_E	Remarks.
6.45	-.123	-.550	+.673	+1.00					-.107				+.086		.013			.058	Elast. Analysis (Elast. Limit).
7	-.13	-.60	+.73	+1.085	.26	.24	.005	.238	-.114	-.118	.014	.180	+.095	-.061	.014	-.005		.064	Check on first trial.
8	-.15	-.68	+.83	+1.245	.305	.27	.009	.290	-.136	-.132	.016	.210	+.114	-.070	.013				No check: $\Delta_B (=\delta_{BA}) \neq \Delta_C$.
	-.15	-.69	+.84	+1.235	.30	.275	.006	.280	-.134	-.137	.016	.200	+.106	-.070	.017	-.005		.074	Check.
9	-.17	-.78	+.95	+1.385	.36	.33	.008	.330	-.157	-.153	.018	.245	+.130	-.080	.015				No check: $\Delta_B \neq \Delta_C$.
	-.18	-.78	+.96	+1.380	.36	.33	.008	.325	-.154	-.150	.016	.235	+.126	-.080	.017	-.010		.086	Check
10	-.20	-.90	+1.10	+1.5						-.175	.021		+.142	-.0925	.021	-.0125	+.0292	.100	Plastic Hinge at E.
11	-.26	-1.12	+1.38	+1.5						-.215	.025			-.125		-.031	+.057		No check.
	-.22	-1.14	+1.36	+1.5						-.230	.030		+.186	-.122	.029	-.033	+.055	.148	Check
12		-1.5	+1.5	+1.5						∞			∞		∞			∞	Collapse.

* multiply by $\frac{M_{TP}L}{EI}$; ** multiply by $\frac{M_{TP}L^2}{EI}$.

Table 2 : Computations for Prob. 2.

Application of the Method to Different Cross Section Members

The entire preceding discussion has been concerned with beams of rectangular cross section. It remains to mention the applicability of the suggested method to the analysis of beams of different cross section.

Above all, it should be noted that the basic method may be used for members of any cross section whatsoever. These separate steps would be required to analyze members of any particular cross section:

1. Establishment of an expression or expressions relating the unit angle change to the applied moment.
2. Integration of the unit angle change for various moment variations to arrive at expressions for total angle change and tangential deviation.
3. Drawing up of curves relating deformations to applied loads.
4. Once the curves of Step 3 have been drawn up, the remaining analysis would follow strictly the example problems presented.

Several points should be mentioned in connection with this procedure. The rigorous treatment of I-beams would result in considerable difficulty. There are actually two distinct inelastic stages in an I-beam in bending: Under increasing moment, once the elastic capacity of the beam has been exceeded, first the elasto-plastic frontier will be in the flange, then in the web as the ultimate moment is approached. While the relation between unit angle change and moment for the latter stage is simple, the integration of the expression for the first inelastic stage is quite involved.

Also, for rigorous results, each I-beam shape would require a separate set of calculations and curves, obviously an excessive requirement.

On the other hand, it should be noted that, due to the smaller inelastic range of I-beams, approximate methods which simplify the moment-curvature relationships beyond the proportional limit yield much better results for I-beams than for beams of rectangular cross section.

CONCLUSION

The proposed method offers an "exact" solution of inelastic deflections simpler than others heretofore devised. It might prove useful in establishing and comparing the validity of any approximate methods of finding inelastic deflections which have been or might be suggested.

NOMENCLATURE

a	Fraction of length of beam from End A to point of maximum moment.
b	Fraction of length of beam from End B to point of maximum moment.
c	Distance from neutral axis of beam to extreme fiber.
C_1	Dimensionless coefficient pertaining to tangential deviation: $\delta = C_1 \frac{M_{yp} L^2}{EI}$.
C_2	Dimensionless coefficient pertaining to angle change: $\theta = C_2 \frac{M_{yp} L}{EI}$.
E	Modulus of Elasticity.

h	End moment on beam, divided by M_{yp}.
k	End moment on beam, divided by M_{yp}.
I	Moment of Inertia of cross section of beam.
L	Length of beam.
M	Bending moment on beam.
M_{yp}	Bending moment causing yield point stress in extreme fiber of beam.
P	Concentrated load on structure.
s_{yp}	Yield point stress.
t	Width of cross section of rectangular beam.
w	Uniform load on structure.
x	Distance along beam.
y	Distance from neutral axis of beam to elasto-plastic frontier.
Δ_A	Deflection of Point A of member, normal to axis of member.
Δ_{AB}	Deflection of Point A of member, calculated by traversing deflected shape of structure from Point B.
δ_{AB}	Deviation of Point A of member, with respect to a tangent from Point B of the member.
θ_{AB}	Total angle change between Points A and B of the Member.
θ_A	Slope of member at Point A.
ϵ_{Ext}	Strain in extreme fiber of beam.
ϵ_{yp}	Yield point strain.
ϕ	Curvature (unit angle change) of beam.

ACKNOWLEDGMENT

This paper is based on part of a thesis written in partial fulfillment of the requirements for the Ph.D. degree in the Department of Civil Engineering of the University of Colorado, Boulder, Colo.

Journal of the
ENGINEERING MECHANICS DIVISION
Proceedings of the American Society of Civil Engineers

LATERAL BUCKLING OF I-BEAMS SUBJECTED TO UNEQUAL END MOMENTS

J. W. Clark,[1] and J. R. Jombock,[2] Junior Members, ASCE
(Proc. Paper 1291)

SYNOPSIS

An experimental investigation into elastic and inelastic lateral buckling of aluminum alloy I-beams subjected to unequal end moments is reported. An approximate method is presented for determining the inelastic buckling strength of I-beams with this type of loading. Suggestions are made by which nonuniform bending could be handled more accurately in present design specifications.

INTRODUCTION

The strength of beams as determined by lateral buckling in the elastic stress range has been calculated for a wide variety of conditions of loading and support. Knowledge of the elastic buckling strength is not very useful for design purposes, however, unless means are available for extending the elastic buckling solution into the inelastic stress range. An analytical solution for the inelastic buckling strength of beams is difficult because the resistance of the material to bending and twisting can vary both through the depth of the beam and along its length. The problem can be studied more easily by means of tests.

Until recently, investigations of the buckling strength of beams, either elastic or inelastic, had been confined largely to cases in which the bending moment diagram was symmetrical about the center of the span. Recently, the mathematical solution has been obtained for the elastic buckling strength

Note: Discussion open until December 1, 1957. Paper 1291 is part of the copyrighted Journal of the Engineering Mechanics Division of the American Society of Civil Engineers, Vol. 83, No. EM 3, July, 1957.

1. Research Engr., Alcoa Research Labs., Aluminum Co. of America, New Kensington, Pa.
2. Research Engr., Alcoa Research Labs., Aluminum Co. of America, New Kensington, Pa.

of beams subjected to unequal end moments.(1) The experimental investigation described in this paper was carried out to study both elastic and inelastic buckling of beams subjected to unequal end moments. Tests were made in which the values of the ratio, r, of the moment at one end of the beam to the moment at the other end were 1.0, 0.5, 0, -0.5 and -1.0. The beams were restrained at the ends against rotation in the horizontal plane, rotation about their longitudinal axes, and displacement in the horizontal plane.

Description of Specimens

The specimens were lengths of 2014-T6 aluminum alloy extruded I-section with nominal dimensions of 2-3/8-in. depth, 1-in. flange width and .094-in. thickness for both flanges and web. Average measured cross-sectional dimensions and section properties are shown in Fig. 1.

The material used for these specimens is a typical structural aluminum alloy. Average mechanical properties of the beams in the longitudinal direction are shown in Table I. The compressive yield strengths, tensile yield strengths and tensile strengths of all specimens were within 2 per cent of the average values listed. A compressive stress-strain curve for strains up to about 7 per cent is shown in Fig. 2. The modulus of elasticity for 2014-T6 aluminum alloys is 10,600,000 psi and the modulus of rigidity three-eighths as great.

Description of Tests

The beams were tested in pairs in a 40,000-lb. capacity Amsler testing machine with the auxiliary fittings illustrated in Fig. 3. The pairs of beams when assembled in the end fittings provided a stronger unit for handling prior to testing and provided more resistance to rotation of the end fittings in a horizontal plane during testing than individual beams would have provided. The end fittings, shown in detail in Fig. 4, were designed to give an end condition approaching complete fixity. Counterbalances were used so that no moment was introduced into the specimens from the weight of the end fittings. The loading beams and knife-edge arrangement by which the end moments were applied to the specimens were designed to give the maximum practical resistance to horizontal rotation of the end fittings during the tests.

Special care was used in assembling the two-specimen units and in the alignment of the units in the testing machine to prevent initial out-of-straightness of the specimens. Before testing the specimens, a load of 200 lbs. was applied to each specimen and the out-of-straightness of the top flange (that is, the horizontal deviation from a straight line through the ends) was measured. For specimens failing by inelastic buckling, the maximum out-of-straightness for the 200-lb load was less than L/1800, L being the specimen length. For specimens failing by elastic lateral buckling, the maximum out-of-straightness was found to be less than L/800 for the 200-lb load.

About a third of the specimens tested had type A5-1 SR-4 electrical resistance wire strain gages mounted on the flanges at each end, top and bottom, at a distance of 1 in. from the end fitting. Clamped to these same specimens at the approximate location of maximum horizontal deflection were light aluminum alloy plates from which linen lines were led to 100-ohm Helipot continuous-rotation linear potentiometers. This arrangement made it possible to measure the lateral deflection and rotation of the specimens. The electrical signals from the strain gages, potentiometers, and a Baldwin SR-4 fluid

pressure cell in the testing machine hydraulic system were recorded with a Hathaway S8-C recording oscillograph, providing continuous records of deformations of the specimens and the corresponding loads.

For all specimens, the load was increased continuously until the ultimate load was reached. Fig. 5 is a photograph of one of the specimens taken after failure.

Results and Discussion

A. Elastic Lateral Buckling

Table II lists the maximum applied bending moments and the corresponding nominal critical bending stresses (hereafter termed experimental critical stresses) at the centroids of the flanges, computed by the usual flexure formula. For moments greater than about 12,500 in.-lb., the experimental critical stresses are higher than the proportional limit of the material and, therefore, are slightly greater than the actual flange stresses at failure. The experimental critical stresses are shown graphically in Fig. 6, which also shows the corresponding theoretical critical stresses for beams with ends fixed against rotation in the horizontal plane.(1) The expression from Ref. 1 used for evaluating the critical moments from which the stresses were found is

$$M_{cr} = \mu_r K_{o,1} \frac{\sqrt{BC}}{\alpha L} \qquad (1)$$

where M_{cr} = maximum bending moment in beam when buckling occurs, in.-lb.,

μ_r = a magnification factor reflecting the influence of the end moment ratio r and the end conditions,*

$K_{o,1} = \sqrt{1 + \frac{\pi^2 a^2}{(\alpha L)^2}}$ = a factor dependent on the section properties, beam length, and end conditions,

$a^2 = \frac{h^2 B}{4C}$ = an index of the section's strength against warping, in.^{2},

h = distance between centroids of flanges, in.,

B = EI_y = minimum flexural rigidity of the beam, lb.-in.^{2},

E = modulus of elasticity, psi,

I_y = minimum moment of inertia of the beam, in.^{4},

C = GJ = torsional rigidity of the beam, lb.-in.^{2},

G = modulus of rigidity, psi,

J = torsion constant, in.^{4},

L = laterally unsupported length of beam, in.,

* One of the significant contributions of Professor Salvadori's paper[1] is the demonstration that the effect of the conditions of restraint at the ends on the value of μ_r is sufficiently small that for design purposes μ_r may be considered to be independent of the end conditions.

α = reduced length factor (α = 1.0 when ends are simply supported in lateral direction and 0.5 when ends are fixed in lateral direction).

In Fig. 6 the experimental critical stresses generally fall below the theoretical curves. For the beams that failed at stresses below the proportional limit of the material, this difference presumably resulted from the fact that the ends of the beams were not completely restrained against rotation in the horizontal plane. This behavior has been found in previous investigations of lateral buckling.(2, 3, 4) An evaluation of this effect was made for all specimens of the present investigation that buckled in the elastic range.

Fig. 6 was used to determine the experimental reduced length factor, α, for these specimens. For any specimen, α is the factor which, when applied to the actual specimen length L, gives a reduced length αL that may be used in Equation 1 to obtain the experimental critical stress.

Fig. 7 is a plot of the experimental reduced length factors as a function of the actual beam length for all specimens that failed by elastic lateral buckling. A straight line was fitted to the plotted points by the method of least squares. The equation of this line was found to be

$$\alpha = .610 - .00134L \tag{2}$$

For beams of about 82-in. length, the above expression gives an experimental reduced length factor of 0.5 corresponding to complete fixity. Equation 2 does not apply to beams whose length exceeds 82 in. The fact that α approaches 0.5 as the length of the beam increases is to be expected since for very long beams the stiffness of the test apparatus relative to the stiffness of the beams is very great. For the shortest specimens buckling elastically, this expression gives experimental reduced length factors ranging from about 0.55 to 0.58, corresponding to lengths of 48 in. for r = -1.0 and 21 in. for r = 1.0, respectively.

B. Inelastic Lateral Buckling

The experimental critical stresses for almost half of the specimens were in the inelastic range. The failure in these cases occurred either by inelastic lateral buckling, by local buckling, or a simultaneous development of both. The type of failure was determined by visual observation. A comparison between the test results and calculated critical stresses for inelastic buckling is illustrated in Fig. 8.

To take account of the reduced stiffness of the beam in the inelastic stress range, Equation 1 can be modified by substituting a reduced modulus E' for the modulus of elasticity E. The result can be expressed

$$M_{cr} = \frac{E'}{E} \mu_r K_{o,1} \frac{\sqrt{BC}}{\alpha L} \tag{3}$$

For comparison with test results, it is convenient to rewrite Equation 3 as follows:

$$\sigma_{cr} = E' \left[\frac{\mu_r K_{o,1} \sqrt{BC}}{E \alpha L} \cdot \frac{h}{2I} \right] \tag{4}$$

where σ_{cr} = stress at centroid of flange corresponding to M_{cr}, psi,

I = moment of inertia of beam about principal axis normal to web, in.^{4}

The quantity in brackets in Equation 4 may be thought of as the value of flange strain at which elastic buckling would take place if the material behaved elastically up to failure. This quantity is plotted as the abscissa in Fig. 8 and critical stress as the ordinate. Values of α were calculated from Equation 2, which was assumed to apply in the inelastic as well as the elastic stress range.

Three different values of the reduced modulus E' were used in calculating the curves in Fig. 8. In each case, the value of the reduced modulus was assumed to be governed by the nominal stress at the mean fiber of the compression flange at the point of maximum bending moment in the beam. The lowest curve in Fig. 8 results from using the tangent modulus E_t for E'. Use of the tangent modulus in the buckling formula gives good agreement with tests in the case of inelastic buckling of aluminum alloy columns,(5) and the tangent modulus curve has also been used in establishing design stresses for aluminum alloy beams.(6)

The middle curve in Fig. 8 was based on the double modulus, E_R, given by the formula

$$E_R = \frac{4EE_t}{(\sqrt{E} + \sqrt{E_t})^2} \tag{5}$$

The double modulus curve was found to agree closely with test results in a previous investigation of lateral buckling of beams with uniform bending moment.(3)

The highest curve in Fig. 8 was derived by assuming E' to equal the secant modulus E_s.

The curves in Fig. 8 are cut off at a stress of 70,100 psi, which is the calculated stress for local buckling of the compression flange for the test beams. In calculating the local buckling stress for the flange, the attachment of the flange to the web was considered to be about half way between the fixed and hinged conditions, and the effective modulus was assumed to be the secant modulus (Ref. 7, p. 353). The resulting approximate formula for the flange buckling stress is

$$\sigma_{cr} = 0.62\ E_s\ (t_f/b_f)^2 \tag{6}$$

where t_f = thickness of flange, in.,

b_f = width of outstanding portion of flange, in.

For these beams, Equation 6 gives a buckling stress equal to 0.024 E_s, which is equivalent to 70,100 psi. One of the assumptions on which this value is based is that the stress is uniform along the flange. The flange buckling stress would be expected to be higher when the beam is subjected to nonuniform bending moment, so that the maximum stress occurs at only one point. The nominal stress values at which failures occurred that involved local buckling, including cases in which lateral buckling and local buckling occurred simultaneously, varied from 69,200 to 81,600 psi.

Measured and calculated critical stresses are further compared by the bar graphs of Fig. 9, which show the ranges of the ratio of experimental to calculated critical stress. The four bars for each value of end moment ratio in Fig. 9 correspond to the four sets of calculated critical stresses.

The first set of calculated critical stresses was based on the assumption that the critical stress for any beam subjected to unequal end moments may be approximated by the calculated critical stress for the beam subjected to uniform bending, using the tangent modulus as the reduced modulus in calculating inelastic critical stresses. The reason for comparing calculated critical stress based on uniform bending with experimental critical stresses for beams with nonuniform bending moment is that design specifications(6, 9) for allowable stresses in beams are generally based on the uniform-bending case (or a loading condition that gives nearly the same buckling stress, such as uniform load on the top flange). Fig. 9 shows that the beams with r = 0 carried up to 96 per cent more bending moment (considering both elastic and inelastic buckling) than would the same beams subjected to uniform bending. When r was -0.5 and -1.0, bending moments at failure were as much as 160 per cent greater than would be expected from considerations of the uniform bending case. This comparison shows that current design requirements for beams may be very conservative when the beams are subjected to reverse bending.

The second set of calculated critical stresses was obtained from the elastic buckling solution for the type of bending moment that the beams were actually subjected to, with the elastic modulus replaced by the tangent modulus. The comparison between the values obtained in this way and the experimental critical stresses is the same as the comparison between the tangent modulus curve and the test points in Fig. 8. It is reasonable to expect the tangent modulus curve to be conservative when applied to beams (Ref. 7, p. 165), and this is borne out by the test results, as shown in Fig. 9. The experimental critical stresses ranged from 8 per cent less to 39 per cent more than the calculated critical stresses.

This second method of calculating critical stresses is essentially the same as the "equivalent slenderness ratio" method. The equivalent slenderness ratio for a beam is equal to the slenderness ratio of a column that would have the same elastic buckling stress as the beam. The equivalent slenderness ratio is used in conjunction with a curve of column buckling stress to determine the buckling stress (either elastic or inelastic) for the beam. If the column curve is based on the tangent modulus, the resulting calculated beam strengths are the same as those determined by substituting the tangent modulus for the modulus of elasticity in the elastic buckling formula for beams. Similar results would also be achieved by applying the equivalent slenderness ratio method in combination with the straight-line formula for aluminum alloy columns,(10) since the straight-line formula agrees closely with the tangent-modulus curve.

A third set of calculated stresses was obtained by the use of the double modulus in the elastic buckling solution. As in a previous investigation,(3) use of the double modulus gives good agreement between experimental and calculated critical stresses for beams under uniform bending moment, the experimental values being from 8 per cent less to 9 per cent more than the calculated critical stresses (see Fig. 9). For beams with nonuniform bending moment, the double modulus curve is conservative, as has been predicated,(8) since the modulus is reduced by the maximum amount in but a small portion

of the beam, while the remainder of the beam is stiffer. Including all the test results, the experimental critical stresses were from 8 per cent less to 34 per cent more than the calculated values.

Finally, a fourth set of calculated critical stresses was obtained by the use of the secant modulus in the elastic buckling solution. The computed values were cut off at the calculated local buckling stress. It can be seen in Fig. 9 that the experimental critical stresses ranged from 12 per cent below to 19 per cent above the computed values. Considering only the beams for which the end moment ratio was zero or less, the experimental buckling stresses are from 7 per cent less to 19 per cent above the values computed on the basis of the secant modulus. A rational basis for expecting the secant-modulus buckling stress to give a reasonable approximation to the true value for values of r between zero and -1.0 is explained in the appendix.

Based on the results of these tests as summarized in Fig. 9, the critical stress for beams subjected to more or less uniform bending (r = 1.0 to 0.5) may be calculated by the use of the double modulus in Equation 4 and critical stress for beams with smaller end-moment ratios may be calculated by the use of the secant modulus in Equation 4.

C. Recommendations Concerning Design Methods

As the tests show, design specifications for beams based on the assumption of a uniform bending moment or a uniform top flange loading can be very conservative when applied to beams with unequal end moments. However, the extra strength of beams subjected to unequal end moments could be taken into account approximately without making any radical changes in current specifications. Present design specifications give formulas or charts that relate the allowable beam stress to a function of the dimensions of the beam, such as $L/\sqrt{B_1/S_c}$ in the ASCE specifications for aluminum alloy structures[6] or ld/bt in the AISC specifications for steel structures.[9] These same formulas or charts could be applied to beams with unequal end moments if the function of the dimensions were multiplied by a coefficient whose value would depend on the ratio of the end moments, r. For example, the quantity $L/\sqrt{B_1/S_c}$ in the ASCE specifications would be replaced by $CL/\sqrt{B_1/S_c}$. Values of the coefficient C corresponding to various values of r would be given in a table or chart.

The coefficient C described in the preceding paragraph is equal to $1/\sqrt{\mu_r}$.* Fig. 10 shows minimum safe values of μ_r plotted versus r for beams with any condition of lateral support at the ends, as given by Salvadori.[1] It has been shown in the present investigation that these values of μ_r apply approximately to inelastic buckling, as well as to the case of elastic buckling for which they were calculated. The test results also help to show that an appreciable improvement in accuracy of design specifications would result from the introduction of a coefficient such as that suggested.

CONCLUSIONS

The following conclusions have been drawn from the results of this

* If a coefficient of this kind were applied to the factor ld/bt used in the ASCE specifications, the value of the coefficient would be proportional to $1/\mu_r$.

investigation of the lateral buckling of aluminum alloy I-beams subjected to unequal end moments:

1. The experimentally determined elastic buckling stresses are generally lower than theoretical critical stresses calculated on the basis of the assumption that the beam ends are fixed against rotation in the horizontal plane. Satisfactory agreement between experimental elastic buckling stresses and theoretical values is obtained by the use of an empirical reduced length factor in the theoretical solution. The reduced length factor varied from about 0.50 to 0.58.

2. Beams under unequal end moments can develop much higher stresses (as much as 160 per cent higher in these tests) than the same beams when subjected to uniform bending moment. Therefore, design specifications based on the case of uniform bending moment, or some other loading giving similar values of critical stress, can be very conservative when applied to beams with unequal end moments.

3. Critical stresses in the inelastic range for beams under unequal end moments can be estimated conservatively by substituting the tangent modulus corresponding to the maximum stress for the modulus of elasticity in the elastic buckling formula. This method of calculation gives the same result as the use of the "equivalent slenderness ratio" method in conjunction with a curve of column buckling strength. Experimental critical stresses were from 8 per cent below to 39 per cent above the values calculated by this method.

4. The use of the double modulus for the effective modulus in the elastic buckling solution gives inelastic critical stresses in reasonable agreement with test results for beams subjected to more or less uniform bending ($r = 1.0$ and $r = 0.5$) but results in conservative inelastic critical stresses for beams with smaller end-moment ratios. For all tests, the experimental critical stresses varied from 8 per cent less to 34 per cent more than the values calculated using the double modulus.

5. The use of the secant modulus for the effective modulus in the elastic buckling solution gives inelastic critical stresses in reasonable agreement with test results for beams with unequal end moments. Critical stresses for the test beams with $r = 0$, -0.5, or -1.0 were from 7 per cent below to 19 per cent above the secant-modulus calculated values.

6. Current design specifications could be modified easily to take approximate account of the greater strength of beams subjected to unequal end moments as compared to beams loaded by equal end moments or uniformly distributed load. The charts and formulas for beam strength already in use would apply to the case of unequal end moments if the function of the beam dimensions (for example, $L/\sqrt{B_1/S_C}$ in Ref. 6 or ld/bt in Ref. 9) were multiplied by coefficient whose value would depend on the end moment ratio, r. Values of the coefficient could be presented in a table or chart.

REFERENCES

1. M. G. Salvadori, "Lateral Buckling of Eccentrically Loaded I-Columns," Proceedings ASCE, Separate No. 607, January, 1955.

2. H. N. Hill, "The Lateral Instability of Unsymmetrical I-Beams," Journal of the Aero. Sciences, Vol. 9, No. 5, March, 1942.

3. C. Dumont and H. N. Hill, "The Lateral Stability of Equal-Flanged Aluminum Alloy I-Beams Subjected to Pure Bending," NACA Technical Note No. 770, August, 1940.

4. H. N. Hill, "Lateral Buckling of Channels and Z-Beams," Transactions ASCE, Vol. 119, 1954.

5. R. L. Templin, R. G. Sturm, E. C. Hartmann and M. Holt, "Column Strength of Various Aluminum Alloys," Technical Paper No. 1, Aluminum Research Laboratories, Aluminum Company of America, Pittsburgh, Pa., 1938.

6. Second Progress Report of the Committee of the Structural Division on Design in Lightweight Structural Alloys, "Specifications for Structures of Aluminum Alloy 6061-T6," Paper 970, Journal of the Structural Division of the American Society of Civil Engineers, Vol. 82, No. ST3, May, 1956.

   Third Progress Report of the Committee of the Structural Division on Design in Lightweight Structural Alloys, "Specifications for Structures of Aluminum Alloy 2014-T6," Paper 971, Journal of the Structural Division of the American Society of Civil Engineers, Vol. 82, No. ST3, May, 1956.

7. F. Bleich, "Buckling Strength of Metal Structures," McGraw-Hill Book Company, Inc., New York, 1952.

8. S. Timoshenko, "Theory of Elastic Stability," McGraw-Hill Book Company, Inc., New York, 1936, p. 273.

9. "Specifications for the Design, Fabrication and Erection of Structural Steel for Buildings," American Institute of Steel Construction, New York, 1946.

10. H. N. Hill and J. W. Clark, "Straight-Line Column Formulas for Aluminum Alloys," Technical Paper No. 12, Aluminum Research Laboratories, Aluminum Company of America, Pittsburgh, Pa., 1955.

APPENDIX

Application of the secant modulus to the calculation of buckling stresses for beams with nonuniform bending moment can be given some rational justification by using the following reasoning: Let E_x' be the effective modulus for the beam cross section at the point x. Assume that the buckling strength can be calculated by substituting an average value of $1/E_x'$ for the quantity $1/E$ in the elastic buckling formula. To understand the meaning of this assumption, consider the expression for the strain energy of lateral bending, V_B, of the beam, including a variable modulus E_x'. This expression is

$$V_B = \frac{I_y}{2} \int_0^L E_x' \left(\frac{d^2u}{dx^2}\right)^2 dx \qquad (7)$$

where I_y is the lateral moment of inertia, u is the lateral deflection, and x is

distance along the longitudinal axis. An approximate value of V_B can be obtained by using the following expression instead of Equation 7:

$$V_B = \frac{\frac{I_y}{2}\int_0^L \left(\frac{d^2u}{dx^2}\right)^2 dx}{\frac{1}{L}\int_0^L \frac{1}{E'_x}\,dx} \tag{8}$$

Rough calculations indicate that the use of Equation 8 rather than Equation 7 can introduce fairly large errors in the values of V_B (as much as 20 or 30 per cent), but the resulting errors in the value of critical stress are considerably smaller. Values of V_B given by Equation 8 can be either higher or lower than the correct values, depending on the variation of du/dx and E'_x along the beam.

If a modification similar to that described above is made in the expressions for strain energy of twisting and flange bending, the resulting equation for total energy of the beam is the same as the equation for elastic strain energy,[1] except that the quantity 1/E is replaced by the quantity in the denominator on the right-hand side of Equation 8. This quantity is the average value of $1/E'_x$ for the beam. Therefore, the resulting critical bending moment is equal to that obtained from the elastic solution by substituting the average value of $1/E'_x$ for 1/E.

Assume that the effective modulus E'_x is the tangent modulus E_{tx} corresponding to the stress in the compressive flange at the point x. Since the beam twists as well as bends when buckling occurs, the actual effective modulus should be greater than the tangent modulus. Thus, the use of the tangent modulus will tend to make the resulting calculated critical moments conservative. The reciprocal of the tangent modulus is

$$\frac{1}{E_t} = \frac{d\epsilon}{d\sigma} \tag{9}$$

where ϵ = unit strain

and σ = unit stress.

For a beam of length L, the average value of $1/E_{tx}$, designated by $1/\bar{E}_t$, is

$$\frac{1}{\bar{E}_t} = \frac{1}{L}\int_0^L \frac{d\epsilon}{d\sigma}dx \tag{10}$$

Assume that the flange stress varies linearly from σ_0 at one end of the beam to σ_L at the other end. For the beams of this investigation, the bending moment varied linearly. The assumption that the flange stress has a linear variation is only an approximation when some of the stresses exceed the proportional limit. Then

$$\frac{d\epsilon}{d\sigma} = \frac{d\epsilon}{dx}\frac{dx}{d\sigma} = \frac{L}{\sigma_L - \sigma_o}\frac{d\epsilon}{dx} \tag{11}$$

Combining Equation 10 and 11 gives

$$\frac{1}{E_t} = \frac{1}{\sigma_L - \sigma_o}\int_o^L d\epsilon \tag{12}$$

Integrating Equation 12 gives

$$\frac{1}{E_t} = \frac{\epsilon_L - \epsilon_o}{\sigma_L - \sigma_o} \tag{13}$$

Thus the average value of the reciprocal of the tangent modulus is equal to the reciprocal of the slope of the line connecting the two points on the stress-strain curve corresponding to the stresses at the two ends of the beam. If the end moment ratio is 0.0 or -1.0, the slope of this line is the secant modulus corresponding to the maximum stress in the beam. Therefore, when r has the value 0.0 or -1.0, and when the expressions for the various types of strain energy in the beam are assumed to be similar to Equation 8, with E'_x being the tangent modulus at the point x, the resulting critical stress values are the same as though the secant modulus corresponding to the maximum stress were substituted for the modulus of elasticity in the elastic buckling formula. This does not mean that a theoretically correct solution of the buckling problem is obtained by substituting the secant modulus for the elastic modulus in the elastic buckling formula. It indicates only that there is reason to expect this use of the secant modulus to give an approximation of the correct solution.

TABLE I

MECHANICAL PROPERTIES OF 2014-T6
ALUMINUM ALLOY EXTRUDED I-BEAMS

Tensile Strength,* psi	63,800
Tensile Yield Strength,* 0.2 per cent offset, psi	60,300
Compressive Yield Strength,** 0.2 per cent offset, psi	60,800
Elongation,* per cent in 2-in. gage length	11.5

* Determined from standard 1/2-in. wide rectangular tension specimens cut from web and machined to uniform thickness, see ASTM Standards, 1955, Part 2, E8-54T, p. 1246-1260.

** Determined from 5/8-in. wide 2.63-in. long rectangular compressive specimens, cut from flange and machined to uniform thickness (tested in subpress with Montgomery-Templin type jig), ibid., E9-52T, p. 1261-1267.

TABLE II

SUMMARY OF EXPERIMENTAL CRITICAL STRESSES

Spec. No.	Length, in.	End Moment Ratio, r	Maximum Applied Moment, M_m, in.-lb.	Experimental Critical Stress, $\frac{M_m h}{2I}$, psi
0.5	60	1.0	2 800	10 600
1	48	1.0	4 140	15 600
1.5	42	1.0	4 700	17 600
2	36	1.0	5 910	22 200
2.5	30	1.0	7 530	28 300
3	24	1.0	9 690	36 400
3.5	21	1.0	11 820	44 400
4	18	1.0	13 560	51 000
5	12	1.0	15 270	57 400
5.5	6	1.0	18 760	70 500 [a]
6	57	0.5	3 800	14 300
7	39	0.5	6 740	25 300
8	30	0.5	9 960	37 400
9	21	0.5	15 080	56 700
10	12	0.5	18 400	69 200 [a]
10.5	6	0.5	21 200	79 800 [b]
11	54	0	5 790	21 800
12	45	0	8 120	30 500
13	36	0	10 480	39 400
14	30	0	13 050	49 100
15	24	0	14 980	56 300
16	18	0	18 430	69 300
16.5	9	0	19 670	74 000 [b]
17	72	-0.5	6 220	23 400
18	54	-0.5	8 350	31 400
19	36	-0.5	13 470	50 600
20	27	-0.5	17 000	63 900
21	18	-0.5	21 000	79 000 [a]
21.5	9	-0.5	21 700	81 600 [b]
22	84	-1.0	4 710	17 700
23	66	-1.0	6 520	24 500
24	48	-1.0	9 310	35 000
25	36	-1.0	13 000	48 900
26	30	-1.0	14 940	56 200
27	24	-1.0	17 540	65 900
28	18	-1.0	20 100	75 700 [b]
29	12	-1.0	20 500	77 200 [b]

a Failed by combined local buckling of flange and web and lateral buckling
b Failed by local buckling of flange and web

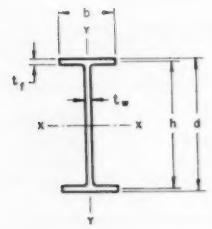

DIMENSION	AVERAGE MEASURED DIMENSIONS, INCHES
b	0.989
d	2.361
h	2.272
t_w	0.0866
t_f	0.0888

SECTION PROPERTIES BASED ON AVERAGE MEASURED DIMENSIONS:

MOMENT OF INERTIA ABOUT X-X AXIS, I_x,	0.302 IN.^{4}
MOMENT OF INERTIA ABOUT Y-Y AXIS, I_y,	0.0144 IN.^{4}
TORSION CONSTANT, J,	0.000955 IN.^{4}
TORSION BENDING CONSTANT, C_s,	0.0186 IN.^{6}

FIG. 1 DIMENSIONS AND SECTION PROPERTIES OF 2014-T6 ALUMINUM ALLOY EXTRUDED I-BEAMS

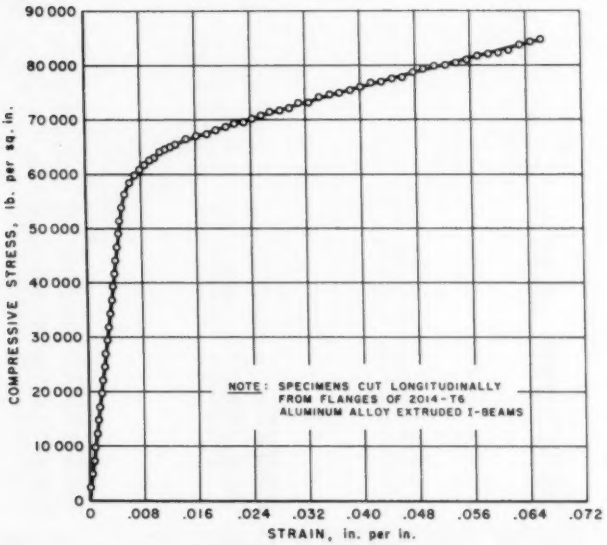

FIG. 2 AVERAGE COMPRESSIVE STRESS-STRAIN CURVE FOR ALUMINUM ALLOY EXTRUDED I-BEAM

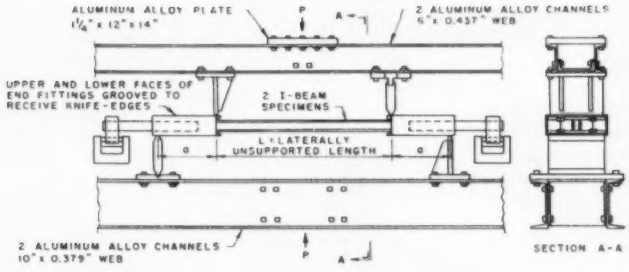

FIG. 3 ARRANGEMENT FOR TESTING PAIR OF I-BEAM SPECIMENS

(KNIFE-EDGES ARRANGED AS SHOWN ABOVE GIVE UNIFORM BENDING MOMENT, i.e., r = 1; FOR OTHER VALUES OF r, PLACE KNIFE-EDGES AS SHOWN BELOW)

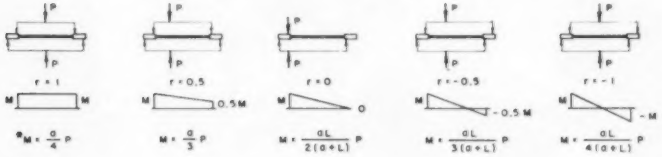

* M = BENDING MOMENT PER SPECIMEN IN ALL CASES

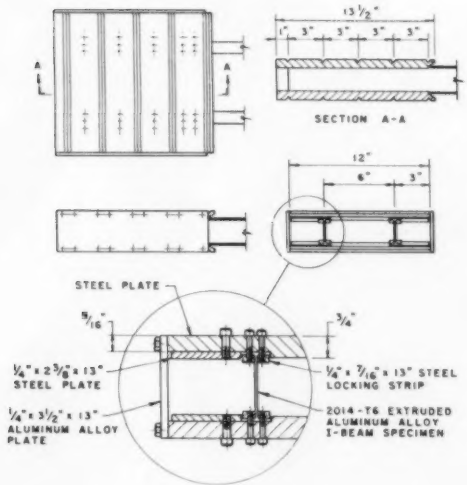

FIG. 4 DETAILS OF END FITTINGS

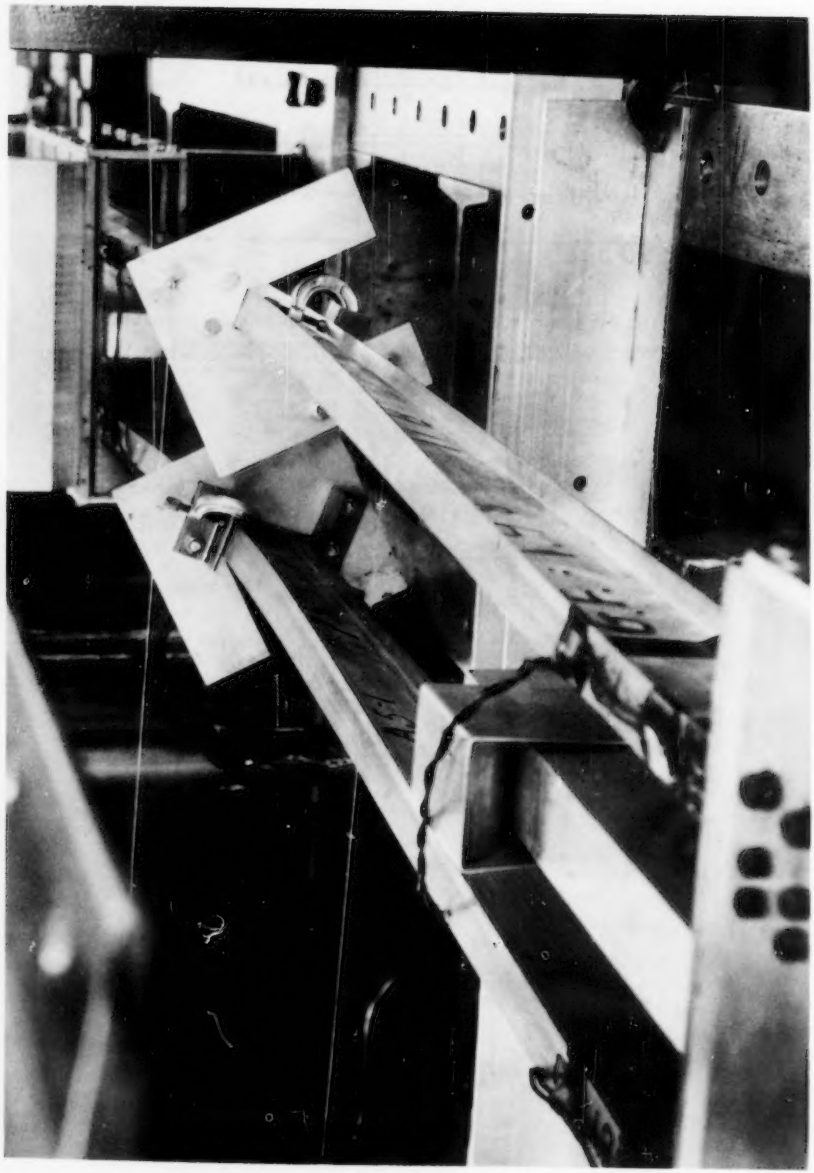

Fig. 5. SPECIMEN 11, r = 0, L = 54 IN., AFTER FAILURE BY ELASTIC LATERAL BUCKLING.

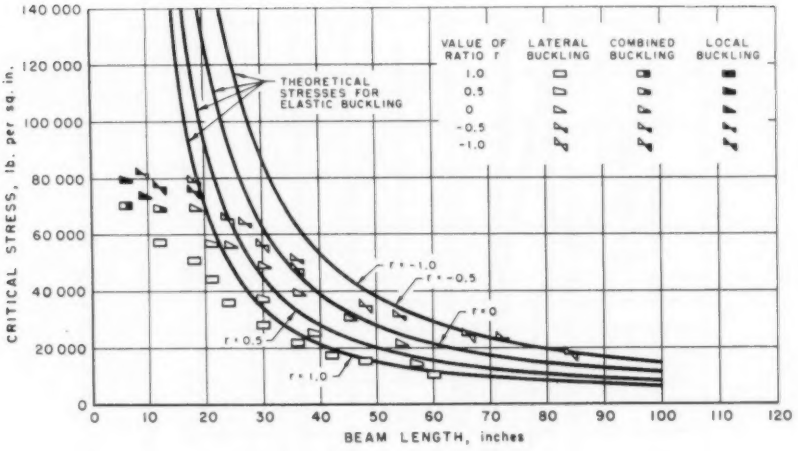

FIG. 6 EXPERIMENTAL AND THEORETICAL CRITICAL STRESSES

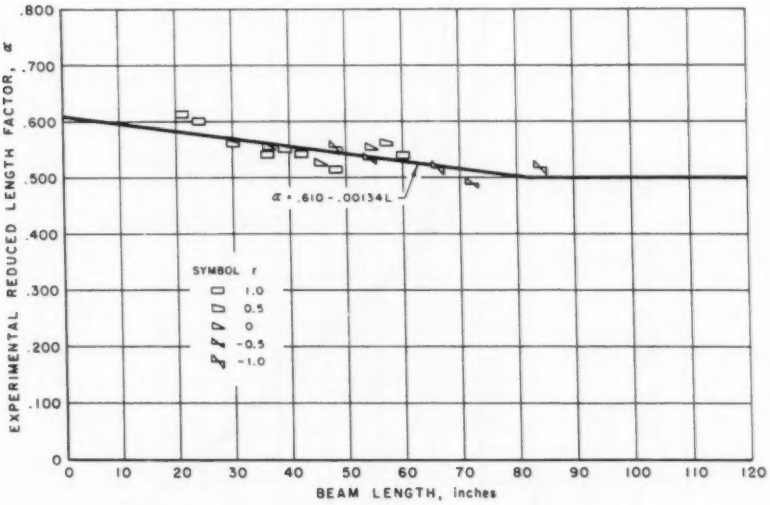

FIG. 7 EXPERIMENTAL REDUCED LENGTH FACTOR

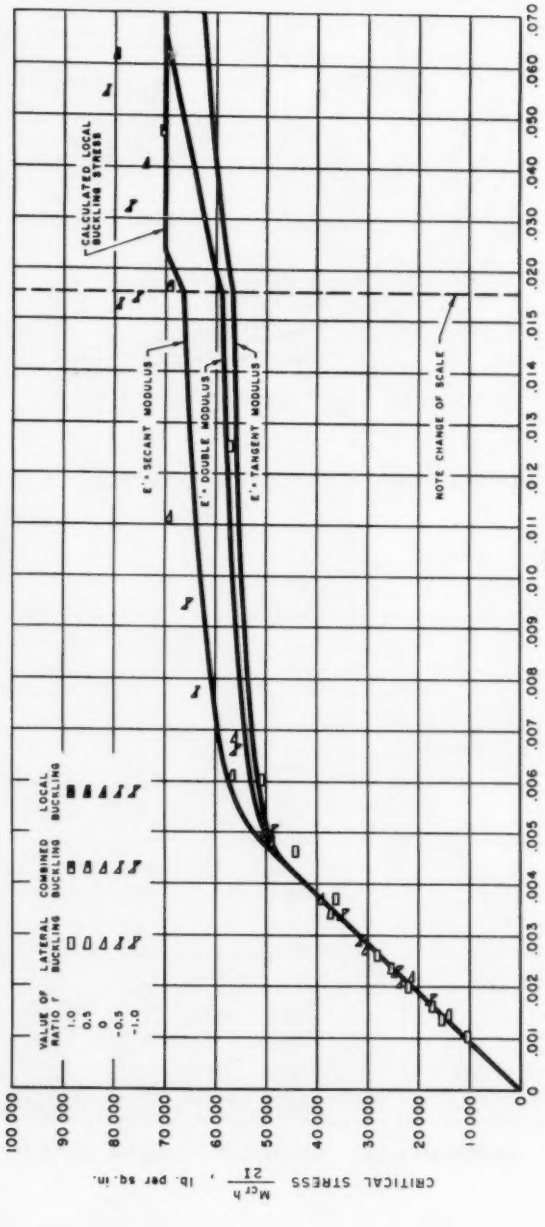

FIG. 8 EXPERIMENTAL CRITICAL STRESSES AND VARIOUS CALCULATED RELATIONSHIPS

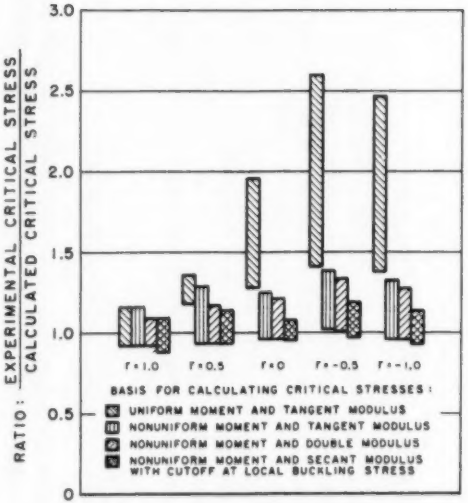

FIG. 9 COMPARISON OF EXPERIMENTAL AND CALCULATED CRITICAL STRESSES

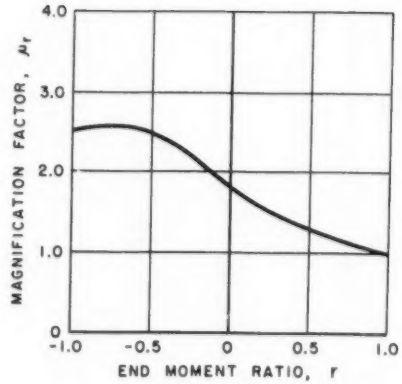

FIG. 10 VALUES OF MAGNIFICATION FACTOR μ_r FOR DESIGN PURPOSES (FROM FIG. 2, REF. 1)

Paper 1292 EM 3

Journal of the
ENGINEERING MECHANICS DIVISION
Proceedings of the American Society of Civil Engineers

THE LATERAL RIGIDITY OF SUSPENSION BRIDGES

I. K. Silverman,[1] A.M. ASCE
(Proc. Paper 1292)

SYNOPSIS

The behaviour of a suspended structure under lateral loads is shown to depend upon the values of three dimensionless parameters

$$\alpha = \frac{Hh_t}{pl^2} \; ; \; \beta = \frac{Hh_c}{pl^2} \; ; \; \lambda = \frac{Hl^2}{2\pi^2 E I_v}.$$

For the important case of a uniform load over the entire span curves, applicable to moderately long span are presented for moment, shear, and deflection coefficients as a function of the parameter λ. The spring constant for small vibrations in the horizontal plane is also derived.

Action under Static Lateral Forces

When the suspended structure of a suspension bridge is deflected out of its plane by lateral forces, restoring forces due to existing suspender loads are brought into play. Since the suspender forces are a measure of the cable tension the behaviour of the suspended structure depends upon the cable stiffness in addition to its own stiffness. The lateral stiffness of a suspension bridge can be expressed in terms of a parameter which is the ratio of cable stiffness to lateral truss system stiffness. Due to this interaction, lateral loads acting on the suspended structure are transferred to the towers in part by the cable.

The Uniform Distribution Assumption

By making the simplifying, but inaccurate, assumption that the load transferred to the cable is uniform, the condition for equality of deflection of the

Note: Discussion open until December 1, 1957. Paper 1292 is part of the copyrighted Journal of the Engineering Mechanics Division of the American Society of Civil Engineers, Vol. 83, No. EM 3, July, 1957.

1. Engr., Bureau of Reclamation, U.S. Dept. of the Interior, Denver, Colo.

cable and truss at the bridge mid span results in a direct solution of a load distribution between cable and truss systems. (See Appendix "A" for notation.)

Under the uniform distribution assumption and for uniform wind load over the full length of the span, which is the most important case, the restoring force z is given by [1][2]

$$z = \frac{w_t}{1 + b/a} - \frac{w_c}{1 + a/b}$$

$$\frac{b}{a} = 9.6\left(\frac{h_t}{h_c}\right)\frac{EI_v}{Hl^2} = 4.8\left(\frac{h_t}{h_c}\right)\frac{1}{\pi^2\lambda}$$

where $\lambda = \frac{Hl^2}{2\pi^2 EI_v}$

Using $w_t = 0.9w$ and $\left(\frac{h_t}{h_c}\right) = 1.02$

$$z = w_t\left[\frac{1}{1 + \frac{0.496}{\lambda}} - \frac{1}{9\left(1 + \frac{\lambda}{0.496}\right)}\right]$$

Coefficients for deflection, bending moment and tower reaction at truss level are given by curves of Figures 5, 6, 7, and 8 marked "Uniform Distribution" for various values of λ.

The Elastic Distribution Method

The Elastic Distribution Method as developed by Moissief and Lienhard [1] is a trial and error method for determining the distribution of load between truss and cable. By assuming an initial distribution of the restoring forces z, the final distribution is obtained by preserving geometrical continuity between truss and cable. This fundamental method has the disadvantage of all trial and error solutions in not being a direct solution.

Differential Equation of Deflected Wind Truss

Using the notation of Appendix "A" and Figures 1 and 2, the following relations may be written:

$$q = w_t - z = EI_v\frac{d^4v}{dx^4} = EI_v v^{IV}$$

$$M = -EI_v\frac{d^2v}{dx^2} = -EI_v v'' = M_w - Hu$$

$$z = p\left(\frac{v-u}{h}\right)$$

$$M_w = \frac{w}{2}x(l-x)$$

2. Numbers in brackets refer to the Bibliography at the end of the paper—Appendix B.

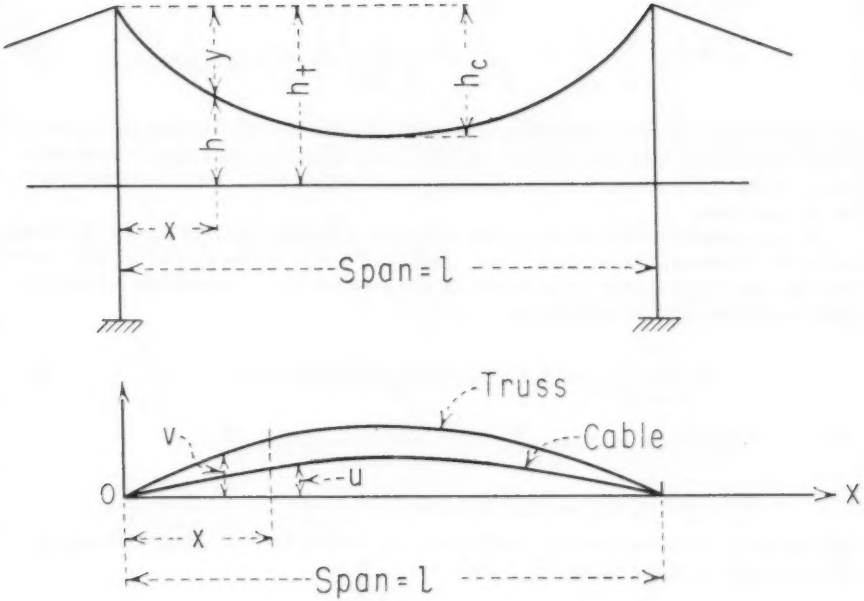
y
h
h+
hc
x
Span = l
Truss
Cable
v
u
0
X
x
Span = l

FIG. 1

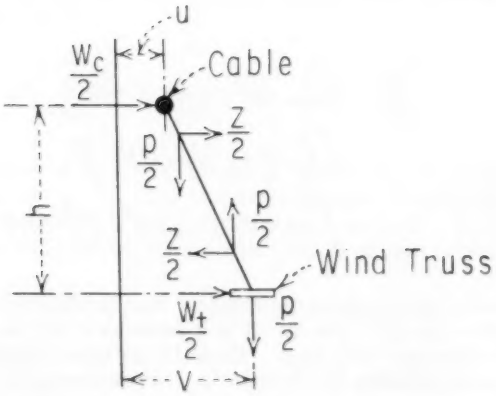
u
Wc/2
Cable
Z/2
p/2
p/2
h
Z/2
Wind Truss
Wt/2
p/2
V

FIG. 2

Eliminating Z and u, the remaining unknown, v, is defined by the following differential equation:

$$L \equiv h v^{IV} - \frac{b}{h} v'' + \frac{b}{E I_v} v - \frac{1}{E I_v}\left(\frac{b M_w}{H} + w_t h\right) = 0 \qquad (1)$$

No solution of (1) in closed form is known. Power series, collocation, and finite difference methods [2], [3], [4] have been used successfully. None of these solutions however are in general terms which involve the parameters of the problem.

An approximate solution of (1) in terms of a Fourier Series can be obtained using the Principle of Virtual Work, [5] [6]. For the uniform lateral load over the full span previously considered, an expression for v satisfying all boundary conditions can be written as

$$v = \frac{l^4}{E I_v}\left[a_1 \sin m_1 x + a_3 \sin m_3 x + a_5 \sin m_5 x + \cdots\right]. \qquad (2)$$

$$\text{where } m_1 = \frac{\pi}{l};\ m_3 = \frac{3\pi}{l};\ \cdots\ m_n = \frac{n\pi}{l}$$

Independent variations of the coefficients a_n yields the following expression for a virtual displacement, δv.

$$\delta v = \delta a_1 \sin m_1 x + \delta a_3 \sin m_3 x + \cdots$$

The Principle of Virtual Work requires that the following conditions be satisfied:

$$\left.\begin{aligned} &\int_0^l L \sin m_1 x\, dx = 0 \\ &\int_0^l L \sin m_3 x\, dx = 0 \\ &\cdots\cdots\cdots\cdots \\ &\int_0^l L \sin m_n x\, dx = 0 \end{aligned}\right\} \qquad (3)$$

The expression for L under the integral sign is obtained by inserting (2) and its derivatives into (1). Unless (2) is a solution of (1) the resulting expression will be different from zero. From (3) as many independent equations are obtained as unknown coefficients a_n. Performing the integrations a set of simultaneous equations for a_n are obtained, the general form of any equation being given by:

$$a_n\left\{(n\pi)^4\left(\frac{\beta}{3} - \frac{\alpha}{2}\right) + (n\pi)^2\left(\beta - \frac{1}{2}\right) - \frac{Hl^2}{2EI_v}\right\} - \sum_i a_i \frac{16\beta\pi^2(ni^5)}{(n-i)^2(n+i)^2} = R_n \qquad (4)$$

$$\alpha = \frac{Hh_t}{pl^2}\ ;\ \beta = \frac{Hh_c}{pl^2}\ ;\ R_n = \frac{4}{(n\pi)^3}\left[4\beta w_t - \frac{w}{2}\right] - \frac{2\alpha w_t}{(n\pi)}$$

$$n = 1, 3, 5 \cdots$$

i may have any odd integral value except n, depending upon the number of terms assumed in (2). For three terms in (2) the set of simultaneous equations obtained is the following:

$$a_1\left\{(\pi\cdot1)^4\left(\frac{\beta}{3} - \frac{\alpha}{2}\right) + (\pi\cdot1)^2\left(\beta - \frac{1}{2}\right) - \frac{Hl^2}{2EI_v}\right\} - a_3\frac{16\beta\pi^2(1\cdot3^5)}{(1-3)^2(1+3)^2}$$
$$- a_5\frac{16\beta\pi^2(1\cdot5^5)}{(1-5)^2(1+5)^2} = \frac{4}{\pi^3}\left[4\beta w_t - \frac{w}{2}\right] - \frac{2\alpha w_t}{\pi} \qquad (5a)$$

$$- a_1\frac{16\beta\pi^2(3\cdot1^5)}{(3-1)^2(3+1)^2} + a_3\left\{(3\pi)^4\left(\frac{\beta}{3} - \frac{\alpha}{2}\right) + (3\pi)^2\left(\beta - \frac{1}{2}\right) - \frac{Hl^2}{2EI_v}\right\}$$
$$- a_5\frac{16\beta\pi^2(3\cdot5^5)}{(3-5)^2(3+5)^2} = \frac{4}{(3\pi)^3}\left[4\beta w_t - \frac{w}{2}\right] - \frac{2\alpha w_t}{3\pi} \qquad (5b)$$

$$- a_1\frac{16\beta\pi^2(5\cdot1^5)}{(5-1)^2(5+1)^2} - a_3\frac{16\beta\pi^2(5\cdot3^5)}{(5-3)^2(5+3)^2} + a_5\left\{(5\pi)^4\left(\frac{\beta}{3} - \frac{\alpha}{2}\right) + (5\pi)^2\left(\beta - \frac{1}{2}\right) - \frac{Hl^2}{2EI_v}\right\} =$$
$$\frac{4}{(5\pi)^3}\left[4\beta w_t - \frac{w}{2}\right] - \frac{2\alpha w_t}{5\pi} \qquad (5c)$$

The parameters in terms of which a_n can be expressed by simultaneous solution of (4) are defined by

$$\alpha = \frac{Hh_t}{pl^2}\ ;\ \beta = \frac{Hh_c}{pl^2}\ ;\ \gamma = \frac{Hl^2}{2EI_v}.$$

The right hand members of (4) are in terms of α, β, ω_t, ω_c. For any given set of values of α, β, ω_t, ω_c the simultaneous solution of (5) gives numerical values of the coefficients a_n. Thus when applied to Proposed Design No. 2 as given in [1] with the following physical characteristics:

$l = 4000$ feet	$w_t = 1150$ lbs. per ft.
$h_c = 509$ feet	$w_c = 150$ lbs. per ft.
$h_t = 519$ feet	$w = 1300$ lbs. per ft.
$p = 22$ kips/ft	$H = 110{,}000$ kips (due to p+c)
$E = 29{,}000$ kips/in.^{2}	$I_v = 1{,}620{,}000$ in.^{2}ft^2

$C = 6$ kips/ft.

the dimensionless parameters

$$\alpha = \frac{110{,}000 \times 519}{22 \times 4000^2} = 0.1622$$

$$\beta = \frac{110{,}000 \times 509}{22 \times 4000^2} = 0.1591$$

$$\gamma = \frac{110{,}000 \times 4000^2}{2 \times 29{,}000 \times 1{,}620{,}000} = 18.73$$

$$\frac{\alpha}{\beta} = \frac{h_t}{h_c} = 1.02$$

The numerical values of a_n for a five term series (2) are:

$a_1 = 0.003{,}883{,}558$ kips/ft.

$a_3 = 0.000{,}117{,}131$ "

$a_5 = 0.000{,}002{,}242{,}01$ "

$a_7 = 0.000{,}001{,}091{,}31$ "

$a_9 = 0.000{,}000{,}398{,}1$ "

Moment and deflection curves are shown in Figures 3 and 4.

The parameter of greatest influence is defined by

$$\lambda = \frac{Hl^2}{2\pi^2 E I_v} = \frac{\gamma}{\pi^2} \qquad (6)$$

For given values of α and β, for example $\alpha = 0.162$ and $\beta = 0.159$, and with the relation $\omega_t = 0.9\,\omega$ the simultaneous equations for a_n reduce to those shown in Table I, where n = 1, 2, 5, 7 and 9 and λ is taken as the variable. Solving these equations for various values of λ the coefficients k_0, k_1, k_2, and k_3 are given in Figures 5, 6, 7, and 8. Table II gives a compilation of such coefficients for representative spans. Practically, the shape of the (λ, k) curves are independent of α, β, ω_t, and ω_c values. For moderately long spans values of the coefficients from Figures 5 to 8, inclusive, are sufficiently accurate for design purposes regardless of the actual α, β, ω_t, and ω_c values, since actual values of α, β, ω_t/ω_c are confined within narrow limits of variation. For $\lambda = 0$ the (λ, k) curves pass thru the points $k_0 = 5/384$; $k_1 = 0.125$; $k_2 = 3/32$; and $k_3 = 0.5$. For large values of λ the values of k_1 may change sign from plus to minus.

Oscillations in the Horizontal Plane

Small vibrations in the horizontal plane about the position of equilibrium are described by means of the following differential equation:

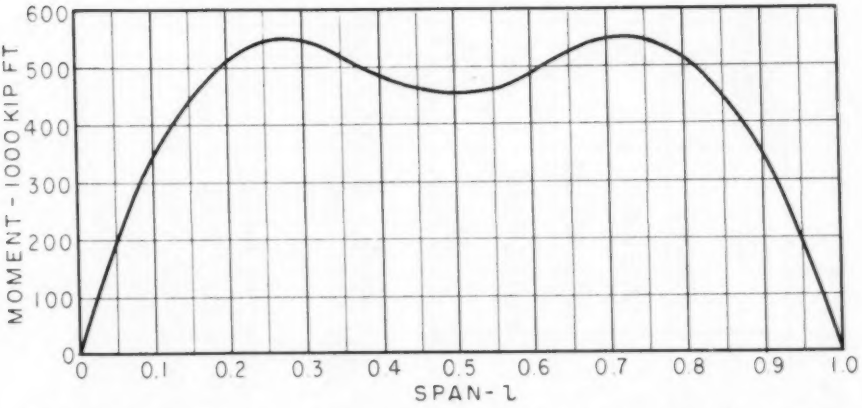

BENDING MOMENT IN WIND TRUSS - UNIFORM LOAD
FIG. 3

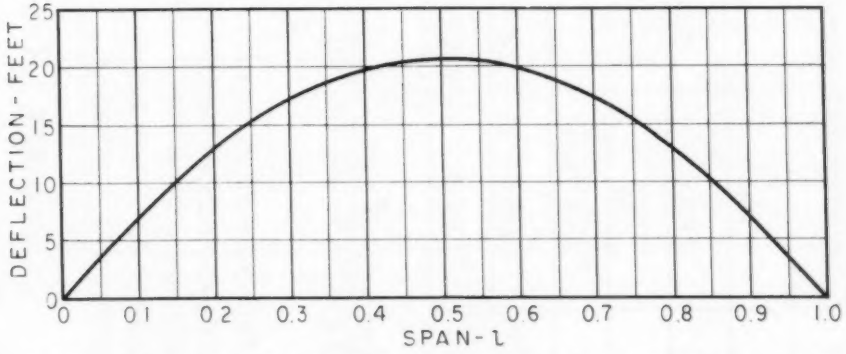

DEFLECTION(v) OF WIND TRUSS - UNIFORM LOAD
FIG. 4

TABLE I: NUMERICAL COEFFICIENTS FOR EQS. (4).

Eq. \ a_n	a_1	a_3	a_5	a_7	a_9	RIGHT HAND MEMBER
1	D_1	243.0	347.22°	466.861°	590.49	$\bar{R}_1$
2	3.0	D_3	2343.75	2016.84	2187.0	$\bar{R}_3$
3	0.55°	303.75	D_5	9337.2°	6025.408163	$\bar{R}_5$
4	0.194°	68.04	2430.55°	D_7	25,833.9375	$\bar{R}_7$
5	0.09	27.0	573.979,591,837	9453.9375	D_9	$\bar{R}_9$

$$D_n = -\frac{4n^2}{\beta}\left\{(n\pi)^2\left(\frac{\beta}{3}-\frac{\alpha}{2}\right)+\left(\beta-\frac{1}{2}\right)\right\}+\frac{4}{\beta}\lambda \; ; \; R.H.M.=\bar{R}_n=\frac{4}{\beta\pi^2}\left[\frac{2\alpha w_t}{(n\pi)}-\frac{4}{(n\pi)^3}\left(4\beta w_t-\frac{w_t}{2}\right)\right]$$

$D_1 = 15.541,532 + 25.147743\lambda$
$D_3 = 641.544,454 + 25.147743\lambda$
$D_5 = 4569.134,291 + 25.147743\lambda$
$D_7 = 17,174.619,119 + 25.147743\lambda$
$D_9 = 46,409.239,37 + 25.147743\lambda$

$\bar{R}_1 = 0.239,738,409\, w_t$
$\bar{R}_3 = 0.086,830,390\, w_t$
$\bar{R}_5 = 0.052,430,279\, w_t$
$\bar{R}_7 = 0.037,515,562\, w_t$
$\bar{R}_9 = 0.029,199,979\, w_t$

$\alpha = 0.1622$; $\beta = 0.1591$; $w_t = 0.9w$

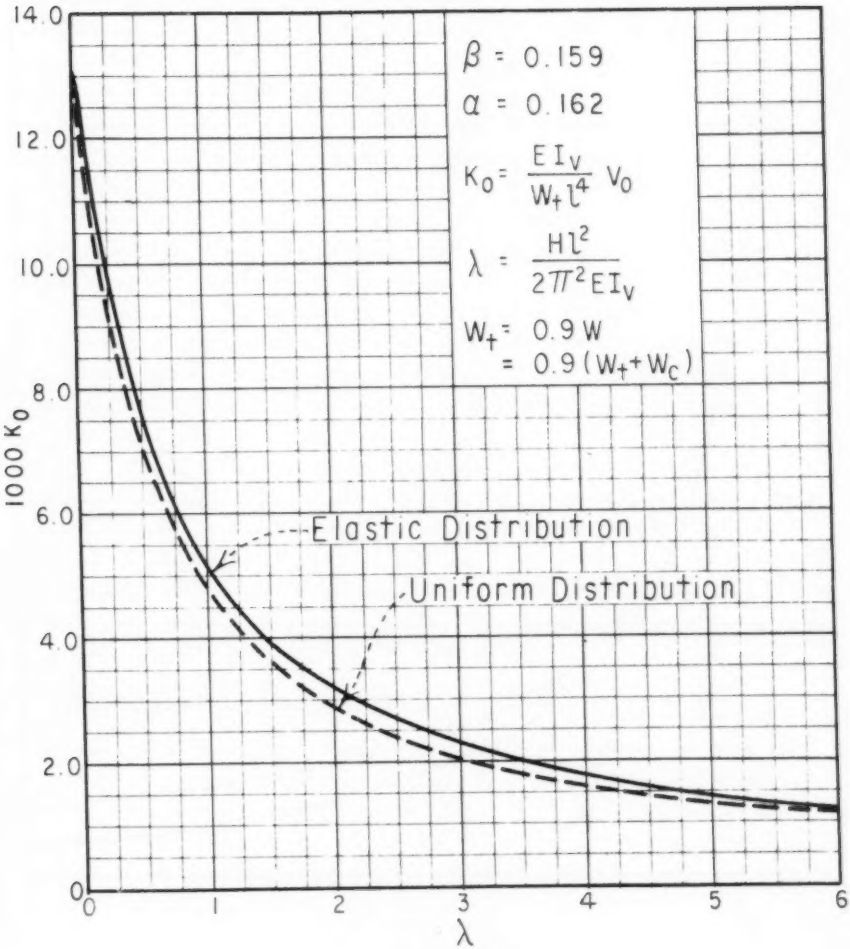
β = 0.159
α = 0.162
$K_0 = \frac{EI_v}{W_t l^4} V_0$
$\lambda = \frac{Hl^2}{2\pi^2 EI_v}$
$W_t = 0.9W$
$= 0.9(W_t + W_c)$
Elastic Distribution
Uniform Distribution
1000 K_0
λ
14.0
12.0
10.0
8.0
6.0
4.0
2.0
0
0
1
2
3
4
5
6

FIG. 5

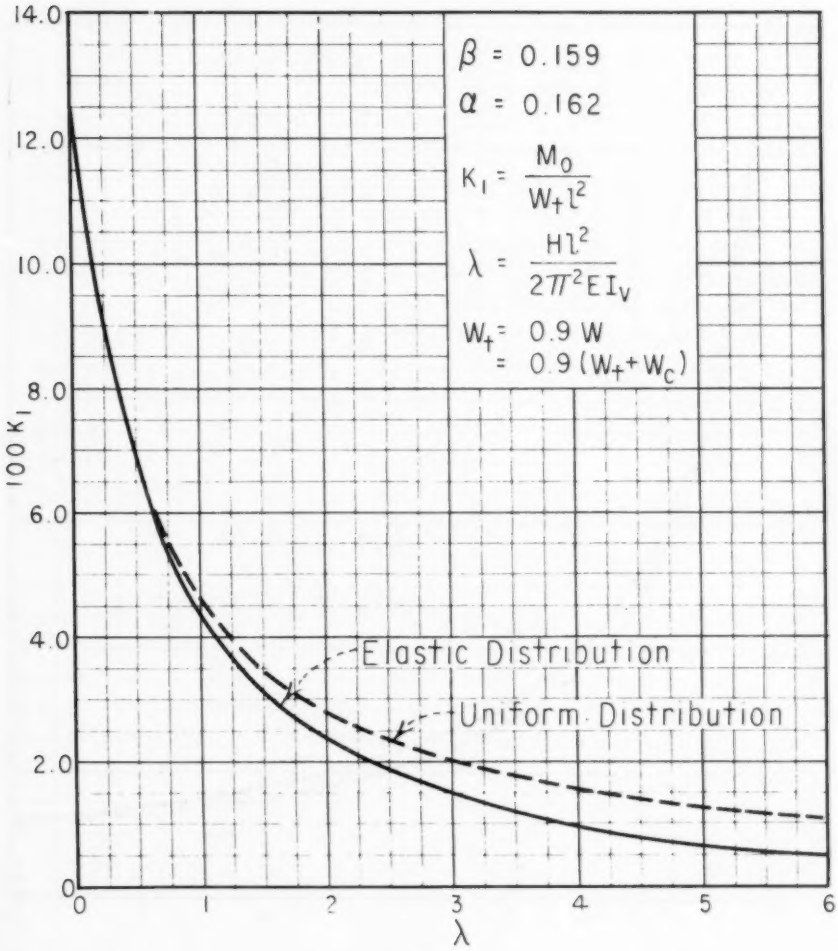
β = 0.159
α = 0.162
K1 = M0 / W+l2
λ = Hl2 / 2π2EIv
W+ = 0.9 W
= 0.9 (W+ + Wc)
Elastic Distribution
Uniform Distribution
100 K1
λ
14.0
12.0
10.0
8.0
6.0
4.0
2.0
0
0
1
2
3
4
5
6

FIG. 6

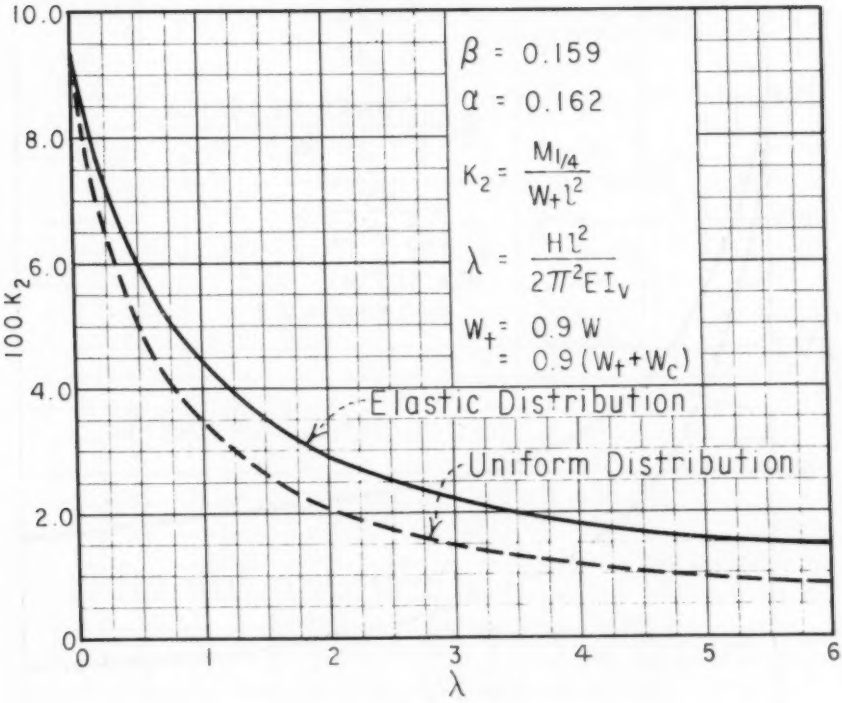
10.0
8.0
6.0
4.0
2.0
0
100 K2
0
1
2
3
4
5
6
λ
β = 0.159
α = 0.162
K2 = M1/4 / W+l2
λ = Hl2 / 2π2EIv
W+ = 0.9 W
= 0.9 (W+ + Wc)
Elastic Distribution
Uniform Distribution

FIG. 7

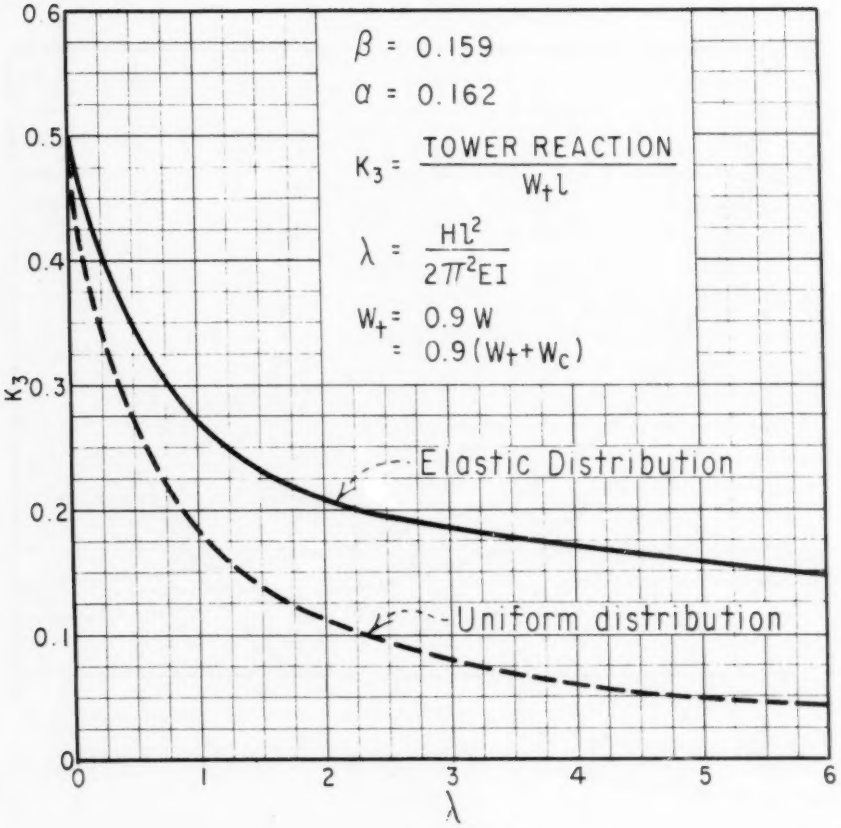
β = 0.159
α = 0.162
K3 = TOWER REACTION / Wt l
λ = Hl² / 2π²EI
Wt = 0.9 W
= 0.9 (Wt + Wc)
Elastic Distribution
Uniform distribution
K3
λ
0 6
0.5
0.4
0.3
0.2
0.1
0
0
1
2
3
4
5
6

FIG. 8

TABLE II: DEFLECTION, MOMENT, AND SHEAR COEFFICIENTS
REPRESENTATIVE SPANS

Bridge	Center Span (feet)	H (pounds)	Mom. of Inertia Wind Truss (I_w) ($in^2 ft^2$)	λ	$1000K_0$	$100K_1$	$100K_2$	K_3
Golden Gate	4200	118.3×10^6 (b)	1,236,000	2.95	2.35	1.52	2.3	0.19
Washington (double deck)	3500	195×10^6 (b)	903,000	4.62	1.75	0.75	1.68	0.16
Tacoma Narrows (1940)	2800	24×10^6 (a)	95,000	3.46	2.02	1.2	2.03	0.18
Transbay	2310	54.3×10^6 (a)	743,000	0.68	6.5	5.7	5.3	0.32
Bronx-Whitestone	2300	36.4×10^6 (a)	410,000	0.821	5.85	5.05	4.9	0.3
Detroit	1840	25.8×10^6 (a)	304,000	0.503	7.75	6.85	5.95	0.35
Manhattan	1470	63.8×10^6 (b)	1,580,000	0.153	10.7	9.8	7.7	0.42

(a) Dead Load Only

(b) Dead+Live + Temp.

$$L \equiv EI_v v^{IV} - \frac{p}{h}\frac{EI_v}{H} v'' + \frac{pv}{h} + m\ddot{v} = 0 \qquad (7)$$

where $\ddot{v} = \frac{d^2v}{dt^2}$

and m = mass of suspended structure per unit of length = p/g. Assuming modes of vibration of the form

$$v = a_n \sin \frac{n\pi x}{l} \sin \omega_n t$$

where ω_n = circular frequency

the requirement that

$$\int_0^t L\,\delta v = 0$$

leads to the following expression for

$$\omega_n^2 = \frac{\left(\frac{n\pi}{l}\right)^2 EI_v \left[\frac{1}{2} + \frac{1}{n^2}\frac{Hl^2}{2\pi^2 EI_v} + \frac{H}{p}\left(\frac{n\pi}{l}\right)^2 \left\{\left(\frac{h_t}{2} - h_c\left(\frac{1}{3} + \frac{1}{n^2\pi^2}\right)\right)\right\}\right]}{\frac{H}{p} m\left[\frac{h_t}{2} - h_c\left(\frac{1}{3} + \frac{1}{n^2\pi^2}\right)\right]}$$

$$= \frac{H}{ml^2}\left[\frac{1}{\chi}\left(8 + \frac{4n^2}{\lambda}\right)\left(\frac{p}{p+c}\right) + \frac{\pi^2 n^4}{2\lambda}\right]$$

$$\chi = \left(\frac{h_t}{h_c} - \frac{2}{3} - \frac{2}{n^2\pi^2}\right); \quad H = \frac{1}{8}\frac{(p+c)l^2}{h_c}$$

c = total weight of cables per ft. of bridge

The spring constant defined as $m\omega_n^2$ becomes

$$K = m\omega_n^2 = \frac{H}{l^2}\left[\frac{1}{\chi}\left(8 + \frac{4n^2}{\lambda}\right)\left(\frac{p}{p+c}\right) + \frac{\pi^2 n^4}{2\lambda}\right]$$

The natural frequency is given by

$$N = \frac{\omega_n}{2\pi} = \frac{1}{2\pi}\sqrt{\frac{K}{m}} = \frac{1}{2\pi}\sqrt{\frac{K}{p}g}$$

Using a value of χ = 0.15 which corresponds to a value of $\frac{h_t}{h_c}$ = 1.02 and n = 1 the natural frequencies for representative bridges are given in Table III.

TABLE III: NATURAL FREQUENCIES - REPRESENTATIVE SPANS ($n=1$)

Bridge	Center Span (feet)	Wt. of suspended Span (p) (lb. per ft.)	Wt. of cables (c) (lb. per ft.)	p + c (lb. per ft.)	H (Dead load) (lbs.)	Mom. of Inertia Wind Truss (I_v) ($in.^2 ft^2$)	λ	K (lb/ft^3)	N c.p.m.
Golden Gate	4200	15,370	5,660	21,035	97.7×10^6	1,236,000	2.45	270	7.2
Washington (single deck)	3500	20,710	10,880	31,590	151.8×10^6	481,000	6.76	463	8.1
Tacoma Narrows (1940)	2800	4,400	1,300	5,700	24×10^6	95,000	3.46	148	9.9
Transbay	2310	15,170	3,570	18,740	54.3×10^6	743,000	0.68	837	12.7
Bronx-Whitestone	2300	8,950	2,050	11,000	36.4×10^6	410,000	0.82	522	13.1
Detroit	1840	10,800	1,600	12,400	25.8×10^6	304,000	0.503	778	14.5

APPENDIX A

a_n = coefficients of Fourier Series

c = weight of all cables per foot of bridge

g = acceleration due to gravity

h_c = sag of cable (Figure 1)

h_t = sag of cable plus length of hanger at midspan (Figure 1)

h = length of hanger at distance X from end of span (Figure 1)

k_0 = coefficient of deflection at span center (Figure 5)

$$= \frac{E I_v}{\omega_t l^4} v_0$$

k_1 = coefficient of moment at span center (Figure 6)

$$= \frac{M_0}{\omega_t l^2}$$

k_2 = coefficient of moment at quarter point (Figure 7)

$$= \frac{M_{1/4}}{\omega_t l^2}$$

k_3 = coefficient of tower reaction at truss level (Figure 8)

$$= \frac{V}{\omega_t l}$$

l = length of center suspended span (Figure 1)

m = mass of suspended span per unit of length

p = total vertical load carried by hangers per foot of bridge

q = $\omega_t - z$

t = time variable

u = deflection of cable at distance X from end of span (Figure 2)

v = deflection of lateral wind truss at distance X from end of span (Figure 2)

ω = $\omega_t + \omega_c$

ω_c = horizontal wind pressure on cables per foot of bridge

ω_t = horizontal wind pressure on suspended structure per foot of bridge

X = distance measured from end of span (Figure 1)

y = vertical distance from top of tower to cable at distance (Figure 1)

z = force of restitution due to inclination of hangers per foot of bridge

E = modulus of elasticity = 29,000,000 lbs. per sq. in.

H = horizontal component of pull of all cables due to vertical loads. The increase in H due to wind loads is neglected.

I_v = equivalent moment of inertia of lateral wind truss

K = spring constant for horizontal oscillations

M_w = bending moment in wind truss, simply supported, due to wind loading

α = dimensionless parameter = $\frac{Hh_t}{pl^2}$

β = dimensionless parameter = $\frac{Hh_c}{pl^2}$

γ = dimensionless parameter = $\frac{Hl^2}{2EI_v}$

λ = dimensionless parameter = $\frac{Hl^2}{2\pi^2 EI_v} = \frac{\gamma}{\pi^2}$

ω_n = circular frequency

$\chi = \left(\frac{h_t}{h_c} - \frac{2}{3} - \frac{2}{n^2\pi^2}\right)$

APPENDIX B—BIBLIOGRAPHY

1. "Suspension Bridges Under the Action of Lateral Forces," Moisseiff and Lienhard, Trans. Am. Soc. C. E. 1933, p. 1080.

2. Ibid, p. 1109.

3. "Stationarer Winddruck auf Hangebrucken," B. Topaloff, Der Stahlbau, May 1954, p, 109.

4. "Lateral Bending of Suspension Bridges," C. A. Erzen, Separate No. 663, Proceedings Am. Soc. C. E.

5. "Eine Wichtige Vereinfachung der Methode von Ritz zur angenaherten Behandlung von Variationsproblemen," H. Hencky, Zeitschrift fur angew. Mathematik und Mechanik, Vol. 7, 1927, p. 80.

6. Discussion to "On the Method of Complementary Energy," by H. M. Westergaard, Trans. Am. Soc. C. E., 1942, p. 798 and 799.

Paper 1293 EM 3

Journal of the
ENGINEERING MECHANICS DIVISION
Proceedings of the American Society of Civil Engineers

BUCKLING OF PLATES UNDER NON-HOMOGENEOUS STRESS

P. P. Bijlaard,* M. ASCE
(Proc. Paper 1293)

SUMMARY

Plastic buckling stresses are calculated for long plates, clamped at their unloaded edges and subject to longitudinal bending or eccentric compression in their plane. As in the author's earlier work on simply supported plates to this end the governing partial differential equation is reduced to ordinary finite-difference equations, using second-order differences. The plastic buckling stresses of clamped and hinged flanges are calculated by the energy method. For clamped and hinged flanges also the elastic buckling stresses are calculated. Simple design formulas and graphs are presented for the plastic reduction factors with which the buckling stresses for the associated elastic cases have to be multiplied for obtaining the plastic buckling stresses.

INTRODUCTION

This paper is sequential to reference 1, where, after some discussion of the basic principles of the author's theory of plastic buckling of plates,(2, 3, 4) the plastic buckling stresses were computed for long simply supported plates under eccentric compression or bending in their plane. The same method, using second-order finite difference equations, is used in the present paper for calculating the plastic buckling stresses of long clamped plates under the same loadings. It was shown in reference 1 that the resulting plastic reduction factor η is practically not influenced by the shape of the stress-strain curve and depends mainly on the maximum edge stress and edge strain. Therefore, as the most convenient way to calculate η , only material with a stress strain diagram as applies for mild steel was considered. (As to the actual applicability of the theory to mild steel and other metals the reader is referred to the "Conclusions.")

For computing the plastic buckling stresses of long clamped flanges an

Note: Discussion open until December 1, 1957. Paper 1293 is part of the copyrighted Journal of the Engineering Mechanics Division of the American Society of Civil Engineers, Vol. 83, No. EM 3, July, 1957.

* Prof. of Structural Eng., Cornell Univ., Ithaca, N. Y.

energy method was used, expressing the variation of the buckling deflections in the lateral direction in terms of the normal modes of vibration of a clamped-free beam, as was done earlier for computing elastic buckling stresses in references 6 and 7. Since for the elastic range the present equations reduce to another form than used in reference 7 for calculating the elastic buckling stresses of clamped flanges, also the elastic buckling stresses were computed for this case. The plastic buckling stresses for hinged flanges were computed by the energy method as well as by a more simple method, comparing deflecting and restraining moments with respect to the hinged edge, acting upon an elementary strip bdx, where b is the flange width and x is measured in the longitudinal direction.

Long Clamped Plate Subjected to Longitudinal Bending or Eccentric Compression in Its Plane

The Finite-Difference Buckling Equations

Dividing the plate (Fig. 1) into imaginary longitudinal strips of width

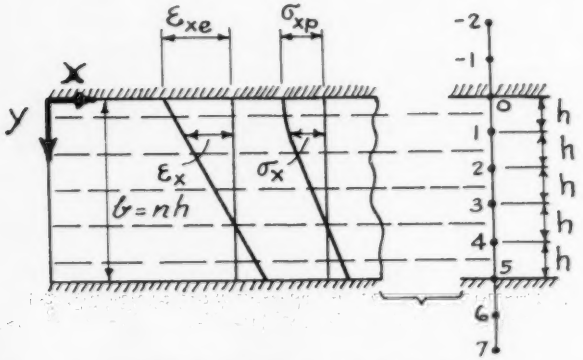

FIG. 1 CLAMPED PLATE SUBJECTED TO ECCENTRIC COMPRESSION IN ITS PLANE

h = b/n, for each of these strips the plasticity parameters A, B, D and F can be considered to be constants, so that for each of the strips the differential equation(2, 3, 4)

$$EI\left[A\frac{\partial^4 w}{\partial x^4} + 2(B+2F)\frac{\partial^4 w}{\partial x^2 \partial y^2} + D\frac{\partial^4 w}{\partial y^4}\right] + t\sigma_x\frac{\partial^2 w}{\partial x^2} = 0 \qquad (1)$$

applies.(1) E is the elastic modulus and $I = t^3/12$, where t is the plate thickness. σ_x is the appropriate compressive stress in the strip. Assuming the buckling deflection as

$$w = Y \sin(\pi x/a) = Y \sin \lambda x \qquad (2)$$

where Y is a function of y alone, and a is the half wave length, this differential equation reduces to the following ordinary finite-difference equation for a pivotal point k (Equation (9) of reference 1):

$$-D_k Y_{k-3} + C_{1k} Y_{k-2} + C_{2k} Y_{k-1} + \left(C_{3k} - 6\lambda^2 h^4 \rho_k \varphi^2\right) Y_k + C_{2k} Y_{k+1} + C_{1k} Y_{k+2} - D_k Y_{k+3} = 0 \qquad (3)$$

where

$$\left.\begin{aligned} C_{1k} &= 12 D_k + (B+2F)_k \lambda^2 h^2 \\ C_{2k} &= -39 D_k - 16 (B+2F)_k \lambda^2 h^2 \\ C_{3k} &= 56 D_k + 30 (B+2F)_k \lambda^2 h^2 + 6 A_k \lambda^4 h^4 \end{aligned}\right\} \qquad (4)$$

$$\varphi^2 = t\sigma_{xp} / EI \qquad (5)$$

$$\rho_k = \sigma_x / \sigma_{xp} \qquad (6)$$

Here σ_{xp} is the maximum edge stress (Fig. 1). The plasticity parameters A_k, B_k, D_k and F_k in a pivotal point k are given by Eq. (22) and (23) of reference 2 or Eq. (21) and (21a) of reference 4. For pure compression, as occurs in all problems considered in the present paper

$$\left.\begin{aligned} A_k &= \left[1 + 3\left(E_t/E_s\right)\right]/\psi \\ B_k &= \left[2 - 2(1-2\nu)\left(E_t/E\right)\right]/\psi \\ D_k &= 4/\psi \\ F_k &= 1/(2+2\nu+3e) \\ \psi &= (5-4\nu+3e) - (1-2\nu)^2 \left(E_t/E\right) \\ e &= \left(E/E_s\right) - 1 \end{aligned}\right\} \qquad (A)$$

where ν is Poisson's ratio. These values can also be read directly from charts in reference 5, as functions of the tangent and secant modulus ratios E_t/E and E_S/E, belonging to σ_x at the pivotal point. However, as shown in reference 1, to take account of the variation in the Y-direction of ρ_k, C_{1k}, C_{2k}, and C_{3k}, instead of their values at the pivotal points, their statically equivalent concentrated values at these points were used, as determined by Eq. (12) and (13) of reference 1.

With n = b/h = 5 (Fig. 1), assuming imaginary points outside the plate, Eq. (3) can be written down for the points 1, 2, 3, and 4 in Fig. 1, resulting

in the four linear homogeneous equations (14) of reference 1. For the present case with clamped edges the boundary conditions are (Fig. 1)

$$Y_{-2} = Y_2;\ Y_{-1} = Y_1;\ Y_0 = 0;\ Y_5 = 0;\ Y_6 = Y_4;\ Y_7 = Y_3$$

Inserting this into the four linear homogeneous equations they contain only the unknown deflections Y_1, Y_2, Y_3 and Y_4 and can yield deflections differing from zero only if the determinant of the system is zero. This leads to

$$\begin{vmatrix} C_{11}+C_{31}-6\lambda^2 h_1^4 \rho \varphi^2 & C_{21}-D_1 & C_{11} & -D_1 \\ C_{22}-D_2 & C_{32}-6\lambda^2 h_2^4 \rho \varphi^2 & C_{22} & C_{12} \\ C_{13} & C_{23} & C_{33}-6\lambda^2 h_3^4 \rho \varphi^2 & C_{23}-D_3 \\ -D_4 & C_{14} & C_{34}-D_4 & C_{14}+C_{34}-6\lambda^2 h_4^4 \rho \varphi^2 \end{vmatrix} = 0 \quad (7)$$

Assuming a ratio a/b, the only unknown is this determinant is the product $\epsilon 2_b 2$. With

$$\sigma_{xp} = k_p \frac{\pi^2 N}{b^2 t} \quad (8)$$

where N is the flexural rigidity of the plate, from Eq. (18) of reference 1,

$$k_p = \varphi^2 b^2 / 10.856 \quad (9)$$

Numerical Results

To save space only the determinant for n = 5 was presented here. Actually, like in reference 1, $\epsilon\, 2_b 2$ was solved from eighth order determinants, obtained by assuming n = b/h = 9. Expressing the strains ϵ_x (Fig. 1) as

$$\varepsilon_x = \varepsilon_{xc}\left[1-(\alpha y/b)\right] \quad (10)$$

and assuming a stress-strain diagram like that of mild steel, k_p was computed for the case $\alpha = 2$ (pure bending) with $(E_s/E)_e = 0.6$ at the upper edge (Fig. 2b) and for $\alpha = 1$, where σ_x is zero at the lower edge, with $(E_s/E)_e = 0.5$ at the upper edge (Fig. 2c). In both cases E_t/E is zero at the upper edge. Choosing several half wave lengths, the minimum buckling stress coefficients k_p and the optimum half wave length a were found. They are given in Table 1. The plastic reduction coefficients η are found as $\eta = k_p/k_e$, where k_e is the buckling stress coefficient for the associated elastic case, that is the case with the same strain distribution from Eq. (10) as the plastic case. Hence for the associated elastic case

$$\sigma_x = \sigma_{xe}\left[1-(\alpha y/b)\right] \quad (11)$$

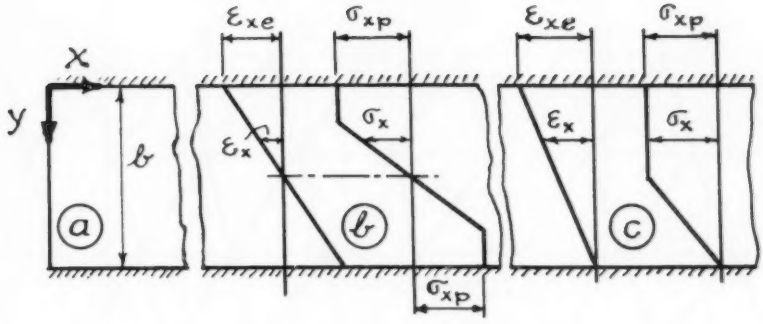

FIG. 2 CLAMPED PLATE SUBJECTED TO BENDING OR ECCENTRIC COMPRESSION IN ITS PLANE

where σ_{xe} is the edge stress at the upper edge. The coefficients k_e for $\alpha = 2$ and $\alpha = 1$ from references 6 and 7 are 39.6 and 13.56, respectively. For the two cases in Table 1 this gives $\eta = 22.3/39.6 = 0.563$ and $\eta = 5.95/13.56 = 0.439$, respectively, as also shown in Table 1.

Table 1. Results of Calculations

α	$(E_s/E)_e$	$(a/b)_{opt}$	k_p	η	η [13]
2	0.6	0.435	22.3	0.563	0.552
1	0.5	0.60	5.95	0.439	0.435

For $\alpha = 0$, that is, for pure compression, from Table 5 of reference 4, the plastic reduction factor is

$$\eta_o = 0.598\sqrt{AD} + 0.312(B + 2F) \qquad (12)$$

Charts for the plastic reduction factors η_0 for various cases of homogeneous compression were made at the Bell Aircraft Corporation and were partly published in reference 9. Fig. 3 gives η_0 from Eq. (12) for the present case of a clamped plate as presented in reference 5. Since for this case η_0 is smaller than for a plate with simply supported edges, also, for example, for the case $\alpha = 2$ it was found that η is slightly smaller than $(E_s/E)_e$, while for the same case for a simply supported plate, in reference 1, η was found about equal to $(E_s/E)_e$.

This applies for a diagram like that of mild steel. If, as another extreme, a hypothetical diagram like that of Fig. 4 is assumed, where $E_t/E = E_s/E$, it may be seen from Eqs. (21) and (21a) of reference 4 or more directly from the charts of reference 5 that A, B + 2F and D become a little more than E_s/E times their elastic values $1/(1-\nu^2)$. Hence for any loading and boundary conditions the plastic reduction factor is a little more than E_s/E. Therefore in

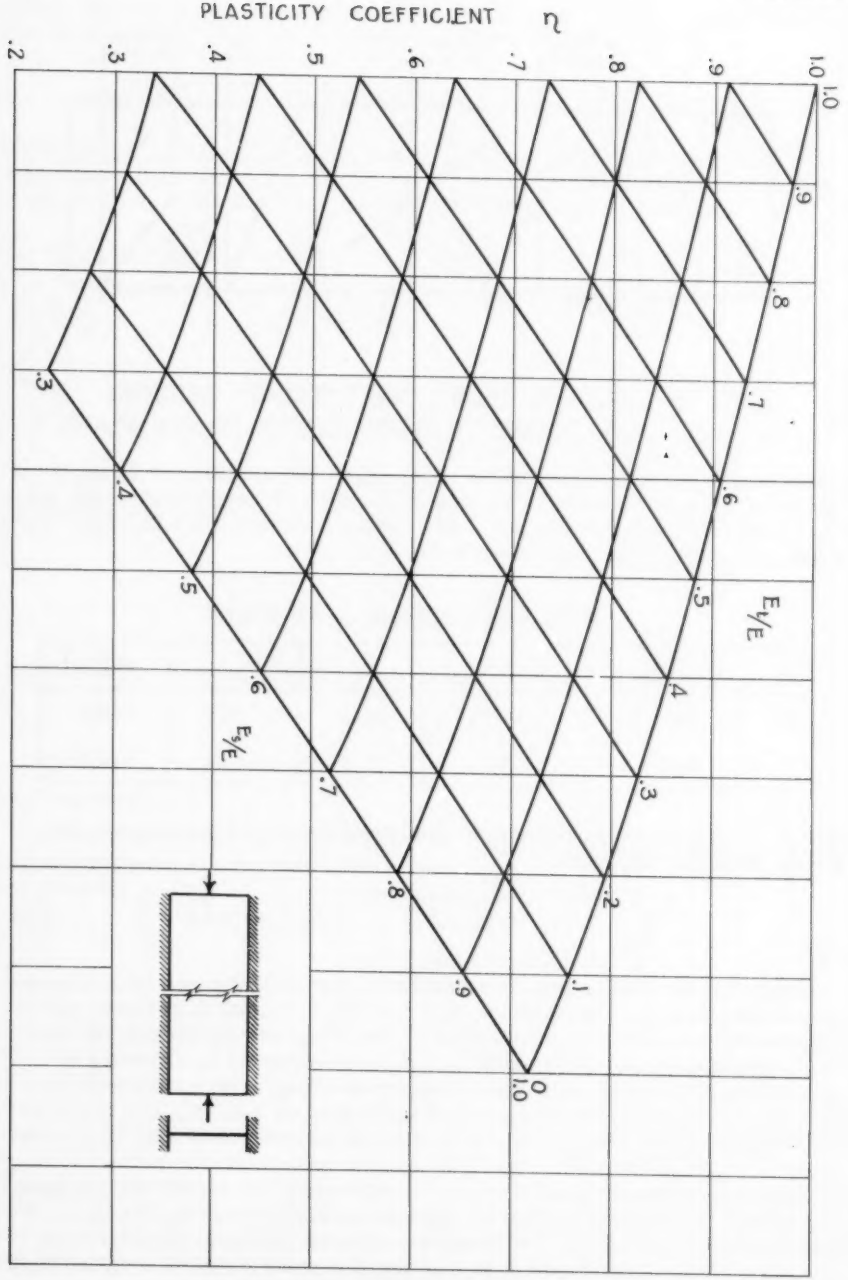

FIG. 3 PLASTIC REDUCTION FACTOR η FOR A CLAMPED PLATE UNDER HOMOGENEOUS COMPRESSION, AS A FUNCTION OF E_s/E and E_t/E

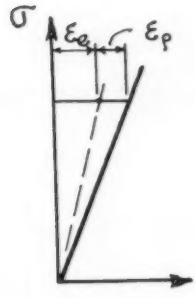

FIG. 4 HYPOTHETICAL STRESS-STRAIN DIAGRAM WHERE $E_s/E = E_t/E$

the present case, for all values of α, η would be somewhat more than E_s/E. Also η_0 crom Eq. (12) would be somewhat more than E_s/E, as is seen directly from Fig. 3.

Design Formula

To take all these circumstances into account the plastic reduction factor for any stress-strain diagram and values α between zero and two may be calculated sufficiently accurately from the formula

$$\eta = \sigma_{xp}/\sigma_{xe} = k_p/k_e = 0.46\alpha(E_s/E)_e + (1-0.46\alpha)(\eta_0)_e \qquad (13)$$

$(E_s/E)_e$ and $(\eta_0)_e$ refer to the upper edge of the plate, where the compressive stress is highest. η_0 is given by Eq. (12) and can be read from Fig. 3 for E_s/E and E_t/E at the upper edge. η from Eq. (13) is given in Table 1 as η (13), for comparison with the computed η values. For $\alpha = 0$, for any stress strain curve, Eq. (13) yields $\eta = (\eta_0)_e$, as given by Eq. (12).

The plastic buckling stress coefficient k_p is equal to ηk_e, where k_e refers to the associated elastic case, having the same strain distribution (α) as the actual plastic case. For convenience k_e from references 10 and 11 is given graphically in Fig. 5.

Long Clamped Flange Subjected to Longitudinal Bending or Eccentric Compression in Its Plane

Derivation of Buckling Condition

This case is most conveniently solved by an energy method, expressing the variation of the deflection in the Y-direction (Fig. 6) in the normal modes of vibration of a clamped-free beam, as was done in reference 6 for clamped plates and in reference 7 for clamped flanges, both for elastic buckling. Hence the buckling deflection

$$w = X \sum_{m=1}^{\infty} a_m Y_m \qquad (14)$$

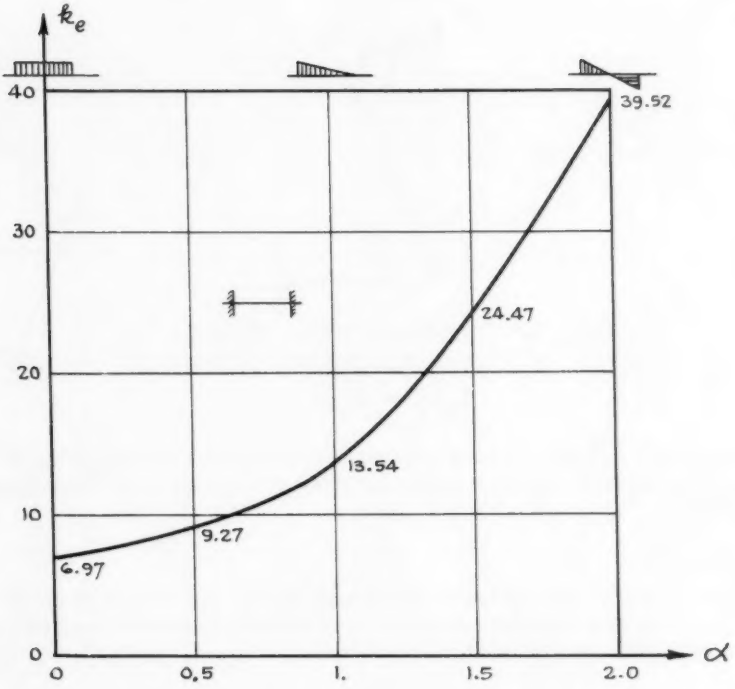

FIG. 5 ELASTIC BUCKLING STRESS COEFFICIENT k_e FOR A CLAMPED PLATE UNDER VARIOUS LOADINGS

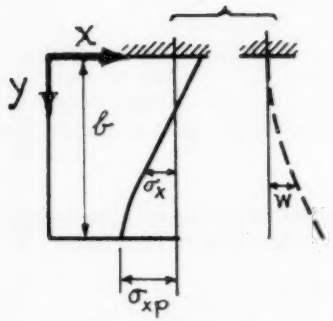

FIG. 6 STRESSES BEFORE BUCKLING AND DEFLECTION AT INCIPIENT BUCKLING FOR CLAMPED FLANGE

with

$$X = \sin(\pi x/a) = \sin \lambda x \tag{15}$$

where a is the half wave length. From references 7 and 12, imposing the condition that

$$\int_0^b Y_m^2 \, dy = b \tag{16}$$

where b is the flange width (Fig. 6),

$$Y_m = \cos(p_m y/b) - \cosh(p_m y/b) - C_m \left[\sin(p_m y/b) - \sinh(p_m y/b)\right] \tag{17}$$

with

$$C_m = \frac{\cos p_m + \cosh p_m}{\sin p_m + \sinh p_m} \tag{18}$$

Here p_m has to satisfy the condition

$$\cos p_m \cosh p_m + 1 = 0 \tag{19}$$

As was expected, also in the plastic range this series converges very satisfactory, so that only three terms are needed in Eq. (14).

In the elastic range, from the principle of virtual displacements, at incipient buckling the energy

$$U = \text{constant} + V_i - V_e \tag{20}$$

reaches an extreme value. If in here V_i and V_e are the work done during buckling by the internal stresses and by the external forces, respectively, this remains true for plastic buckling. This is evident if one considers that the relative decrease of the buckling stress in the plastic range is due to the decrease of the secant and tangent moduli, but is not influenced by the fact that the plastic deformations are not reversible, since nowhere reversal of stress occurs. In other words, the plate behaves as an elastic plate with the same decreased rigidities as the plastic one, so that the principle of virtual displacements remains valid.

From Eq. (59) of reference 13 the work done by the internal stresses during buckling is

$$V_i = \tfrac{1}{2} EI \iint \left[A\left(\frac{\partial^2 w}{\partial x^2}\right)^2 + 2B \frac{\partial^2 w}{\partial x^2} \frac{\partial^2 w}{\partial y^2} + D\left(\frac{\partial^2 w}{\partial y^2}\right)^2 + 4F\left(\frac{\partial^2 w}{\partial x \partial y}\right)^2 \right] dx\,dy \tag{21}$$

where A, B, D and F are the plasticity parameters mentioned in the foregoing. The external work during buckling is, considering compressive stresses as positive,

$$V_e = \tfrac{1}{2} t \iint \sigma_x \left(\frac{\partial w}{\partial x}\right)^2 dx\,dy \tag{22}$$

where σ_x is a function of y (Fig. 6). From Eq. (14), (20), (21) and (22), for a plate length a

$$U = \tfrac{1}{2} \int_0^a \int_0^b \Big\{ EI\Big[AX''^2 (\Sigma a_m Y_m)^2 + 2BXX'' \sum_1^m \sum_1^n a_m a_n Y_m Y_n'' + DX^2 (\Sigma a_m Y_m'')^2 + 4FX'^2 (\Sigma a_m Y_m')^2\Big] - t\sigma_x X'^2 (\Sigma a_m Y_m)^2 \Big\}\, dx\,dy \tag{23}$$

where a prime and a dot mean differentiation with respect to x or y, respectively. Since U should reach an extreme value, a_1, a_2, etc. should be chosen such that

$$\partial U / \partial a_i = 0 \tag{24}$$

where i = 1, 2, etc. This leads to equations of the general form

$$\int_0^a \int_0^b \Big\{ EI\Big[AX''^2 Y_i \Sigma a_m Y_m + BXX''(Y_i'' \Sigma a_m Y_m + Y_i \Sigma a_n Y_n'') + DX^2 Y_i'' \Sigma a_m Y_m'' + 4FX'^2 Y_i' \Sigma a_m Y_m'\Big] - t\sigma_x X'^2 Y_i \Sigma a_m Y_m \Big\}\, dx\,dy = 0 \tag{25}$$

Integration of this equation in the X-direction gives, after division by a/2 and denoting all term numbers of the sums by m again

$$EI \int_0^b \Big[A\lambda^4 Y_i \Sigma a_m Y_m - B\lambda^2 (Y_i'' \Sigma a_m Y_m + Y_i \Sigma a_m Y_m'') + DY_i'' \Sigma a_m Y_m'' + 4F\lambda^2 Y_i' \Sigma a_m Y_m'\Big]\, dy - t\lambda^2 \int_0^b \sigma_x Y_i \Sigma a_m Y_m\, dy = 0 \tag{26}$$

Case 1

First the case of pure bending of a flange in its plane is considered (Case 1), assuming a stress-strain diagram as that of mild steel and a stress distribution as shown in Fig. 7a, where at both edges $E_S = 0.5\ E$. Here in the plastic parts $\sigma_x = \pm\ \sigma_{xp}$ and in the elastic parts $\sigma_x = \sigma_{xp}\ [-2 + (4y/b)]$, so that in Eq. (26)

$$\int_0^b \sigma_x Y_i \sum a_m Y_m\, dy = \sigma_{xp}\left\{-\int_0^{\frac{1}{4}b} Y_i \sum a_m Y_m + \int_0^b Y_i \sum a_m Y_m + \int_{\frac{1}{4}b}^{\frac{3}{4}b} \left[-2 + (4y/b)\right] Y_i \sum a_m Y_m \right\} dy$$

$$= \sigma_{xp}\left[-2\int_0^b Y_i \sum a_m Y_m + \int_0^{\frac{1}{4}b} Y_i \sum a_m Y_m + 3\int_{\frac{1}{4}b}^b Y_i \sum a_m Y_m + \frac{4}{b}\int_{\frac{1}{4}b}^{\frac{3}{4}b} y\, Y_i \sum a_m Y_m\right] dy \qquad (27)$$

The normal modes Y_m are orthogonal functions, so that, if $i \neq m$,

$$\int_0^b Y_i Y_m\, dy = 0 \qquad (28)$$

Dividing in Eq. (26) the expression to the left by $\lambda^2 \pi^2\ EI/b^2$ one obtains, using Eqs. (8), (16), (27) and (28),

$$\int_0^b \psi_i\, dy - k_p \phi_i / (1-\nu^2) = 0 \qquad (29)$$

where ν is Poisson's ratio and

$$\psi_i = \left(\frac{1}{\beta^2}\right) A Y_i \sum a_m Y_m - \left(b^2/\pi^2\right)\left[B\left(\ddot{Y}_i \sum a_m Y_m + Y_i \sum a_m \ddot{Y}_m\right) - 4F \dot{Y}_i \sum a_m \dot{Y}_m\right] + \left(\beta^2 b^4/\pi^4\right) D \ddot{Y}_i \sum a_m \ddot{Y}_m \qquad (30)$$

$$\phi_i = -2a_i b + \left[\int_0^{\frac{1}{4}b} Y_i \sum a_m Y_m + 3\int_{\frac{3}{4}b}^b Y_i \sum a_m Y_m + \left(\frac{4}{b}\right)\int_{\frac{1}{4}b}^{\frac{3}{4}b} y\, Y_i \sum a_m Y_m\right] dy \qquad (31)$$

$$\beta = \frac{a}{b} \qquad (32)$$

The first term of Eq. (29) can be more conviently written as

$$\int_0^b \psi_i \, dy = \int_0^b \psi_{ei} \, dy - \int_0^{\frac{1}{4}b} (\psi_e - \psi_p)_i \, dy - \int_{\frac{3}{4}b}^b (\psi_e - \psi_p)_i \, dy \qquad (33)$$

where the subscripts e and p refer to elastic and plastic, respectively. For elastic deformation, where $E_s = E_t = E$, with $\nu = 0.3$: $A = D = 1/(1 - \nu^2) = 1.099$, $B = \nu/(1 - \nu^2) = 0.329$ and $F = 1/(2 + 2\nu) = 0.385$.
Hence

$$\int_0^b \psi_{ei} \, dy = \left[(1.099/\beta^2) a_i - 0.1645 \left(\Sigma a_m J_{mi} + \Sigma a_m J_{im} \right) + 0.77 \Sigma a_m R_{mi} + 1.099 \beta^2 a_i S_i \right] b \qquad (34)$$

where

$$\left. \begin{aligned} J_{mi} &= \frac{2b}{\pi^2} \int_0^b Y_m Y_i'' \, dy \quad ; \quad R_{mi} = \frac{2b}{\pi^2} \int_0^b Y_m' Y_i' \, dy \\ S_{mi} &= \frac{b^3}{\pi^4 a_i} \Sigma \int_0^b a_m Y_m'' Y_i'' \, dy \end{aligned} \right\} \qquad (35)$$

J_{mi} and R_{mi} have been calculated in reference 7, from which, for $m \neq i$,

$$J_{mi} = \frac{8 p_i^2}{\pi^2 (p_i^4 - p_m^4)} \left\{ (p_i C_i - p_m C_m) \left[p_i^2 (-1)^{m+1} + p_m^2 \right] \right\} \qquad (36)$$

$$R_{mi} = \frac{8 p_i C_i}{\pi^2} (-1)^{m+1} - J_{mi} \qquad (37)$$

and for $m = i$

$$J_{ii} = \frac{2}{\pi^2} \left(2 p_i C_i - p_i^2 C_i^2 \right) \qquad (38)$$

$$R_{ii} = \frac{8 p_i C_i}{\pi^2} - J_{ii} \qquad (39)$$

The expression S_i can be calculated by integration by parts. One obtains, since at $y = 0$, $Y = Y' = 0$ and at $y = b$, $y'' = Y''' = 0$,

$$\int_0^b Y_m'' Y_i'' \, dy = \int_0^b Y_m'''' Y_i \, dy = (p_m/b)^4 \int_0^b Y_m Y_i \, dy$$

Hence, in connection with Eq. (16) and (28), from Eq. (35),

$$S_i = (p_m/\pi)^4 \tag{40}$$

Using three terms of the series in Eq. (14), from Eqs. (18) and (19)

$$\left.\begin{aligned} p_1 &= 1.85710 \;;\; p_2 = 4.69474 \;;\; p_3 = 7.85476 \\ C_1 &= 0.73410 \;;\; C_2 = 1.01845 \;;\; C_3 = 0.999224 \end{aligned}\right\} \tag{41}$$

and from Eq. (36) = (39)

$$\begin{aligned} J_{11} &= 0.17391 \;;\; J_{12} = -2.38018 \;;\; J_{13} = 5.56315; \\ J_{21} &= 0.37969 \;;\; J_{22} = -2.69482 \;;\; J_{23} = -1.83184; \\ J_{31} &= 0.31703 \;;\; J_{32} = 0.65440 \;;\; J_{33} = -9.27126 \\ R_{11} &= 0.94184 \;;\; R_{12} = R_{21} = -1.49543 \;;\; R_{13} = R_{31} = 0.79871; \\ R_{22} &= 6.57043 \;;\; R_{23} = R_{32} = -4.53002 \;;\; R_{33} = 15.63312 \end{aligned} \tag{42}$$

Choosing values for β, the right hand side of Eq. (34) can then be calculated in terms of a_1, a_2 and a_3, for m = 1, 2 and 3 and i = 1, 2 and 3. The second and third integral to the right in Eq. (33), containing the plasticity parameters A, B, D and F, that vary with y, were evaluated by Simpson's rule, dividing the plate width b into 8 equal spacings (Fig. 7a). A, B, D and F in the point

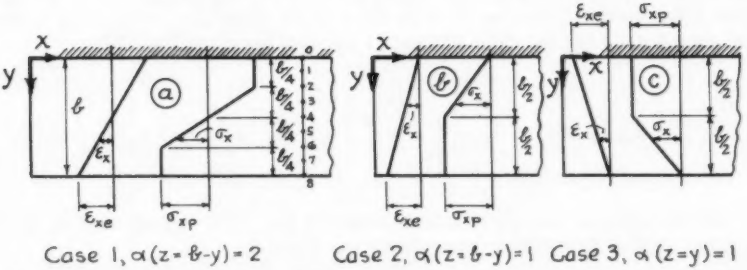

FIG. 7 CLAMPED FLANGE SUBJECTED TO BENDING OR ECCENTRIC COMPRESSION IN ITS PLANE

0, 1, 2, 6, 7 and 8 follow from Eqs. (21) and (21a) of reference 4 or can be read from the charts in reference 5 as functions of E_s/E and E_t/E. In all these points $E_t = 0$ and E_s/E is 0.5 for points 0 and 8, 2/3 for points 1 and 7 and 1 for points 2 and 6. The ordinates Y_i and Y_m in the points 0 to 8 follow from Eq. (17); their derivatives are obtained by simple differentiations.

The integrals in Eq. (31) lead to rather extensive expressions, so that it was more convenient and accurate to evaluate them too by Simpson's rule, especially since the Y_m values for points 3, 4 and 5 had to be calculated anyway for evaluating the first term in Eq. (29) for the next Cases 2 and 3.

Hence Eq. (29), for chosen values of β, leads to 3 homogeneous linear equations in the 3 unknown coefficients a_1, a_2 and a_3. Equating the denominator determinant of these equations to zero, k_p is the only unknown and can be solved from a cubic equation (Approximation III). The convergence of the

solution can be checked by assuming as a first and second approximation $a_2 = a_3 = 0$ and $a_3 = 0$, respectively (Approximations I and II).

Table 2. Values $k_p/(1-\nu^2)$ for Case 1

β	$k_p/(1-\nu^2)$		
	I	II	III
1.3	1.224	1.223	1.216
1.4	1.214	1.212	1.205
1.5	1.215	1.211	1.205
1.6	1.226	1.221	1.213

Table 2 shows that the convergence is very satisfactory. $k_p = 0.91\ (1.20) =$ 1.092 at the optimum half wave length a = 1.45b.

Case 2

Similar calculation were made for eccentric compression with a stress distribution as shown in Fig. 7b, where at the free edge $E_s/E = 0.5$ and $E_t = 0$. Eq. (26) also applies here, but now in the plastic range $\sigma_x = \sigma_{xp}$ and in the elastic range $\sigma_x = (2y/b)\,\sigma_{xp}$, so that in the last term of Eq. (26)

$$\int_0^b \sigma_x Y_i \sum a_m Y_m \, dy = \sigma_{xp}\left[\frac{2}{b}\int_0^{\frac{1}{2}b} y\, Y_i \sum a_m Y_m + \int_{\frac{1}{2}b}^{b} Y_i \left[\sum a_m Y_m\right] dy\right] \qquad (43)$$

Hence, in Eq. (29), where ψ_i remains given by Eq. (30), except that A, B, D and F have values that differ from those for Case 1.

$$\phi_i = \left[\left(\frac{2}{b}\right)\int_0^{\frac{1}{2}b} y\, Y_i \sum a_m Y_m + \int_{\frac{1}{2}b}^{b} Y_i \sum a_m Y_m\right] dy \qquad (44)$$

Further, instead of Eq. (33),

$$\int_0^b \psi_i \, dy = \int_0^b \psi_{ei} \, dy - \int_{\frac{1}{2}b}^{b} (\psi_e - \psi_p)_i \, dy \qquad (45)$$

The first integral to the right is given by Eq. (34). All other integrals were calculated by Simpson's rule. Eq. (29) yields the results given in Table 3.

Table 3. Values $k_p/(1-\nu^2)$ for Case 2

β	$k_p/(1-\nu^2)$		
	I	II	III
1.00	0.838	0.838	0.835
1.10	0.828	0.828	0.812
1.20	0.831	0.831	0.828

Hence $k_p = 0.91\ (0.81) = \underline{0.737}$ at the optimum half wave length of about $a = \underline{1.11b}$.

Case 3

For this case the assumed stress distribution is shown in Fig. 7c. Here at the clamped edge $E_s/E = 0.5$. In a similar way as in the other cases one finds that in Eq. (29), where ψ_i remains given by Eq. (30),

$$\phi_i = 2a_i b - \left[\int_0^{\frac{1}{2}b} Y_i \sum a_m Y_m - \left(\frac{1}{b}\right)\int_{\frac{1}{2}b}^{b} y\, Y_i \sum a_m Y_m\right] dy \qquad (46)$$

Further, instead of Eq. (33),

$$\int_0^b \Psi_i\, dy = \int_0^b \Psi_{ci}\, dy - \int_0^{\frac{1}{2}b} (\Psi_c - \Psi_p)_i\, dy \qquad (47)$$

The results for this case are given in Table 4.

Table 4. Values $k_p/(1-\nu^2)$ for Case 3

β	$k_p/(1-\nu^2)$		
	I	II	III
1.6	3.350	2.702	2.701
1.7	3.305	2.695	2.695
1.8	3.286	2.706	2.706

This gives $k_p = 0.91(2.695) = \underline{2.452}$ at the optimum half wave length $a = \underline{1.7b}$.

Elastic Buckling Stresses for the Associated Cases 1a, 2a, and 3a

In order to express the strain distribution in Cases 1, 2 and 3 by a uniform formula it is convenient to write

$$\varepsilon_x = \varepsilon_{xe}\left[1-(\alpha z/b)\right] \tag{48}$$

where ϵ_{xe} is the maximum edge strain, occurring at one of the edges, and z is the distance from that edge. Hence, from Fig. 7, for Cases 1 and 2, z = b-y and for Case 3, z = y. Further for Cases 1, 2 and 3, α is 2, 1 and 1, respectively. For the associated elastic Cases 1a, 2a and 3a

$$\sigma_x = \sigma_{xe}\left[1-(\alpha z/b)\right] \tag{49}$$

Using Eqs. (14) - (20) the elastic buckling stresses for Cases 1a, 2a and 3a were calculated in reference 7. However, these calculations are partly based on Eq. (19) of that reference, which, to the present writer's opinion, does not apply for the present boundary conditions. Therefore these elastic buckling stresses were calculated by reducing the formulas, used in the foregoing for calculating the plastic buckling stresses, to the elastic range. For Case 1a, with z = b-y and $\alpha = 2$,

$$\sigma_x = \sigma_{xe}\left[-1+(2y/b)\right] \tag{50}$$

and in Eq. (26), in connection with Eqs. (16) and (28),

$$\int_0^b \sigma_x Y_i \Sigma a_m Y_m \, dy = \sigma_{xe}\left(-a_i + 2\Sigma a_m H_{mi}\right) b \tag{51}$$

where

$$H_{mi} = \frac{1}{b^2}\int_0^b y Y_m Y_i \, dy \tag{52}$$

From references 7, for $m \neq i$,

$$H_{mi} = \frac{8 p_m p_i}{(p_m^4 - p_i^4)^2} C_m C_i \left[-2 p_m^2 p_i^2 + (p_m^4 + p_i^4)(-1)^{m+1}\right] \tag{53}$$

and for m = i,

$$H_{ii} = \frac{1}{2} + \frac{2 C_i^2}{p_i^2} \tag{54}$$

from which

$$H_{11} = 0.80654 \; ; \; H_{12} = H_{21} = -0.15343 \; ; \; H_{13} = H_{31} = 0.02032;$$
$$H_{22} = 0.59412 \; ; \; H23 = H_{32} = -0.19090 \; ; \; H_{33} = 0.53239 \tag{55}$$

Eq. (29) now becomes

$$\int_0^b \psi_{oi}\, dy - k_e \phi_i / (1-\nu^2) = 0 \tag{56}$$

where k_e is determined by

$$\sigma_{xe} = k_e \frac{\pi^2 N}{b^2 t} \tag{57}$$

The first term in Eq. (56) is given by Eq. (34) and from Eqs. (26), (51) and (56)

$$\phi_i = (-a_i + 2 \Sigma a_m H_{mi})\, b \tag{58}$$

Hence Eq. (56) can be evaluated. The results are given in Table 5.

Table 5. Values $k_e/(1-\nu^2)$ for Case 1a

β	$k_e/(1-\nu^2)$		
	I	II	III
1.57	2.378	2.377	2.374
1.6	2.372	2.371	2.369
1.63	2.367	2.366	2.3640
1.7	2.367	2.366	2.3641

This gives $k_e = 0.91\ (2.362) = \underline{2.149}$ at an optimum half wave length a = 1.66b. As may be easily verified, for Case 2a, with z = b-y and $\alpha = 1$, in Eq. (56)

$$\phi_i = b \sum a_m H_{mi} \tag{59}$$

which leads to the results given in Table 6.

Table 6. Value $k_e/(1-\nu^2)$ for Case 2a

β	$k_e/(1-\nu^2)$		
	I	II	III
1.6	1.803	1.784	1.7816
1.63	1.800	1.781	1.7789
1.7	1.799	1.782	1.7798

Hence $k_e = 0.91\ (1.778) = \underline{1.618}$ for a = 1.66b.

For Case 3a, with z = y and $\alpha = 1$, in Eq. (56)

$$\phi_i = \left(a_i - \Sigma\, a_m H_{mi}\right) b \qquad (60)$$

The results for Case 3a are given in Table 7.

Table 7. Value $k_e/(1-\nu^2)$ for Case 3a

β	$k_e/(1-\nu^2)$		
	I	II	III
1.5	7.600	6.850	6.570
1.57	7.535	6.536	6.517
1.6	7.518	6.546	6.529
1.63	7.502	6.580	6.556
1.7	7.502	6.609	

This gives $k_e = 0.91\ (6.517) = \underline{5.930}$ at a = 1.57b.

Design Formula

The values k_p and k_e, calculated for Cases 1, 2 and 3 and their associated elastic cases 1a, 2a and 3a, respectively, are assembled in Table 8. For all cases, at the most loaded edge $(E_s/E)_e = 0.5$ and $E_t/E = 0$ (Fig. 7). The resulting plastic reduction factors $\eta = k_p/k_e$ are given in the sixth column. Also η for homogeneous compression ($\alpha = 0$) is listed. It is calculated as the ratio σ_B/σ_E from Table 5 of reference 4, using Eq. (21) and (21a) of that reference or can be read directly from a chart in reference 5, for $E_s/E = 0.5$ and $E_t/E = 0$. This chart is given here as Fig. 8.

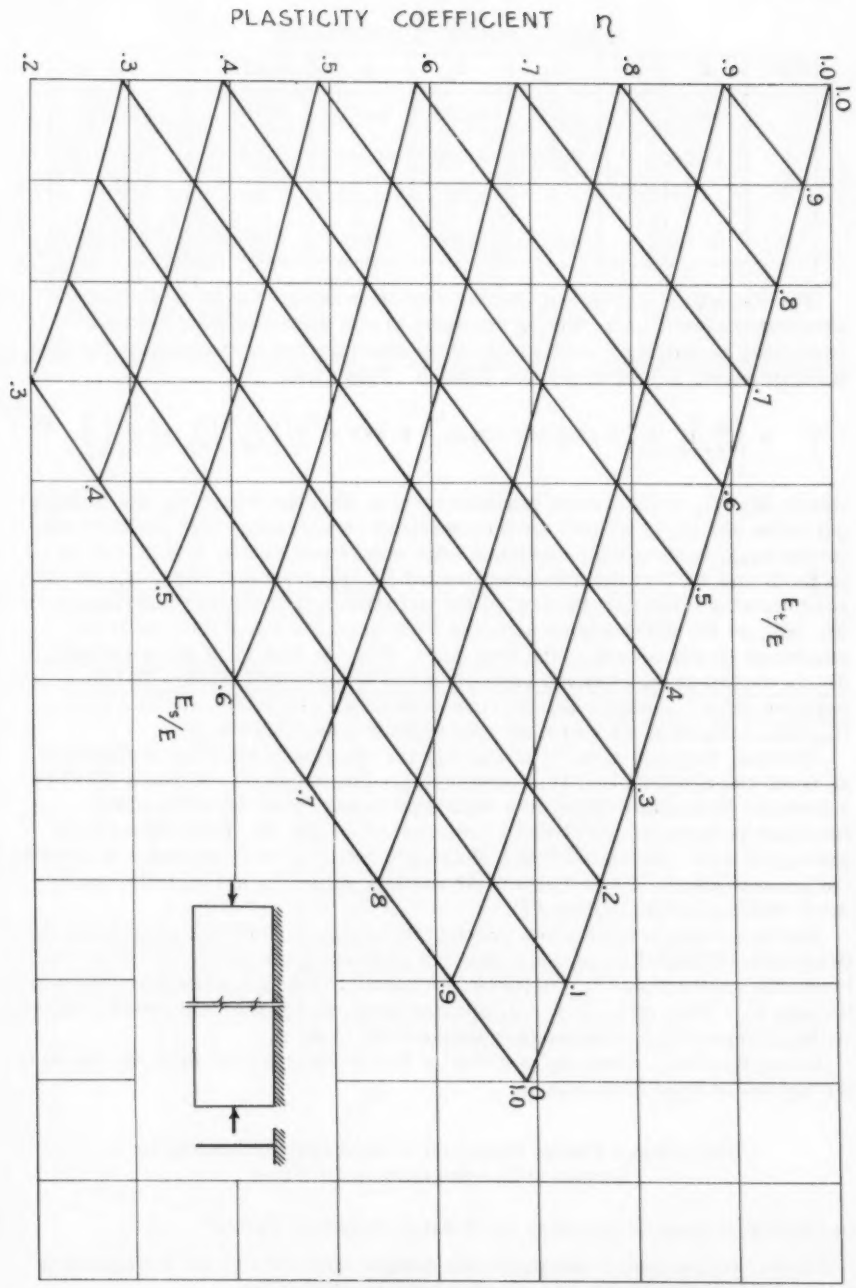

FIG. 8 PLASTIC REDUCTION FACTOR η FOR A CLAMPED FLANGE UNDER HOMOGENEOUS COMPRESSION, AS A FUNCTION OF E_s/E and E_t/E

Table 8. Results of Computations

Case	z	α	k_p	k_e	η	$k_e(7)$	$k_e(11)$
1	b-y	2	1.092	2.149	0.51	2.142	2.134
2	b-y	1	0.737	1.618	0.455	1.636	1.608
		0		1.28	0.333	1.28	1.28
3	y	1	2.452	5.930	0.414	6.259	5.905

For any value of α in Eq. (48) the reduction factor η with respect to the associated elastic case, having the same strain distribution as the plastic case, may be assumed to be given by the third degree curve passing through the four known values of η from Table 8. This gives

$$\eta = (\eta_o)_e + (0.37\alpha + 0.575\alpha^2 - 0.255\alpha^3)\left[(E_s/E)_e - (\eta_o)_e\right] \quad (61)$$

where $(E_s/E)_e$ is the secant modulus ratio at the edge where σ_x has its highest value and $(\eta_0)_e$ applies for homogeneous compression with a stress and strain equal to the actual maximum edge stress and strain, that is, belonging to E_s/E and E_t/E at the maximum loaded (in compression) edge. η_0 can be read directly from Fig. 8. For α, the parameter of the strain distribution in Eq. (48), in Eq. (61) the plus sign has to be used if z = b-y, that is, if the maximum strain occurs at the free edge. If z = y, that is, if the maximum strain occurs at the clamped edge, α has to be inserted into Eq. (61) as a negative value. Actually Eq. (61) has been chosen such that, for $\alpha = 2$, $\eta = (E_s/E)_e$, instead of 2% more, as would follow from Table 8.

Further, in Table 8, $k_e(7)$ and $k_e(11)$ are the elastic buckling coefficients k_e from references 7 and 11, respectively. The values in reference 11 were calculated from finite-difference equations based on the equation of the funicular polygon, as developed in references 14 and 10. Both values $k_e(7)$ and $k_e(11)$ were calculated with a Poisson's ratio $\nu = 0.3$, as was also used in the present paper. From Table 8 the present values k_e are in better agreement with $k_e(11)$ than with $k_e(7)$.

For convenience k_e is given graphically in Fig. 9. No data is available between α(z = y) equal to zero and one, but in drawing the pertinent curve between the known points it was taken into account that its continuation should go through $k_e = 0$ for α(z = b-y) = 1, because there k_e for the compressive stress at the clamped edge, where α(z = y) refers to, is zero.

Hence $k_p = \eta k_e$, where k_e is given by Fig. 9 and η by Eq. (61). In the latter η_0 can be read from Fig. 8.

Long Hinged Flange Subjected to Longitudinal Bending or Eccentric Compression in Its Plane

Derivation of Explicit Formula for Plastic Reduction Factor

Similar to the case of homogeneous compression ($\alpha = 0$) for a long flange it is sufficiently accurate to assume a buckling deflection

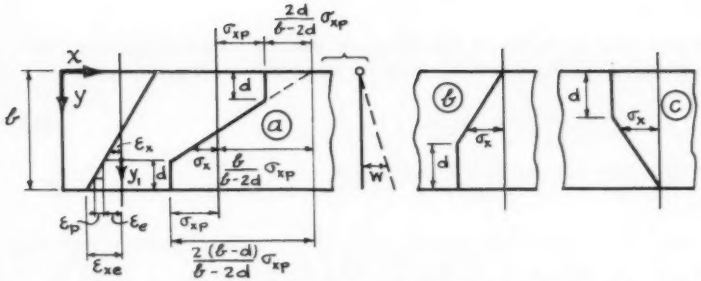

FIG. 10 HINGED FLANGE SUBJECTED TO BENDING OR ECCENTRIC COMPRESSION IN ITS PLANE

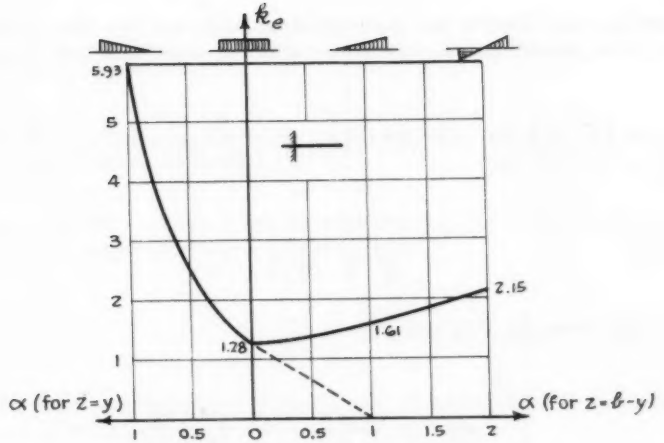

FIG. 9 ELASTIC BUCKLING STRESS COEFFICIENT k_e FOR A CLAMPED FLANGE UNDER VARIOUS LOADINGS

$$\omega = Ky \sin(\pi x/a) \tag{62}$$

Using the condition that at incipient buckling the work V_i done by the internal stresses must be equal to the work V_e done by the external forces, or

$$V_i = V_e \tag{63}$$

from Eqs. (21) and (62), for one half wave length

$$V_i = (\pi^2 K^2 EI/a)\int_0^b F\,dy \tag{64}$$

From Eq. (21) of reference 4

$$F = \frac{1}{2 + 2\nu + 3e} \tag{65}$$

Case 1

Assuming pure bending and a stress strain diagram like that of soft steel (Case 1), with plastic zones of arbitrary width d, from reference 4 and Fig. 10a,

$$e = (E/E_s) - 1 = \varepsilon_p/\varepsilon_e = \frac{y_1}{(\frac{b}{2} - d)} = \frac{2}{1-2\delta} \cdot \frac{y_1}{b} \tag{66}$$

where

$$\delta = d/b \tag{67}$$

With $\nu = 0.3$, from Eq. (65) and (66)

$$\int_0^d F\,dy_1 = \frac{1-2\delta}{6}\, b \ln \frac{13+4\delta}{13(1-2\delta)} \tag{68}$$

In the elastic part, where e = 0, F = 0.385, so that

$$\int_0^b F\,dy = (1-2\delta)\left[0.385 + \frac{1}{3} \ln \frac{13+4\delta}{13(1-2\delta)}\right] b \tag{69}$$

From Eqs. (22) and (62)

$$V_e = (\pi^2/4a)\, K^2 t \int_0^b \sigma_x y^2\,dy \tag{70}$$

From Fig. 10a, in here

$$\int_0^b \sigma_x y^2 dy = -\frac{b}{b-2d}\sigma_{xp}\int_0^b y^2 dy + \frac{2d}{b-2d}\sigma_{xp}\int_0^d y^2 dy + \frac{2}{b-2d}\sigma_{xp}\int_d^{b-d} y^3 dy + \frac{2(b-d)}{b-2d}\sigma_{xp}\int_{b-d}^b y^2 dy$$

$$= \frac{1}{6}\left(1+2\delta-2\delta^2\right) b^3 \sigma_{xp} \tag{71}$$

Inserting V_i and V_e into Eq. (63), it yields, with $EI = (1-\nu^2)N$,

$$\sigma_{xp} = \frac{24(1-\nu^2)(1-2\delta)}{\pi^2(1+2\delta-2\delta^2)}\left[0.385 + \left(\frac{1}{3}\right)\ln\frac{13+4\delta}{13(1-2\delta)}\right]\frac{\pi^2 N}{b^2 t} \tag{72}$$

For the associated elastic case, for which in Eq. (49) z = b-y and $\alpha = 2$ (pure bending), from reference 7,

$$\sigma_{xe} = 0.85\,\frac{\pi^2 N}{b^2 t} \tag{73}$$

so that for this value of α

$$\eta_\alpha = \frac{\sigma_{xp}}{\sigma_{xe}} = \frac{1-2\delta}{1+2\delta-2\delta^2}\left[1+0.867\ln\frac{13+4\delta}{13(1-2\delta)}\right] \tag{74}$$

According to Eq. (66) in here δ can be expressed in the secant modulus ratio $(E_S/E)_e$ at the compressed edge, where $y_1 = d$:

$$\delta = \frac{1}{2}\left[1-(E_s/E)_e\right] \tag{75}$$

The plastic reduction factor η_α from Eq. (74) is given in Table 9 for various ratios $(E_S/E)_e$ in the column marked z = b-y, $\alpha = 2$.

Table 9. Plastic Reduction Factors

$(E_s/E)_e$	z / α	b-y / 2	b-y / 1	0	y / 1
0.875		0.884	0.890	0.860	0.865
0.750		0.768	0.785	0.722	0.705
0.625		0.696	0.726	0.590	0.580
0.500	η_α	0.605	0.645	0.465	0.444
0.375		0.505	0.550	0.342	0.320
0.250		0.390	0.432	0.224	0.210

In contrast with the preceding cases, for pure bending ($\alpha = 2$) η is here greater than $(E_S/E)_e$, especially for small ratios $(E_S/E)_e$. In reference 1 it

was shown, using its Fig. 13, that for a simply supported plate η will be about equal to $(E_s/E)_e$. As explained in the foregoing, for a clamped plate η is a little smaller. For a clamped flange, from Table 8, where for all cases $(E_s/E)_e = 0.5$, η is indeed about equal to $(E_s/E)_e$.

For the present case of a hinged flange, however, the same reasoning is not valid. It is based on the assumption that the shape of the deflection for the plastic case is the same as for the elastic case, so that the restraining forces are reduced in the ratio of about $(E_s/E)_e$. In the present case for both the plastic and the elastic case the deflection may be assumed as Eq. (62), but the deflecting forces depend on the fourth order partial derivatives of the deflection, which, for an infinitely long plate, from Eq. (62) are all zero or infinitely small of higher order. Hence, with the same approximate deflection, the restraining forces in the plastic case may still have a distribution different from $(E_s/E)_e$ times those in the elastic case. By considering a strip bdx of the flange (Fig. 11) it is seen that its equilibrium requires that the moment M_{dp}, given by the deflecting forces D about the hinged edge y = 0, must be equal to the difference M_{rp} between the twisting moments at both edges x = const. of the strip. Using Eq. (62), the deflecting forces acting on an element dx dy of the strip are

$$D = -t\sigma_x\left(\partial^2 w/\partial x^2\right)dx\,dy = \left(\pi^2/a^2\right)t\sigma_x K y \sin(\pi x/a)\,dx\,dy = C_1\sigma_x\, y\,dy \tag{76}$$

where C_1 is a constant for the strip considered. Hence the total moment about the hinge is (Fig. 11)

$$M_{dp} = C_1\int_0^b \sigma_x\, y^2\,dy \tag{77}$$

where the integral is given by Eq. (71).
From Eq. (22) of reference 4 the difference between the twisting moments is (Fig. 11)

$$M_{rp} = -\int_0^b \left(\partial M_{xy}/\partial x\right)dx\,dy = -2EI\int_0^b F\left(\partial^3 w/\partial x^2\partial y\right)dx\,dy = C_2\int_0^b F\,dy \tag{78}$$

where the integral is given by Eq. (69). At incipient buckling

$$M_{dp} = M_{rp} \tag{79}$$

Denoting the deflecting and restraining moments in the associated elastic case as M_{de} and M_{re}, since also $M_{de} = M_{re}$,

$$M_{dp} = \frac{M_{rp}}{M_{re}}\,M_{de} \tag{80}$$

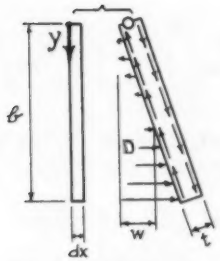

FIG. 11 DEFLECTING AND RESTRAINING FORCES ACTING AT INCIPIENT BUCKLING UPON AN ELEMENT OF A HINGED FLANGE, SUBJECTED TO BENDING IN ITS PLANE

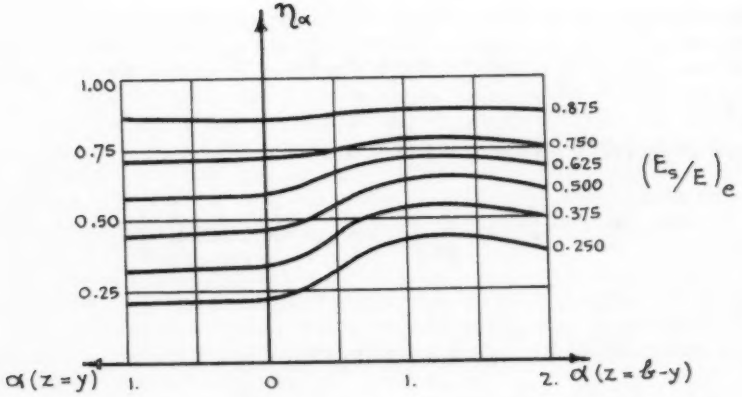

FIG. 12 PLASTIC REDUCTION FACTOR η_α FOR A HINGED FLANGE UNDER VARIOUS LOADINGS, AS A FUNCTION OF E_s/E AT THE EDGE WITH HIGHEST COMPRESSIVE STRAIN

In a similar way as was calculated in Eqs. (71) and (77), in the associated elastic case (pure bending)

$$M_{de}/C_1 = \int_0^b \sigma_x y^2 dy = -\sigma_{xe}\int_0^b y^2 dy + \left(\frac{z}{b}\right)\sigma_{xe}\int_0^b y^3 dy = \left(\frac{1}{6}\right) b^3 \sigma_{xe} \tag{81}$$

where σ_{xe} is the compressive edge stress. In the elastic range, with e = 0, from Eq. (65) F = 0.385, so that, using Eq. (78),

$$M_{re}/C_2 = 0.385\ b \tag{82}$$

Hence in Eq. (80) M_{dp} is given by Eqs. (71) and (77), M_{rp} by Eqs. (69) and (78), M_{de} by Eq. (81) and M_{re} by Eq. (82). Insertion into Eq. (79) leads to the same expression for $\sigma_{xp}/\sigma_{xe} = \eta$ as given by Eq. (74).

In the same way expressions for η were found for Cases 2 and 3.

Case 2

For Case 2, where in Eq. (48) z = b-y and $\alpha = 1$ (Fig. 10b)

$$\eta_\alpha = \frac{3(1-\delta)}{3(1+\delta-\delta^2)+\delta^3}\left[1 + 0.867 \ln \frac{13+2\delta}{13(1-\delta)}\right] \tag{83}$$

where now

$$\delta = d/b = 1-(E_s/E)_e \tag{84}$$

Case 3

Here in Eq. (48) z = y and $\alpha = 1$ (Fig. 10c) and

$$\eta_\alpha = \frac{(1-\delta)^2}{1-\delta^4}\left[1 + 0.867 \ln \frac{13+2\delta}{13(1-\delta)}\right] \tag{85}$$

where

$$\delta = d/b = 1-(E_s/E)_e \tag{86}$$

Values for η_α from Eq. (83) and (84) are given in Table 9 under z = b-y, $\alpha = 1$. Those from Eq. (85) and (86) are shown under z = y, $\alpha = 1$. For homogeneous compression ($\alpha = 0$), from Table 5 of reference 4, $\eta_0 = 2.6$ F, where F is given by the present Eq. (65). In Table 9 values for η_0 are given under $\alpha = 0$. Using the values in Table 9 in Fig. 12 the reduction factor η_α is plotted versus α(z = b-y) and α(z = y) for various ratios $(E_s/E)_e$ at the edge with highest compressive strain. Actually these ratios η_α are valid for the special stress-strain diagram assumed.

As another extreme, let the stress-strain diagram be given by the straight line relation in Fig. 4, in which hypothetical case at any stress the strain consists of an elastic part ϵ_e and a plastic part $\epsilon_p = p\ \epsilon_e$, where p is a constant.

For any stress distribution (Fig. 13) then the ratio $e = \epsilon_p/\epsilon_e = p$ will be equal to that at the maximum compressed edge, so that from Eq. (65) everywhere F will be equal to F_e at that edge. Since in the elastic range $F = 0.385$, this makes the restraining moment M_{rp} in Eq. (78) $F_e/0.385 = 2.6\ F_e$ times that for an elastic flange with the same buckling deflection, so that in Eq. (80) $M_{rp}/M_{re} = 2.6\ F_e$.

The stress distribution for the plastic case is identical to that for the associated elastic case, so that the deflecting moment M_{dp}, as meant in Eq. (77), is σ_{xp}/σ_{xe} times that in the elastic case, σ_{xp} and σ_{xe} being the edge stresses in the plastic and elastic case, respectively. Hence from Eq. (80), for any value α in Eq. (48),

$$\eta = \sigma_{xp}/\sigma_{xe} = 2.6\ F_e \tag{87}$$

where F_e refers to the most compressed edge.

Design Formula

Hence for any actual stress strain diagram, given by the solid curve OPQ in Fig. 14, it seems appropriate to obtain the plastic reduction factor for the maximum compressive edge stress σ_{xp} as

$$\eta = \left(\eta_\alpha A_1 + 2.6 F_e A_2\right)/\left(A_1 + A_2\right) \tag{88}$$

Here A_1 is the area between the actual stress-strain curve OPQ up to the maximum edge stress σ_{xp} and the hypothetical diagram, given by the dashed straight line OQ and A_2 is the area between the actual curve OPQ and the broken dashed line ORQ, which has the same shape as the diagram of soft steel. Further η_α is given by Fig. 12 and F_e is given by Eq. (65), where e is related to E_s/E by Eq. (66). Both η_α and F_e have to be determined for $(E_s/E)_e$ at the most compressed edge. For a diagram like mild steel, $A_2 = 0$, so that Eq. (88) yields $\eta = \eta_\alpha$, as it should. For pure compression ($\alpha = 0$), from Table 5 of reference 4, $\eta_\alpha = \eta_0 = 2.6\ F$, so that from Eq. (88) for any stress strain diagram $\eta = 2.6\ F$, in accordance with Table 5 of reference 4.

The plastic buckling stress coefficient k_p is ηk_e, where the buckling stress coefficient k_e for the associated elastic case is given graphically in Fig. 15. As may be easily calculated in the same way as σ_{xp} was calculated in the foregoing, for cases where the maximum compressive stress occurs at the free edge, that is, where in Eq. (49) $z = b-y$,

$$k_e = \frac{16.8}{\pi^2(4-\alpha)} \tag{89}$$

If the maximum compressive stress occurs at the hinged edge, so that in Eq. (49) $z = y$,

$$k_e = \frac{16.8}{\pi^2(4-3\alpha)} \tag{90}$$

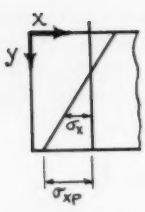

FIG. 13 HINGED FLANGE UNDER ECCENTRIC COMPRESSION IN ITS PLANE, IF $E_s/E = E_t/E$ (FIG. 4)

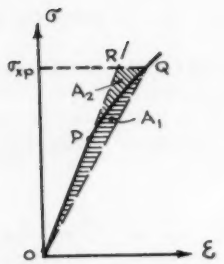

FIG. 14 ARBITRARY STRESS-STRAIN DIAGRAM

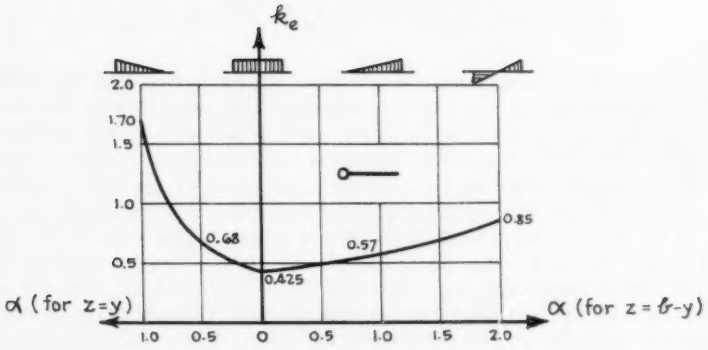

FIG. 15 ELASTIC BUCKLING STRESS COEFFICIENT k_e FOR A HINGED FLANGE UNDER VARIOUS LOADINGS

For α = 1 and 2 Eqs. (89) and (90) yield values k_e that practically agree with those calculated in reference 7.

CONCLUSIONS

As follows from experiments referred to in reference 1, for plates under homogeneous compression the author's theory is in excellent agreement with tests on aluminum alloys. Also for other metals where E_t is always positive, so that no yielding in layers occurs, the same good agreement may be expected. For mild steel that agreement is satisfactory if the stresses are not at the lower yield point, that is, not in the horizontal part of the stress-strain diagram between upper yield point and the strain hardening range. In that region, where $\sigma = \sigma_{ys}$, in the case of homogeneous compression, one can only speak of a critical strain, and from experiments reported in reference 15 the actual critical strain is higher than predicted by the theory, that is, the theory is conservative. This is quite understandable, since it assumes continuous plastic deformation, while at the lower yield point yielding in discrete layers occurs, leaving elastic blocks between them. This, of course, makes the material more rigid than would follow from the theory. This same phenomenon hampers the buckling of columns in this region, as was pointed out in reference 16. Hence the present results may be expected to be accurate for alloys of aluminum, magnesium, titanium, etc. They will also be accurate for steels that do not have a horizontal part in their stress strain diagram and for other steels if the stresses are nowhere at the lower yield point. If the stresses are all or partly at the lower yield point, the present results are conservative.

For all loadings and boundary conditions the plastic buckling stress coefficient in Eq. (8) is given as

$$k_p = \eta k_e \tag{91}$$

For clamped plates and an assumed stress distribution, with maximum edge stress σ_{xp}, k_e refers to the associated elastic case, for which the stress distribution is given by Eq. (11), where α is determined by the strain distribution in the plastic case, as given by Eq. (10). In both Eqs. (10) and (11) y is measured from the edge with the highest compressive stress. k_e can be read from Fig. 5. The plastic reduction factor η is computed from Eq. (13), where $(E_s/E)_e$ and $(\eta_0)_e$ refer to the edge where the maximum compressive stress is acting. η_0 is read from Fig. 3 for E_s/E and E_t/E at that edge. From Eq. (23) of reference 1 the required plate thickness t (without safety factor) is

$$t = 1.05\left(\frac{\sigma_{xp}}{\eta k_e E}\right)^{\frac{1}{2}} b \tag{92}$$

For a clamped flange or a hinged flange the stress distribution in the associated elastic case is given by Eq. (49), with the same α value as occurs in Eq. (48) for the strain distribution in the plastic case, as explained in the text following that equation. For a clamped flange k_e can be read from Fig. 9. The reduction factor η is given by Eq. (61), where $(E_s/E)_e$ and $(\eta_0)_e$ refer to

the edge with maximum compression. η_0 can be read from Fig. 8 for E_s/E and E_t/E at that edge.

k_e for a hinged flange follows from Fig. 15 and η is determined by Eq. (88) as explained in the text following that equation.

For both clamped and hinged flanges the required thickness t is given by Eq. (92).

In reference 17 the case of simply supported plates, under combined shear and eccentric compression in this plane, is dealt with.

ACKNOWLEDGMENT

This investigation was carried out at Cornell University under the sponsorship and with the financial assistance of the Office of Ordnance Research of the U. S. Army. Most of the numerical work was done on a desk calculating machine by Mr. Mohammad Taheri or on I.B.M. machine by Miss. R. B. Lahayne, part of it both ways.

The author wishes to express his thanks and appreciation for the valuable co-operation of all concerned. He also is indebted to the Bell Aircraft Corporation for its permission to present the graphs in Fig. 3 and 8.

BIBLIOGRAPHY

1. "Theory of Plastic Buckling of Plates and Application to Simply Supported Plates Subjected to Bending or Eccentric Compression in Their Plane," by P. P. Bijlaard, ASME Paper No. 55-A-8, Journal of Applied Mechanics, Vol. 23, No. 1, pp. 27-34, March, 1956.

2. "A Theory of Plastic Buckling With Its Application to Geophysics" by P. P. Bijlaard, Proceedings of the Royal Netherlands Academy of Sciences, Amsterdam, Holland, Vol. 41, May 1938, pp. 468-480.

3. "Theory of the Plastic Stability of Thin Plates," by P. P. Bijlaard, Publ. International Association for Bridge and Structural Engineering, Zurich, Switzerland, Vol. 6, 1940-41, pp. 45-69.

4. "Theory and Tests on the Plastic Stability of Plates and Shells," by P. P. Bijlaard, Journal of the Aeronautical Sciences, Vol. 16, September 1949, pp. 529-541.

5. "Plasticity Parameters and Coefficients for Plates and Shells," by A. Krivetsky, Bell Aircraft Corporation Report No. 02-984-019, June 1954.

6. "Biegungsbeulung der Rechteckplatte," by K. Nölke, Ingenieur-Archiv, Vol. 8, 1937, pp. 403-425.

7. "Elastische Beulung von auf einseitigen, ungleichmassigen Druck beanspruchten Platten" and "Reine Biegungsbeulung rechteckiger Platten im elastischen Bereich" by C. F. Kollbrunner and G. Herrmann, Mitteilungen der T.K.V.S.B., Nos. 1 and 2, Verlag A. G. Gebr. Leemann Co., Zurich, Switzerland, 1948-49.

8. "Analysis of the Elastic and Plastic Stability of Sandwich Plates by The Method of Split Rigidities - II," by P. P. Bijlaard, Journal of the Aeronautical Sciences, Vol. 18, December 1951, pp. 790-796, 829.

9. "Plasticity Coefficients for the Plastic Buckling of Plates and Shells," by A. Krivetsky, Journal of the Aeronautical Sciences, Vol. 22, June 1955, pp. 432-435.

10. "Ausbeulen rechteckiger Platten unter Druck, Biegung und Druck mit Biegung" by F. Stussi, C. F. Kollbrunner and H. Wanzenried, Mitteilungen aus dem Institut fur Baustatik a.d. E.T.H., Zurich, Switzerland, No. 26, 1953.

11. "Present Situation in Switzerland with Regard to Experiments on Buckling with Indication of the Buckling Values k," by C. F. Kollbrunner, Fifteenth International Congress of the Steel Information Centres, Brussels, Belgium, October 5-9, 1953.

12. "The Theory of Sound" by Lord Rayleigh, Dover Publications, New York, 1945, Vol. 1, p. 276.

13. "A Theory of Plastic Stability and Its Application to Thin Plates of Structural Steel" by P. P. Bijlaard, Proceedings of the Royal Netherlands Academy of Sciences, Amsterdam, Holland, Vol. 41, September, 1938, pp. 731-743.

14. "Berechnung der Beulspannungen gedruckter Rechteckplatten, by F. Stussi, Publ. International Association for Bridge and Structural Engineering, Zurich, Switzerland, Vol. 8, 1947, pp. 237-248.

15. "Local Buckling of Wide-Flange Shapes," by G. Haaijer and B. Thurlimann, Progress Report X, Fritz Laboratory, Report No. 205E.5, Lehigh University, September 1954.

16. "Exact Computation of the Buckling of the Walls of the Typical Sections Used in Bridge-Building (in Dutch), by P. P. Bijlaard, De Ingenieur in Nederlandsch Indie, Vol. 6, February 1939, pp. I.17-I.23.

17. "Plastic Buckling of Simply Supported Plates Subjected to Combined Shear and Bending or Eccentric Compression in Their Plane," by P. P. Bijlaard, will appear in the Journal of Aeronautical Sciences, 1957.

Journal of the
ENGINEERING MECHANICS DIVISION
Proceedings of the American Society of Civil Engineers

CONTENTS

DISCUSSION
(Proc. Paper 1311)

Discussion of
"SUPPRESSION OF THE FLUID-INDUCED VIBRATION OF CIRCULAR CYLINDERS"

by Peter Price
(Proc. Paper 1030)

PETER PRICE.[1]—The author wishes to thank Mr. Housner for his informative discussion of the response of a stack to intermittent forces. Two points in particular raised by him prompt further discussion. They are: (1) That the stack vibration observations made by him suggest that the flow patterns around actual stacks and around the wind tunnel models may be different, and (2) the influence of damping on the water channel results quoted in the paper.

It is the writer's belief that the observed stack vibration is reconcilable with the wind tunnel results if the level of turbulence in the air streams approaching the stack and the wind tunnel model are kept in mind. The effect of turbulence on the drag coefficient (which reflects the character of flow around the cylinder) has been studied extensively.[2] It has been found that in wind tunnels where the turbulence level is high the critical Reynolds number range may be in the region of 60,000 to 200,000,but may be from 200,000 to 600,000 in a low turbulence tunnel. The 120,000 to 300,000 range reported in the paper reflects the high turbulence level of the Stanford tunnel, caused by a honeycomb located just upstream of the test region.

The turbulence level in a wind tunnel stream is bound to be higher than will be encountered in normal natural airstreams and thus the critical range of Reynolds numbers for a real stack will be higher than wind tunnel tests would indicate. This implies that supercritical flow may not be established around a stack until the Reynolds number approaches 1,000,000.

In this light it seems not unlikely that the stack observed by Mr. Housner was operating in the critical range (Reynolds numbers of 460,000, 663,000, and 1,020,000 for wind speeds of 18, 26 and 40 fps respectively). The larger amplitude at the 26 fps wind speed would then be consistent with the wind tunnel results where critical range vibration amplitude was larger than that encountered in the low supercritical regime. The frequency observations made by Mr. Housner for the 18 fps condition also reinforce this belief. It would be interesting to test the effect of boundary layer trips or extensive surface roughness (devices which artificially produce the turbulent boundary layer typical of supercritical flow) on the vibration amplitude of the stack mentioned. If the stack has been operating in the critical regime the artificially induced supercritical flow conditions should result in a reduced vibration amplitude.

The effect of damping on plain cylinder vibration has been discussed by

1. Athlone Fellow, Royal Aircraft Establishment, Farnborough, Hampshire, England.
2. Goldstein, S: Modern Developments in Fluid Dynamics, Oxford, The Clarendon Press, Vol. II, 1938.

Meier-Windhorst.[3] Damping reduces vibration amplitude substantially and vibration frequency very slightly. If hydrodynamic forces and the fraction of critical damping (c) are constant the product of spring stiffness (k) and maximum double amplitude $(B)_{max}$ should be constant and the curve in Figure 3 should be a straight line. The fact that the run 4 (I = 0.335 in.-lb.-sec.^{2}) produces a kB_{max} factor much lower than that of runs 7 - 11 (I = 2.151 to 6.722 in.-lb.-sec.^{2}) and a maximum amplitude below the projected straight line through the B_{max} values for runs 7 - 11, would indicate that the damping was greater for run 4 than runs 7 - 11, rather than as Mr. Housner suggests.

The proportion of the beneficial effect of the shroud due to increased damping was not directly measured in the water channel tests, which were of an exploratory nature, made solely to pick the most likely form of suppressor. A measure of the importance of damping can be obtained, however, from the information plotted in Figure 5. If the very pessimistic assumption is made that the entire beneficial effect of the shroud at low k values is due to an increase in damping

$$\frac{c_{shroud}}{c_{plain\ cyl.}} = \frac{B_{max\ plain\ cyl.}}{B_{max\ shroud}}$$

This ratio has been computed throughout the k range and is as follows:

k	$\frac{c_{shroud}}{c_{plain\ cyl.}}$
30	1.84
80	1.81
150	1.68
200	1.58
300	2.14
400	5.50
500	20

Since the vibration frequency at maximum amplitude is constant as k is varied, the tip velocity of the vibrating cylinder will diminish as maximum amplitude decreases, with a consequent reduction in damping. It can be seen from the table above that the results predict an increase in damping as k increases and amplitude decreases. It thus becomes apparent that the diminished amplitude is the result of a reduction in the driving force. This reduction is the result of the changed character of the flow around the cylinder caused by the shroud. It is significant that the effect is most marked in the cases where double amplitudes are 0.7 diameters or less, the region of greatest interest.

3. Meier-Windhorst, A.: Flatterschwingungen von Zylindern im gleichmassigem Flüssigkeitsstrom. Mitt. des Hydraulischen Institute der Technischen Hochschule München, Heft 9, Munich, 1939.

Discussion of
"SOME OBSERVATIONS ON OPEN CHANNEL FLOW AT SMALL REYNOLDS NUMBERS"

by Lorenz G. Straub, Edward Silberman, and Herbert C. Nelson
(Proc. Paper 1031)

CORRECTIONS.—The figures to which Prof. Posey refers in his discussion of this paper in Proc. Paper 1154 appear on page 1154-17.

LORENZ G. STRAUB,* M. ASCE, EDWARD SILBERMAN,** and HERBERT C. NELSON,*** A.M. ASCE.—The comments of Professors Lansford and Robertson and Professor Posey augment the paper and their efforts are appreciated. Little additional comment is required.

Regarding the filament of maximum velocity in laminar flow, the measurements described in the paper do not permit making a positive statement. Since about 15 minutes were required for each pitot tube reading, it was not feasible to search for the filament of maximum velocity. Velocities were obtained by the tube at no closer than 0.2 in. below the surface (about 0.25 depth) and at 0.25 in. intervals below this. Within these limitations, no velocity was found which exceeded the surface velocity in laminar flow. On the other hand, for most turbulent velocity measurements, with the same limitations, a maximum was found beneath the surface, even at Reynolds numbers as low as 6,000. Since the original paper was published, another thesis has been completed in which laminar flow velocities were measured by an electrical conductivity method.(1) The closest readings beneath the surface were about 0.2 depth and, again, no maximum was found beneath the surface. It appears, therefore, that the maximum velocity in laminar flow may be at the surface. (The isovels in Professor Posey's figure from Pickett's measurements seem to indicate maximum velocity at the surface, also.)

The conclusions regarding the applicability of laminar flow theory to flow in open channels were intended to apply mainly to friction factor and to wall shear stress—conclusions 1 and 3, page 20. Professor Posey is correct in stating that the predicted velocity profiles are not accurately comparable with theory (at a distance from the wall). It is believed that the discrepancies are surface effects, probably attributable to surface tension. There is every reason to believe that the water and kerosene used in the experiments described in the original paper behaved as Newtonian fluids and that the discrepancies are not explainable by use of differential equations based on non-Newtonian fluids. Had Professor Posey included mean flow data with his figure taken from Pickett's measurements, a better comparison could have been made with the theoretical results (given graphically in Professor Posey's first figure and analytically in Appendix B-4).

* Director, St. Anthony Falls Hydr. Lab., Univ. of Minnesota, Minneapolis, Minn.
** Associate Prof., St. Anthony Falls Hydr. Lab., Univ. of Minnesota, Minneapolis, Minn.
*** Hydr. Engr., Kimberly-Clark Corp., Neenah, Wis.

In connection with Fig. 4 of Lansford and Robertson, the following tabulation of theoretical laminar wall shear distribution for the same channel (taken from Appendix B-3) may be interesting:

LAMINAR WALL SHEAR DISTRIBUTION

90-Degree Triangular Channel

$\xi/1.414d$	$T_o/\overline{T_o}$	$\xi/1.414d$	$T_o/\overline{T_o}$
0.05	0.424	0.25	1.135
0.10	0.700	0.30	1.210
0.15	0.868	0.40	1.323
0.20	1.014	0.50	1.343

Symmetrical about $\xi/1.414d = 0.5$

The following corrections should be made in Appendix B of the paper:

Page 24 - No. 2 - In the formula for w, the fraction after the summation sign should contain in the denominator the factor $\cosh \frac{2n+1}{2}\frac{\pi b}{d}$ rather than $\frac{2n+1}{2}\frac{\pi b}{d}$. Also, the first fraction in the equation for K should contain $\frac{d}{b}$ rather than $\frac{b}{d}$ in the denominator.

Page 25 - No. 3 - In the formula for w, a bracket should enclose the entire expression following d^2.

Page 25 - No. 5 - The factor $(1 + \frac{b^2}{d^2})$ should be eliminated from the numerator and denominator.

Page 26 - No. 6 - In the lower figure only, the coordinate axis should be rotated 90 degrees counter-clockwise, so that the x-axis is vertical, positive upwards, and the y-axis is horizontal, positive to the left.

Page 26 - No. 7 - The superscript over q in the heading of the table refers to the List of References and should be 18 rather than 21.

Page 27 - No. 8 - The formula for w should be $w = \frac{qS}{1500} b^2 H$.

Page 28 - No. 9 - The formula for w should be $w = \frac{qS}{1500} d^2 H$.

Page 28 - No. 10 - The reference for w should be 19 rather than 22.

In Fig. 4 of the discussion by Lansford and Robertson, the ordinate scale should contain T_o rather than T_w to be consistent with Appendix A.

REFERENCES

1. Howe, H. "Laminar Flow Velocity Distribution in a 120° Triangular Channel," Unpublished M. S. Thesis, University of Minnesota, Minneapolis, Minn., 1956, 143 pages.

Discussion of
"THE BOUNDARY LAYER DEVELOPMENT IN OPEN CHANNELS"

by J. W. Delleur
(Proc. Paper 1138)

T. BLENCH* M. ASCE.—With a properly designed parallel throated long-crested weir equipped with suitable gauging in the channel upstream, the discharge equation should be deducible to about 0.5% accuracy if the engineer will observe the velocity distribution at the gauging section and in the vicinity of the critical section in the throat. The equation to use is that expressing the fact that, somewhere near the end of the throat, depth must be critical as expressed strictly by making the energy of flow (specific depth, specific head, still-pond depth) a minimum after allowing for the effect of the kinetic energy correction factor (Ref. A). The principal source of error will then be in estimating the friction loss between the gauging and critical sections. Suitable designs have been in use extensively in the Punjab Irrigation canals since as early as 1927. The present paper interests the writer because it draws attention to the need for observing velocity distribution near the critical section for every accurate rating of a long-crested weir and suggests that further research might permit the velocity distribution to be deduced. But with great accuracy demanded by the practising engineer the reliability of deduction must be fully established. The following queries, with their implied criticisms, are made with this practical object in view; the writer pretends to no expertness in pure boundary layer theory and must expect at least some of his questions to appear rather elementary.

i. Does Fig. 2, or its related theory, indicate that a normal velocity distribution could not be established in the throat of a long-crested weir, no matter how long the crest might be? If so can the theory be accepted as even approximately correct? If not what does a turning value of eta of 0.13 represent practically (see Figs. 2, 8)?

ii. What is H? Is it $\sqrt[3]{q^2/g}$ or $\sqrt[3]{kq^2/g}$ or the value of depth that makes energy of flow, viz $h + hq^2/2g$ a minimum allowing for k being variable, where k is kinetic energy correction factor?

iii. Does the paper apply to anything else but critical, or very nearly critical, conditions? If so, what is the justification for equation (15) which appears to compel critical condition?

iv. Since the phenomenon under investigation is that of the boundary layer, that owes its existence to friction loss and is essentially turbulent, why is friction loss ignored generally and why are the Reynold's stresses ignored in equation (4)?

v. Specifically, concerning equation (4), is it merely an abbreviated way of writing the straightforward momentum equation allowing for pressure gradient

* Prof. of Civ. Eng. and Cons. Engr., Univ. of Alberta; Edmonton, Alta., Canada.

and replacing pressure gradient by its equivalent from the standard hydrodynamic equation of motion which assumes non-pulsating (and therefore non-turbulent) flow (Ref. 3 Chapter IV. Sec. 52)? If so, why is this form used when there is no pressure gradient but there is turbulence which requires the introduction of Reynold's stresses $\rho u' v'$ etc.?

vi. In equations (18) sigma appears to be $H^{3/2}$ divided by itself yet it is used as a variable. How is this explained?

vii. Has the virtual channel the same kinetic energy and momentum per unit weight of fluid as the actual channel? If not what is the justification for using it?

viii. Why is single log paper used for plotting velocity distributions in Figures 5-7 when a seventh root law is used in equation (8)?

REFERENCE

(A) JAEGER, C. Engineering Fluid Mechanics. Blackie & Son. 1956.

Discussion of
"WIND INDUCED VIBRATION OF CYLINDRICAL STRUCTURES"

by Joseph Penzien
(Proc. Paper 1141)

T. AU,* A.M. ASCE.—The investigation on vibration of steel stacks has been activated by the many instances of reported excessive vibrations of welded steel stacks in recent years. A better understanding of the subject is still essential in order to design such structures adequately. The paper has indeed contributed some additional information much needed in this field.

Below the critical range of Reynold's numbers, the vibration of stacks in a direction normal to the wind is generally attributed to the von Karman vortex trail, and the theory has been validated by experimental results. At or above the critical range, hypotheses have been advanced, perhaps without sufficient evidence in some instances, to predict the behavior of vibrations. One of the erroneous conclusions is that since the shedding of vortices become a-periodic beyond the critical range, the turbulent wake would inhibit vibrations. This obviously contradicts some most recent observations reported in literature in which excessive vibrations of stacks involve Reynold's numbers considerably above the critical range. The wind tunnel investigation of the dynamic behavior of cylindrical sections under the action of wind at critical range reported in the paper further confirms the field observations.

A recent investigation of vibrations of full-size stacks by Ozker and Smith[1] has been cited by the author to compare with his own results. Two pertinent points in the former work related to this paper may be elaborated here:

1. The stack vibrates at its own natural frequency at all times regardless of wind velocity probably for all conditions above critical range of Reynold's numbers. The alternating force is automatically resonant with the natural frequency of vibration. This concept is now accepted in a wider circle although the exact mechanism behind the formation of the alternating exciting forces is still a matter of conjecture. As pointed out by Sherlock,[2] for vibration of stacks in wind above critical range, the von Karman theory has served a useful framework on which to hang coefficients based on experience, but it can not be said that the reality of the von Karman trail has been established. The results from wind tunnel tests of cylinders presented in the paper seem to strengthen this impression.

2. The displacement of the top of stacks increases with increasing wind velocity. In other words, once the vibration is initiated, the amplitude of vibration will be increased continuously, following approximately a parabolic curve, as the wind velocity is increased. This conclusion seems to be at variance with the experience of others. Since similar results have been observed from the stacks in several plants of the Detroit Edison Company as reported by Ozker and Smith, there is no reason to believe that it is merely

* Asst. Prof. of Eng. Mech., Univ. of Detroit, Detroit, Mich.

a coincidence. Unfortunately, the paper does not shed any new light on this controversy since the range of Reynold's numbers in the wind tunnel tests is between 10^5 and 10^6 while that of vibrating stacks may be almost as high as 10^7. The pulsating response as indicated by the maximum dynamic reaction in the paper nevertheless casts some shadows on the above conclusion.

The Strouhal number and the drag coefficient for rigid cylinders of 4-inch and 12-inch diameters have been found by Delany and Sorensen[3] for Reynold's number R up to 2.3×10^6. Between $R = 10^5$ and 10^6, the results are remarkably similar to the S-curve of Relf and Simmons and the C_D-curve of Göttingen shown in Fig. 5 of the paper. For R greater than 10^6, the following values are given:

R	C_D	S
10^6	0.40	0.38
1.5×10^6	0.43	0.42
2.0×10^6	0.50	0.35

Note that the value of C_D is increasing with R up to the limit of the range but the curve of S dips for R over 1.5×10^6.

REFERENCES

1. M. S. Ozker and J. O. Smith, "Factors Influencing the Dynamic Behavior of Tall Stacks under the Action of Wind," ASME Transactions, v. 78, August 1956, p. 1381.

2. Ibid., Discussion by R. H. Sherlock, p. 1387.

3. N. K. Delany and N. E. Sorensen, "Low-speed Drag of Cylinders of Various Shapes" NACA Technical Note 3038, Nov. 1953.

Discussion of
"A PRESSURE LINE CONCEPT FOR INELASTIC BENDING"

by Frank Baron
(Proc. Paper 1157)

JOHN A. HRIBAR,[1] J.M. ASCE.—The author has presented here a "tool" that can become quite useful in quickly estimating the effects of plasticity on the behavior of structural elements subjected to flexural loads. The contribution hinges on the pictorial design procedure that is used. If this procedure is used to obtain a quick result, it results in only an estimate unless one is experienced in the method and has a keen sense of judgment in balancing statics pictorially. Of course only an estimate may be the desired result. But for an accurate result several "checks" would have to be made to obtain the best "fit."

This procedure may neither be more rapid nor more accurate than present methods used on certain materials and cross-sections. Two questions are raised. Could not members of steel, that has an easily approximated stress-strain curve and comprises the major portion of structural material, be analyzed by present methods with the same ease? Could not the ultimate load on a structural element of any material and any cross-section be as easily and more accurately calculated by the theory of plasticity? The writer has raised these questions to emphasize that the theory of plasticity may be as rapid, more accurate and less artificial in some cases.

The writer agrees that as the cross-section or the stress-strain curve becomes more unwieldy the "tool" becomes more powerful. Also the by-products of the procedure are quite useful in a thorough analysis of a structure. The pressure line concept will speed up estimates on structural elements of this type. This is a contribution that is well received in a time when there is much discussion of ultimate or plastic design.

1. Graduate Teaching Asst., Dept. of Civ. Eng., Carnegie Inst. of Technology, Pittsburgh, Pa.

Journal of the
ENGINEERING MECHANICS DIVISION
Proceedings of the American Society of Civil Engineers

DISPERSION OF LONGITUDINAL WAVES*

by E. Volterra,** M. ASCE
(Proc. Paper 1322)

SUMMARY

The problem of dispersion of longitudinal waves in elastic rods of infinite lengths and of rectangular cross-section is discussed by applying the one-dimensional theory of wave propagation based on the Method of Internal Constraints. The results given by this theory are compared with those given by the Elementary, Love, Bishop approximate theories, and, in the case of two-dimensional elasticity, with the exact theories given by Lord Rayleigh and Lamb.

NOMENCLATURE

The following nomenclature is used in the text:

$2a, 2b$ = lateral dimensions of the cross-section of the bar

c = phase velocity of longitudinal waves in a bar

c_g = group velocity of longitudinal waves in a bar

$c_p = \sqrt{\frac{E}{\rho(1-\sigma^2)}}$ = plate velocity

c_s = velocity of Rayleigh surface waves

$c_o = \sqrt{\frac{E}{\rho}}$ = velocity of longitudinal waves of infinite wave-length in a bar (bar velocity)

$c_1 = \sqrt{\frac{E(1-\sigma)}{(1+\sigma)(1-2\sigma)\rho}}$ = velocity if dilatation waves in an unbounded medium

Note: Discussion open until December 1, 1957. Paper 1322 is part of the copyrighted Journal of the Engineering Mechanics Division of the American Society of Civil Engineers, Vol. 83, No. EM 3, July, 1957.

* The material in the paper is based on an investigation, conducted at the Rensselaer Polytechnic Institute, Troy, N. Y., under the sponsorship of the Office of Ordnance Research, Contract No. DA-30-115-ORD-709. Project No. 454.13.

** Prof. of Eng. Mechanics, The Univ. of Texas, Austin, Tex.

$c_2 = \sqrt{\frac{E}{2\rho(1+\sigma)}}$ = velocity of distortion waves in an unbounded medium

E = Young's modulus
σ = Poisson's ratio
ρ = density
} for the material of the bar

r_y, r_z = radii of gyration of the cross-section of the bar with respect to the y and z axes

$r_p = \sqrt{r_y^2 + r_z^2}$ = polar radius of gyration of the cross-section of the bar with respect to the x axis

t = time

u, v, w = components of the elastic displacement in the x, y and z axes

x, y, z = rectangular coordinates

$\alpha = \frac{2\sigma}{1-2\sigma}$

$\beta = \frac{b}{a}$

$\gamma = \frac{2\pi}{L}$ = wave number

INTRODUCTION

The paper discusses the problem of the dispersion of longitudinal waves in elastic straight rods of infinite lengths and of rectangular cross-sections by applying the one-dimensional approximate theory of wave propagation based on the "Method of Internal Constraints," which theory was presented in previous papers.(1,2,3)

This theory is based on the assumption that during motion the sections originally normal to the axis of the bar remain plane.

Considering a bar of any cross-section shape referring it to a system of orthogonal cartesian coordinates x, y, z, where x coincides with the axis of the bar and y and z with the principal axes of inertia of the cross-section of the bar, the above condition is satisfied by supposing that the components u, v, w of the elastic displacement along the x, y and z axes are expressed by the following equations:

$$\begin{aligned} u &= \nu(x,t) \\ v &= y\,\lambda(x,t) \\ w &= z\,\mu(x,t) \end{aligned} \qquad (1)$$

where ν, λ and μ are three functions a priori unknown of the variable x and of the time t.

On the assumptions that no external forces (body and surface forces) are applied to the bar, that the inertia characteristics of the cross-section of the bar are constant, that the bar has infinite length, the following equations of motion are derived (see Appendix to the paper):

$$r_z^2 \frac{\partial^2 \lambda}{dx^2} - \frac{2(1-\sigma)}{(1-2\sigma)} \lambda - \frac{2\sigma}{(1-2\sigma)} \frac{\partial \nu}{\partial x} - \frac{2\sigma}{(1-2\sigma)} \mu =$$

$$= 2(1+\sigma) \frac{\rho}{E} r_z^2 \frac{\partial^2 \lambda}{\partial t^2}$$

$$r_y^2 \frac{\partial^2 \mu}{\partial x^2} - \frac{2(1-\sigma)}{(1-2\sigma)} \mu - \frac{2\sigma}{(1-2\sigma)} \frac{\partial \nu}{\partial x} - \frac{2\sigma}{(1-2\sigma)} \lambda = \tag{2}$$

$$= 2(1+\sigma) \frac{\rho}{E} r_y^2 \frac{\partial^2 \mu}{\partial t^2}$$

$$\frac{2(1-\sigma)}{(1-2\sigma)} \frac{\partial^2 \nu}{\partial x^2} + \frac{2\sigma}{(1-2\sigma)} \frac{\partial \lambda}{\partial x} + \frac{2\sigma}{(1-2\sigma)} \frac{\partial \mu}{\partial x} =$$

$$= 2(1+\sigma) \frac{\rho}{E} \frac{\partial^2 \nu}{\partial t^2}$$

In equations (2) the quantities r_y and r_z represent the radii of inertia of the cross-section of the bar, E, σ and ρ respectively Young's modulus, Poisson's ratio and the density of the material of the bar. From equations (2) the dispersion curves, i.e. the relationship between the phase and group velocities of propagation of longitudinal waves c and c_g versus the wave-length L, can be derived.

Dispersion curves are in general obtained by applying the appropriate boundary conditions to the general equations of motion of the medium, and exact solutions can be derived only in particular cases among which are the case of an infinite long rod of circular cross-section and the case of a plate of infinite extent. The first problem was investigated in terms of the general equations of elasticity by L. Pochhammer in the year 1876.[4] An outline of this exact theory is discussed by A. E. H. Love[5] and numerical values of dispersion curves have been calculated by D. Bancroft and R. M. Davies.[6,7]

The second problem was investigated by Lord Rayleigh in the year 1888,[8] by H. Lamb in the year 1917,[9] by R. E. D. Bishop in the year 1953.[10] Numerical values of dispersion curves have been calculated by J. P. Marsden.[11]

Instead, the problem of wave propagation in an elastic bar of rectangular cross-section in terms of the equations of the Mathematical Theory of Elasticity has not been solved and therefore approximate solutions must be sought.

The simplest theory of longitudinal waves in elastic bars predicts that such waves travel with a constant velocity $c_o = \sqrt{\frac{E}{\rho}}$ (bar velocity), and therefore without dispersion.[12] The corresponding equation of motion is:

$$\frac{\partial^2 u}{\partial t^2} - \frac{E}{\rho} \frac{\partial^2 u}{\partial x^2} = 0 \tag{3}$$

If lateral inertia of the elements of the bar is considered, the terms - $\sigma 2 r_p^2 \frac{\partial^4 u}{\partial x^2 \partial t^2}$ must be added to equation (3) to take into account this effect, r_p representing the radius of gyration of the cross-section of the bar about the x axis. The differential equation of motion (3) is modified to the form given by A. E. H. Love in 1934:[13]

$$\frac{\partial^2 u}{\partial t^2} - \frac{E}{\rho}\frac{\partial^2 u}{\partial x^2} - \sigma r_p^2 \frac{\partial^4 u}{\partial x^2 \partial t^2} = 0 \qquad (4)$$

If the shear stresses are taken into account the equation of motion takes the form given by R. E. D. Bishop in 1953:[14]

$$\frac{\partial^2 u}{\partial t^2} - \frac{E}{\rho}\frac{\partial^2 u}{\partial x^2} - \sigma r_p^2 \frac{\partial^4 u}{\partial x^2 \partial t^2} + \sigma r_p^2 \frac{E}{2(1+\sigma)\rho}\frac{\partial^4 u}{\partial x^4} = 0 \qquad (5)$$

Bishop[14] has improved the results of equation (5) by the method of successive approximations. In the Bishop improved theory the geometrical form of the cross-section of the bar has to be introduced. In the particular case of a bar of rectangular cross-section (2a x 2b) the equation of motion becomes:

$$\begin{aligned}
&\frac{\partial^2 u}{\partial t^2} - \frac{E}{\rho}\frac{\partial^2 u}{\partial x^2} - \frac{\sigma^2}{3}(a^2+b^2)\frac{\partial^4 u}{\partial x^2 \partial t^2} + \\
&+ \frac{\sigma^2}{6(1+\sigma)}\frac{E}{\rho}(a^2+b^2)\frac{\partial^4 u}{\partial x^4} + \\
&+ \frac{2\sigma^2(1+\sigma)}{3}\frac{\rho}{E}\left[\frac{a^4+b^4}{5}(1-\sigma) - \right. \\
&\left. - \sigma\frac{a^2b^2}{3}\right]\frac{\partial^6 u}{\partial x^2 \partial t^4} - \frac{2\sigma^2}{3}\left[\frac{a^4+b^4}{5}(1-\sigma) - \right. \\
&\left. - \frac{\sigma}{3}a^2b^2\right]\frac{\partial^6 u}{\partial x^4 \partial t^2} + \\
&+ \frac{\sigma^2}{6(1+\sigma)}\frac{E}{\rho}\left[\frac{a^4+b^4}{5}(1-\sigma) - \frac{\sigma}{3}a^2b^2\right]\frac{\partial^6 u}{\partial x^6} = 0
\end{aligned} \qquad (6)$$

If in equation (6) the terms associated with shear stress are neglected, the Love improved equation is obtained for a bar of rectangular cross-section as derived by Bishop under the following form:

$$\frac{\partial^2 u}{\partial t^2} - \frac{E}{\rho}\frac{\partial^2 u}{\partial x^2} - \frac{\sigma^2}{3}(a^2+b^2)\frac{\partial^4 u}{\partial x^2 \partial t^2} +$$

$$+ \frac{2\sigma^2(1-\sigma^2)}{15}\frac{\rho}{E}(a^4+b^4)\frac{\partial^6 u}{\partial x^2 \partial t^4} - \tag{7}$$

$$- \frac{2\sigma^2(1+\sigma)}{9}\frac{\rho}{E}a^2b^2\frac{\partial^6 u}{\partial x^2 \partial t^4} = 0$$

In the following text the dispersion equations which will be obtained from the above equations will be referred to as derived from:

Elementary Theory	from equation 3
Love Theory	from equation 4
Bishop Theory	from equation 5
Bishop Improved Theory	from equation 6
Love Theory Improved by Bishop	from equation 7
Theory Based on the Method of Internal Constraints	from equation 2

The object of the present paper is to discuss the problem of dispersion of longitudinal waves in elastic rods of infinite lengths and of rectangular cross-sections by applying the approximate one-dimensional theory of wave propagation based on the "Method of Internal Constraints" and to compare the results with those given by the other approximate one-dimensional theories of wave propagation and with the exact theories which are deduced from the Mathematical Theory of Elasticity.

The results of such an analysis clearly show that in the two numerical cases considered, i.e. the case of a bar of square cross-section and the case of a rectangular bar (2a x 2b) having ratio $\beta = \frac{b}{a} = 0.125$, the use of the theory based on the "Method of Internal Constraints" gives the closest values to the exact solutions, which is in accordance with experimental findings. In fact, according to recent experiments by R. W. Morse[15,16] on dispersion effects in bars of rectangular cross-sections, the dispersion curves of a bar of square cross-section should give very close results to those obtained with a bar of circular cross-section if the ratio of the diameter of the cylinder to the side of the square cross-section is 1.13.

The dispersion curves for a bar of rectangular cross-section should be in good agreement with the theoretical plane strain case when the ratio of the lateral dimensions of the cross-section of the bar $\beta = \frac{b}{a} \leqslant 0.125$.

The Phase-Velocity of Longitudinal Waves

Let:

$$u(x,t) = A\, e^{i\gamma(x-ct)} \tag{8}$$

where A is a constant, $\gamma = \frac{2\pi}{L}$ the wave number, L the wave-length, c the phase velocity and $i = \sqrt{-1}$. By substituting equation (8) into equations (3), (4), (5), (6) and (7) one finds the following expressions for the phase velocity:

In the Elementary Theory:

$$Y = \frac{c}{c_o} = 1 \tag{9}$$

In Love Theory:

$$Y = \frac{c}{c_o} = \frac{1}{\sqrt{1 + \frac{\pi^2\sigma^2(1+\beta^2)\delta^2}{3}}} \tag{10}$$

In Bishop Theory:

$$Y = \frac{c}{c_o} = \sqrt{\frac{1 + \frac{\pi^2\sigma^2(1+\beta^2)\delta^2}{6(1+\sigma)}}{1 + \frac{\pi^2\sigma^2(1+\beta^2)\delta^2}{3}}} \tag{11}$$

In Bishop Improved Theory:

$$Y^4\delta^4\pi^4\, 2(1+\sigma)F - Y^2\left[\delta^4\pi^4\, 2F - \delta^2\pi^2\,\frac{\sigma^2}{3}\,(1+\beta^2) - 1\right] + \tag{12}$$

$$+\left[\delta^4\pi^4\,\frac{F}{2(1+\sigma)} - \delta^2\pi^2\,\frac{\sigma^2}{6(1+\sigma)}\,(1+\beta^2) - 1\right] = 0$$

where

$$F = \frac{\sigma^2}{3}\left[\frac{1-\sigma}{5}\,(1+\beta^4) - \frac{\sigma}{3}\,\beta^2\right]$$

In Love Improved Theory:

$$Y^4\delta^4\pi^4\, 2(1+\sigma)F + Y^2\left[\delta^2\pi^2\,\frac{\sigma^2}{3}\,(1+\beta^2) + 1\right] - 1 = 0 \tag{13}$$

Let:

$$\begin{aligned} \nu &= A\, e^{i\gamma(x-ct)} \\ \lambda &= B\, e^{i\gamma(x-ct)} \\ \mu &= C\, e^{i\gamma(x-ct)} \end{aligned} \tag{14}$$

where A, B and C are three constants.

Substituting equations (14) into equations (2) one obtains three homogeneous algebraic equations in A, B and C whose determinant set equal to zero yields the following frequency equation:

$$
\begin{aligned}
&- Y^6 + Y^4 \frac{1}{2(1+\sigma)} \left[\frac{12(\alpha+2)(1+\beta^2)}{(2\pi)^2\beta^2\delta^2} + \alpha + 4 \right] - \\
&- Y^2 \frac{1}{2(1+\sigma)^2} \left[\frac{12(5\alpha+6)(1+\beta^2)(2\pi)^2\delta^2+144(4\alpha+4)}{(2\pi)^4\beta^2\delta^4} + \right. \\
&\left. + 2\alpha + 5 \right] + \\
&+ \frac{4}{2(1+\sigma)^3} \left[\frac{12(1+\alpha)(1+\beta^2)(2\pi)^2\delta^2+144(3\alpha+2)}{(2\pi)^4\beta^2\delta^4} \right] \\
&+ \frac{\alpha+2}{2(1+\sigma)^3} = 0
\end{aligned}
\tag{15}
$$

In equations (9), (10), (11), (12), (13), and (15)

$$Y = \frac{c}{c_o} \qquad \alpha = \frac{2\sigma}{1-2\sigma}$$

$$\beta = \frac{b}{a} \qquad \delta = \frac{2a}{L}$$

From the above equations it follows for the two limiting cases of very long ($\delta \to 0$), or very short waves ($\delta \to \infty$), the following valucs for the phase velocities:

In the Love Theory:

for $\delta \to 0$ $Y = 1$ $c = c_o$

for $\delta \to \infty$ $Y = 0$ $c = 0$

In the Bishop Theory:

for $\delta \to 0$ $Y = 1$ $c = c_o$

for $\delta \to \infty$ $Y = \dfrac{1}{\sqrt{2(1+\sigma)}}$

$$c = \sqrt{\frac{E}{2(1+\sigma)\rho}} = c_2$$

(velocity of distortion waves in an unbounded medium)

In the Bishop Improved Theory:

for $\delta \to 0$ $Y = 1$ $c = c_o$

for $\delta \to \infty$ $Y = \frac{1}{\sqrt{2(1+\sigma)}}$ $c = \sqrt{\frac{E}{2(1+\sigma)\rho}} = c_2$

In the Love Theory Improved by Bishop:

for $\delta \to 0$ $Y = 1$ $c = c_o$

for $\delta \to$ $Y = 0$ $c = 0$

Instead, for $\delta \to \infty$ equation (15) becomes:

$$- Y^6 + Y^4 \left[\frac{\alpha+4}{2(1+\sigma)} \right] - Y^2 \frac{(2\alpha+5)}{2(1+\sigma)^2} + \frac{\alpha+2}{2(1+\sigma)^3} = 0 \qquad (16)$$

The roots of equation (16) are:

$$Y_1 = \sqrt{\frac{1-\sigma}{(1+\sigma)(1-2\sigma)}}$$

$$c = \sqrt{\frac{E(1-\sigma)}{(1+\sigma)(1-2\sigma)\rho}} = c_1$$

(velocity of dilatation waves in an unbounded medium)

$$Y_2 = Y_3 = \sqrt{\frac{1}{2(1+\sigma)}}$$

$$c = \sqrt{\frac{E}{2(1+\sigma)\rho}} = c_2$$

(velocity of distortion waves in an unbounded medium)

In the case of an infinite plate (plane strain case), the relationship between the phase velocity c of sinusoidal waves and their wave length L is given by the following transcendental equation (7), (8), (9):

$$\frac{\tanh nb}{\tanh mb} = \frac{4\gamma^2 mn}{(\gamma^2+n^2)^2} \qquad (17)$$

where $\gamma = \frac{2\pi}{L}$ is the wave number

$$m^2 = \gamma^2 \left[1 - \frac{c^2}{c_1^2} \right]$$

$$n^2 = \gamma^2 \left[1 - \frac{c^2}{c_2^2} \right] \qquad (18)$$

$c_1 = \sqrt{\frac{E(1-\sigma)}{(1+\sigma)(1-2\sigma)\rho}}$ the velocity of dilatation waves in an unbounded medium

$c_2 = \sqrt{\frac{E}{2\rho(1+\sigma)}}$ the velocity of distortion waves in an unbounded medium

$2b$ the thickness of the plate

From equation (17) it follows that for very long waves ($\delta = \frac{2b}{L} \to 0$)

$$c = \sqrt{\frac{E}{\rho(1-\sigma^2)}} = c_p \qquad \text{(plate velocity)} \qquad (19)$$

for very short waves ($\delta \to \infty$): $c \to c_s$ velocity of Rayleigh surface waves (x)(10)

In the case of a very thin beam (plane stress case), the dispersion equation is given by the following transcendental equation (17), (10):

$$\frac{\tanh pa}{\tanh qa} = \frac{4\gamma^2 pq}{(\gamma^2+p^2)^2} \qquad (20)$$

where:

$$p^2 = \gamma^2 \left[1 - \frac{c^2}{c_2^2} \right]$$

$$q^2 = \gamma^2 \left[1 - \frac{c^2}{c_p^2} \right] \qquad (21)$$

$c_2 = \sqrt{\frac{E}{2(1+\sigma)\rho}}$ velocity of distortion waves in an unbounded medium

$c_p = \sqrt{\frac{E}{\rho(1-\sigma^2)}}$ the plate velocity

$2a$ the depth of the bar

From equation (20) it follows that for very long waves

$$(\delta = \frac{2a}{L} \to 0) \qquad c = \frac{E}{\rho} = c_o \qquad \text{bar velocity}$$

for very short waves equation (20) reduces to the cubic equation in $(\frac{c}{c_2})^2$ similar to the equation for Rayleigh surface waves:[10]

$$(\frac{c^2}{c_2^2})^3 - 8(\frac{c^2}{c_2^2})^2 + (\frac{c^2}{c_2^2})(24 - 16\frac{c^2}{c_p^2}) - 16(1 - \frac{c_2^2}{c_p^2}) = 0 \qquad (22)$$

For $\sigma = 0.29$ the principal root of equation (22) is:

$$\frac{c}{c_2} = 0.9154 \qquad \text{i.e.:} \quad \frac{c}{c_o} = 0.5699$$

Equations (17) and (20) have been solved numerically by J. P. Marsden[11] of the Department of Physics at the University College of Wales in Aberystwyth, for values of Poisson's ratio $\sigma = 0.29$.*

In figure 1 the dispersion curves $\frac{c}{c_o}$ versus the ratio $\frac{2a}{L}$ are given for a bar of rectangular cross-section with ratio $\beta = \frac{b}{a} = 0.125$. The results for the lowest mode according to the theory based on the "Method of Internal Constraints" (equation 15) are compared with the results given by the plane stress case (equation 18), by the Elementary Theory (equation 9) and by the Love and Bishop simple and improved theories (equations 10, 11, 12 and 13).

In figure 2 the dispersion curves $\frac{c}{c_o}$ versus the ratio $\frac{2a}{L}$ are given for a bar of rectangular cross-section with ratio $\beta = \frac{b}{a} = 0.125$, according to the theory based on the "Method of Internal Constraints" (equation 15).

Figure 3 gives the dispersion curves $\frac{c}{c_o}$ versus the ratio $\frac{r}{L}$ between

---

* The author is indebted to Professor R. M. Davies, Head of the Department of Physics at the University College of Wales in Aberystwyth, for having furnished him with these numerical data which have been used for comparison in some of the figures enclosed in the text.

radius of gyration of the cross-section and wave-length for a bar of square cross-section. The curves obtained from equation (15) in the case $\beta = 1$ are compared with the curves calculated by R. M. Davies[7] using the Pochhammer's solution for a cylindrical bar.

In figure 4 the results for the lowest mode of the dispersion curves $\frac{c}{c_o}$ versus the ratio $\frac{r}{L}$ for a bar of square cross-section according to the theory based on the "Method of Internal Constraints" (equation (15) are compared with the results given by the other theories, i.e. with the lowest modes of the Pochhammer's solution according to R. M. Davies, with Love, and Bishop simple and improved theories. In the computations of these dispersion curves the value $\sigma = 0.29$ has been assumed for Poisson's ratio of the material of the bar.

The Group Velocity of Longitudinal Waves

The velocity with which the energy of a pulse is propagated is called its group velocity and is given in terms of the phase velocity c and of the wave-length L by the equation:

$$c_g = c - L \frac{dc}{dL}$$

or by:

$$c_g = c + \delta \frac{dc}{d\delta} \tag{23}$$

From equation (23) it follows that the group velocity of longitudinal waves is:

In the Elementary Theory: $c_g = c_o$ (24)

In Love Theory: $c_g = c^3$ (25)

In Bishop Theory:

$$c_g = c \left[1 + \frac{1}{1 + \frac{\pi^2\sigma^2(1+\beta^2)\delta^2}{3}} - \frac{1}{1 + \frac{\pi^2\sigma^2(1+\beta^2)\delta^2}{6(1+\sigma)}} \right] \tag{26}$$

In Love Theory Improved by Bishop:

$$c_g = c \left[1 - \frac{4 \left(\frac{c}{c_o} \right)^2 (1+\sigma) F \pi^4\delta^4 + \frac{\pi^2\sigma^2}{3}(1+\beta^2)\delta^2}{4 \left(\frac{c}{c_o} \right)^2 (1+\sigma) F \pi^4\delta^4 + \frac{\pi^2\sigma^2}{3}(1+\beta^2)\delta^2 + 1} \right] \tag{27}$$

where

$$F = \frac{\sigma^2}{3}\left[\frac{1-\sigma}{5}(1+\beta^4) - \frac{\sigma}{3}\beta^2\right]$$

In Bishop Improved Theory:

$$c_g = c\left[1 - \frac{\left(\frac{c}{c_o}\right)^4 \delta \frac{df_1(\delta)}{d\delta} + \left(\frac{c}{c_o}\right)^2 \delta \frac{df_2(\delta)}{d\delta} + \delta \frac{df_3(\delta)}{d\delta}}{4\left(\frac{c}{c_o}\right)^4 f_1(\delta) + 2\left(\frac{c}{c_o}\right)^2 f_2(\delta)}\right] \quad (28)$$

where:

$$f_1(\delta) = 2(1+\sigma)\,\pi^4 F \delta^4$$

$$f_2(\delta) = -2\pi^4 F \delta^4 + \frac{\pi^2\sigma^2}{3}(1+\beta^2)\delta^2 + 1$$

$$\delta \frac{df_1(\delta)}{d\delta} = 8(1+\sigma)\,\pi^4 F \delta^4$$

$$\delta \frac{df_2(\delta)}{d\delta} = -8\pi^4 F \delta^4 + \frac{2\pi^2\sigma^2}{3}(1+\beta^2)\delta^2$$

$$\delta \frac{df_3(\delta)}{d\delta} = \frac{2\pi^4 F}{(1+\sigma)}\delta^4 - \frac{\pi^2\sigma^2}{3(1+\sigma)}(1+\beta^2)\delta^2$$

$$F = \frac{\sigma^2}{3}\left[\frac{1-\sigma}{5}(1+\beta^4) - \frac{\sigma}{3}\beta^2\right]$$

In the Theory based on the "Method of Internal Constraints:"

$$c_g = c\left\{1 + \frac{\left(\frac{c}{c_o}\right)^4 \delta \frac{df_1(\delta)}{d\delta} - \left(\frac{c}{c_o}\right)^2 \delta \frac{df_2(\delta)}{d\delta} + \delta \frac{df_3(\delta)}{d\delta}}{6\left(\frac{c}{c_o}\right)^6 - 4\left(\frac{c}{c_o}\right)^4 f_1(\delta) + 2\left(\frac{c}{c_o}\right)^2 f_2(\delta)}\right\} \quad (29)$$

where:

$$f_1(\delta) = \frac{3(\alpha+2)}{2(1+\sigma)\pi^2}\,\frac{1+\beta^2}{\beta^2}\,\frac{1}{\delta^2} + \frac{\alpha+4}{2(1+\sigma)}$$

$$f_2(\delta) = \frac{3(5\alpha+6)}{4(1+\sigma)^2\pi^2}\,\frac{1+\beta^2}{\beta^2}\,\frac{1}{\delta^2} + \frac{9(\alpha+1)}{(1+\sigma)^2\pi^4}\,\frac{1}{\beta^2}\,\frac{1}{\delta^4} + \frac{2\alpha+5}{4(1+\sigma)^2}$$

$$\delta\,\frac{df_1(\delta)}{d\delta} = -\,\frac{3(\alpha+2)}{(1+\sigma)\pi^2}\,\frac{1+\beta^2}{\beta^2}\,\frac{1}{\delta^2}$$

$$\delta\,\frac{df_2(\delta)}{d\delta} = -\,\frac{3(5\alpha+6)}{2(1+\sigma)^2\pi^2}\,\frac{1+\beta^2}{\beta^2}\,\frac{1}{\delta^2} - \frac{36(\alpha+1)}{(1+\sigma)^2\pi^4}\,\frac{1}{\beta^2}\,\frac{1}{\delta^4}$$

$$\delta\,\frac{df_3(\delta)}{d\delta} = -\,\frac{3(1+\alpha)}{(1+\sigma)^3\pi^2}\,\frac{1+\beta^2}{\beta^2}\,\frac{1}{\delta^2} - \frac{18(3\alpha+2)}{(1+\sigma)^3\pi^4}\,\frac{1}{\beta^2}\,\frac{1}{\delta^4}$$

$$\alpha = \frac{2\sigma}{1-2\sigma}$$

In figure 5 the dispersion curves $\frac{c_g}{c_o}$ versus the ratio $\frac{2a}{L}$ are given for a bar of rectangular cross-section with ratio $\beta = \frac{b}{a} = 0.125$. The results for the lowest mode according to the theory based on the "Method of Internal Constraints" (equation 29) are compared with the results given for the plane stress case (as computed by J. P. Marsden), by the Elementary Theory (according to equation 30) and by the Love and Bishop simple and improved theories (according to equations (25), (26), (27) and (28).

In figure 6 the dispersion curves $\frac{c_g}{c_o}$ versus the ratio $\frac{2a}{L}$ are given for a bar of rectangular cross-section with ratio $\beta = \frac{b}{a} = 0.125$, according to the theory based on the "Method of Internal Constraints" (equation 29).

In figure 7 the dispersion curves $\frac{c_g}{c_o}$ versus the ratio $\frac{r}{L}$ (between radius of gyration of the cross-section and wave-length) are given for a bar of square cross-section. The curves obtained from equation (29) in the case $\beta = 1$ are compared with the curves calculated by R. M. Davies[7] using the Pochhammer solution for a cylindrical bar.

In figure 8 the results for the lowest mode of the dispersion curves $\frac{c_g}{c_o}$ versus the ratio $\frac{r}{L}$ for a bar of square cross-section according to the theory based on the "Method of Internal Constraints" (equation 29) are compared with

the results given by the other theories, i.e. with the results for the lowest mode of the Pochhammer solution according to R. M. Davies, and of the Love and Bishop simple and improved theories (according to equations (25), (26), (27) and (28) .

APPENDIX

The Equations of Motion for Longitudinal Waves Derived by the "Method of Internal Constraints"

The Strain Energy per unit volume of the bar will be expressed by:

$$V_o = \frac{E(1-\sigma)}{2(1+\sigma)(1-2\sigma)} \left[\epsilon_x^2 + \epsilon_y^2 + \epsilon_z^2\right] +$$

$$+ \frac{\sigma E}{(1+\sigma)(1-2\sigma)} \left[\epsilon_x\epsilon_y + \epsilon_y\epsilon_z + \epsilon_z\epsilon_x\right] \qquad (30)$$

$$+ \frac{E}{4(1+\sigma)} \left[\gamma_{xy}^2 + \gamma_{yz}^2 + \gamma_{zx}^2\right]$$

where:

$$\epsilon_x = \frac{\partial u}{\partial x} = \frac{\partial v}{\partial x} \qquad \gamma_{xy} = \frac{\partial v}{\partial x} + \frac{\partial u}{\partial y} = y\frac{\partial \lambda}{\partial x}$$

$$\epsilon_y = \frac{\partial v}{\partial y} = \lambda \qquad \gamma_{yz} = \frac{\partial w}{\partial y} + \frac{\partial v}{\partial z} = 0 \qquad (31)$$

$$\epsilon_z = \frac{\partial w}{\partial z} = \mu \qquad \gamma_{zx} = \frac{\partial u}{\partial z} + \frac{\partial w}{\partial x} = z\frac{\partial \mu}{\partial x}$$

The Total Potential Energy of the bar will be expressed by:

$$U = \int_v V_o dV = - \int_\ell dx \int_A V_o \, dydz \qquad (32)$$

where V is the volume of the bar, ℓ its length and A its cross-section area.

Substituting equations (31) into equations (30) and (32), and performing the integrations with respect to the variables y and z, calling:

$$I_y = \int_A z^2 \, dA$$

$$I_z = \int_A y^2 \, dA$$

the principal moments of inertia of the cross-section, one obtains the following expression for U:

$$U = -\int_{\ell} \left\{ \frac{E(1-\sigma)}{2(1+\sigma)(1-2\sigma)} \left[\left(\frac{\partial v}{\partial x} \right)^2 + \lambda^2 + \mu^2 \right] A + \right.$$

$$+ \frac{\sigma E}{(1+\sigma)(1-2\sigma)} \left[\frac{\partial v}{\partial x} \lambda + \frac{\partial v}{\partial x} \mu + \lambda\mu \right] A +$$

$$\left. + \frac{E}{4(1+\sigma)} \left[I_z \left(\frac{\partial \lambda}{\partial x} \right)^2 + I_y \left(\frac{\partial \mu}{\partial x} \right)^2 \right] \right\} dx$$

The Kinetic Energy per unit volume of the bar will be expressed by:

$$T_o = \frac{\rho}{2} \left[\left(\frac{\partial u}{\partial t} \right)^2 + \left(\frac{\partial v}{\partial t} \right)^2 + \left(\frac{\partial w}{\partial t} \right)^2 \right] \qquad (33)$$

where ρ is the density of the material of the bar. By substituting into equations (33) the expressions for the components of the displacements u, v, w given by equations (1), performing the integrations over the cross-section of the bar, one obtains the Total Kinetic Energy of the bar expressed by:

$$T = \frac{\rho}{2} \int_{\ell} \left\{ A \left(\frac{\partial v}{\partial t} \right)^2 + I_z \left(\frac{\partial \lambda}{\partial t} \right)^2 + I_y \left(\frac{\partial \mu}{\partial t} \right)^2 \right\} dx$$

On the assumption that no external forces (body and surface forces) are applied to the bar, supposing the bar of infinite length, by applying Hamilton's Principle under the form:

$$\delta \int_{t_1}^{t_2} (U + T)\, dt = 0$$

to the whole bar, supposing the displacement to be zero at t_1 and t_2, the equations of motion (2) are obtained.

BIBLIOGRAPHY

1. "The Equations of Motion for Curved Elastic Bars deduced by the use of the "Method of Internal Constraints" " by E. Volterra ("Ingenieur Archiv," 23. Band, 6. Heft, 1955, pp. 402-409).

2. "A One-Dimensional Theory of Wave-Propagation in Elastic Rods Based on the "Method of Internal Constraints" " by E. Volterra ("Ingenieur Archiv," 23. Band, 6. Heft, 1955, pp. 410-420).

3. "Some Applications of the "Method of Internal Constraints" to Dynamic Problems" by E. Volterra. (Proceedings of the September 1955 Madrid Colloquium of the International Union of Theoretical and Applied Mechanics on Deformation and Flow of Solids. Springer 1956 pp. 236-250.)

4. Pochhammer, L. (1876). Uber die Fortpflanzungsgeschwindigkeiten kleiner Schwingungen in einem unbegrenzten isotropen Kreiszylinder. Journal fur die reine und angewandte Mathematik (Crelle), Vol. 81, p. 324, 1876.

5. "The Mathematical Theory of Elasticity" by A. E. H. Love, paragraphs 199-202. Fourth edition, Cambridge University Press, 1934.

6. "The Velocity of Longitudinal Waves in Cylindrical Bars" by D. Bancroft. The Physical Review, Vol. 59, Second Series 1941, pp. 588-593.

7. "A Critical Study of the Hopkinson Pressure Bar" by R. M. Davies. Philosophical Transactions of the Royal Society of London. Series A. Vol. 240, pp. 375-457, January 1948.

8. "On the Free Vibrations of an Infinite Plate of Homogeneous Isotropic Elastic Matter" by Lord Rayleigh Proceedings of the London Mathematical Society Vol. 20, pp. 225-234, 1889.

9. "On Waves in an Elastic Plate" by H. Lamb, pp. 114-128. Proceedings of the Royal Society of London. Series A. Vol. 93, 1917.

10. "On Dynamic Problems of Plane Stress and Plane Strain" by R. E. D. Bishop, pp. 250-254. The Quarterly Journal of Mechanics and Applied Mathematics, Vol. 6, 1953.

11. "Experiments on the Dispersion of Stress Waves" by J. P. Marsden. (Thesis submitted to the University of Wales in candidature for the degree of Philosophiae Doctor. April 1954) (not yet published).

12. "Stress Waves in Solids" by H. Kolsky, Oxford Clarendon Press, 1953.

13. "The Mathematical Theory of Elasticity" by A. E. H. Love, paragraph 278. Fourth edition, Cambridge University Press, 1934.

14. "Longitudinal Waves in Beams" by R. E. D. Bishop (The Aeronautical Quarterly Vol. 3, pp. 280-293, February 1952.

15. "Dispersion of Compressional Waves in Isotropic Rods of Rectangular Cross-Section" by R. W. Morse (The Journal of the Acoustical Society of America, Vol. 20, 1948, pp. 833-838).

16. "The Velocity of Compressional Waves in Rods of Rectangular Cross-Section" by R. W. Morse (The Journal of the Acoustical Society of America, Vol. 22, 1950, pp. 219-233).

17. "On the Transverse Vibrations of Bars of Uniform Cross-Section" by S. P. Timoshenko. (Philosophical Magazine, Vol. 43, Sixth Series, 1922, pp. 125-131).

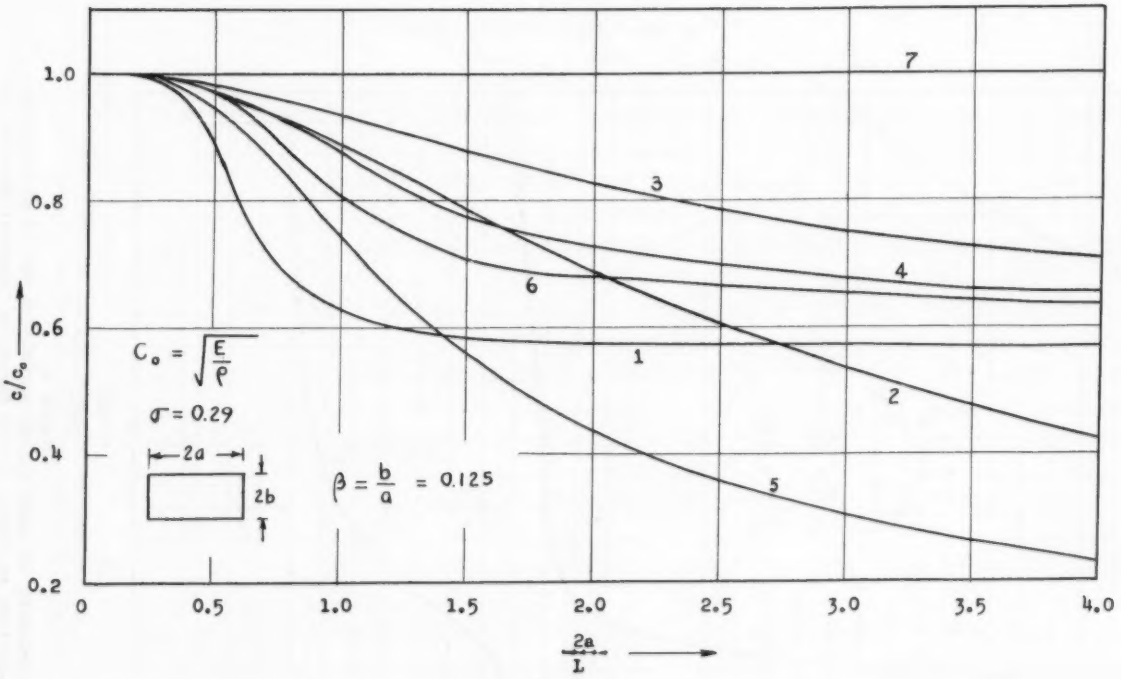

Figure 1
Dispersion Curves For A Bar Of Rectangular Cross-section.

1. Plane stress. 2. Love theory. 3. Bishop theory. 4. Bishop improved theory.
5. Love theory improved by Bishop. 6. Theory of Internal Constraints (1st Mode).
7. Elementary theory.

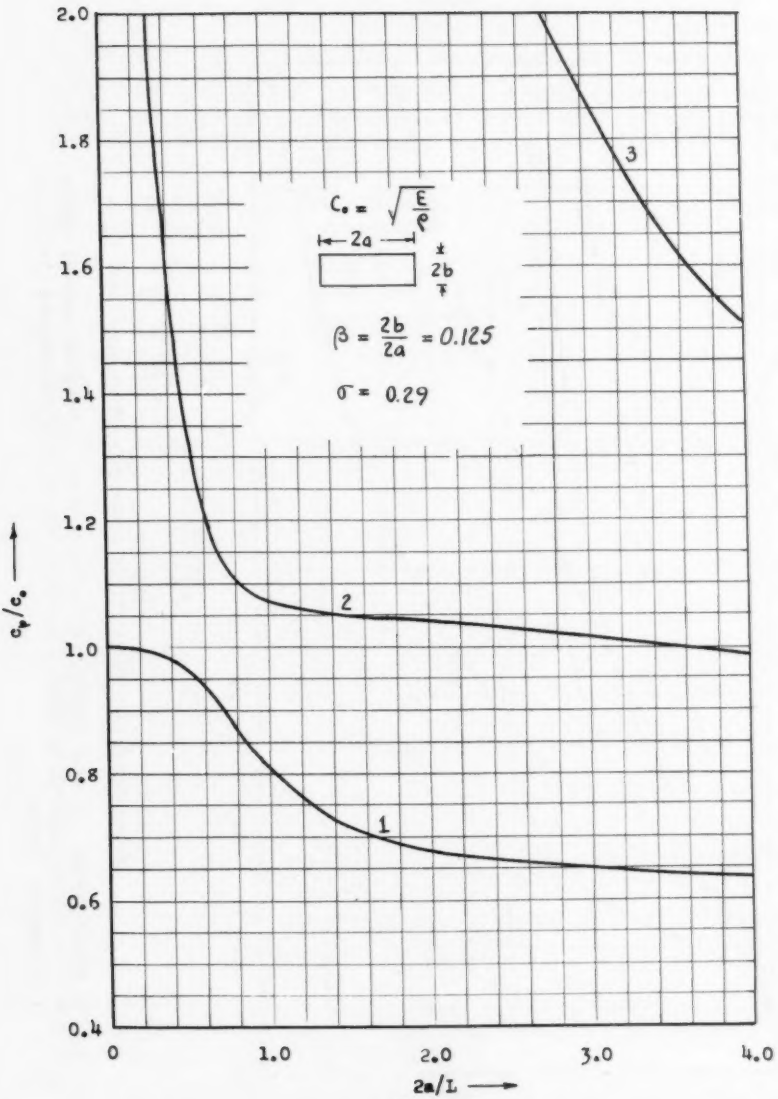

Figure 2

Phase velocity of longitudinal waves in a bar of rectangular cross-section according to the Theory of Internal Constraints (3 Modes).

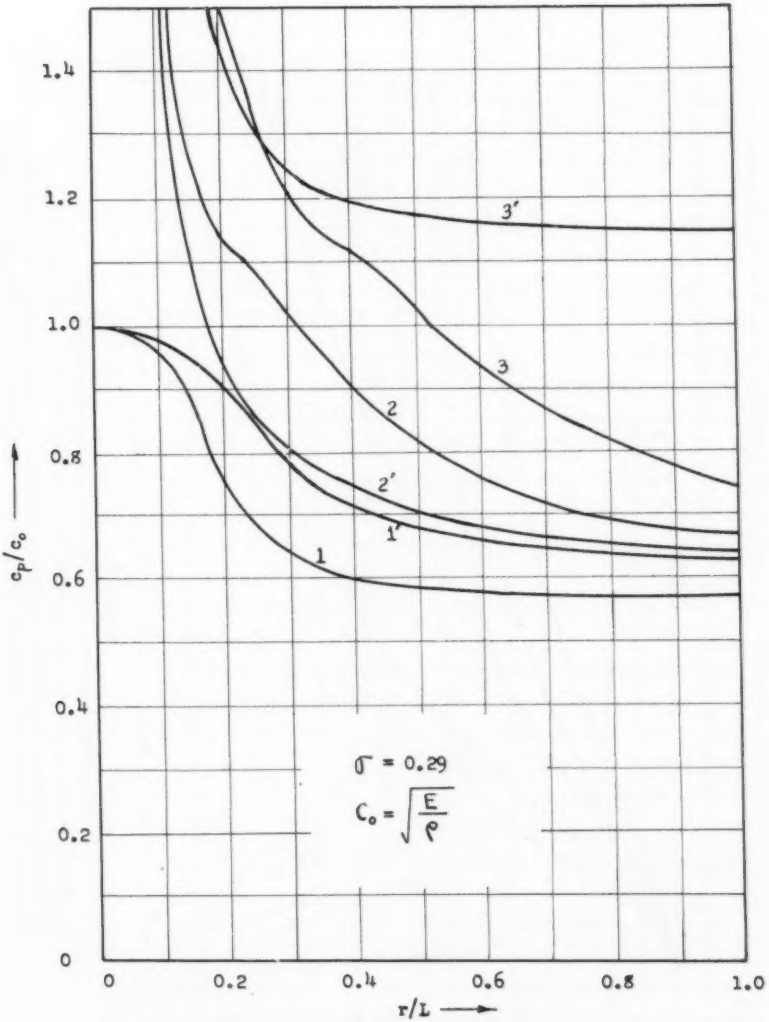

Figure 3

Phase velocity, c_p, of longitudinal waves of wave length L in square cross-section bars of radius of gyration r.

1, 2, 3. Exact theory (According to R. M. Davies), (for cylindrical bars), 3 Modes.

1', 2', 3'. Method of Internal Constraints, 3 Modes.

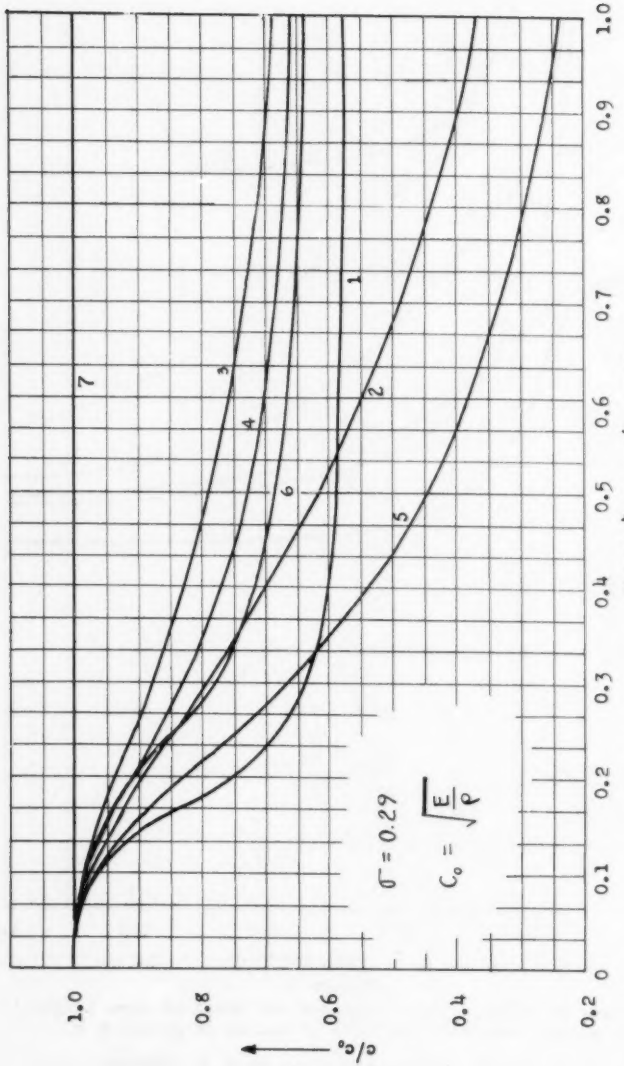

Figure 4

Dispersion Curves For A Bar Of Square Cross-section

1. Exact theory according to Davies for cylindrical bars. 2. Love theory. 3. Bishop theory. 4. Bishop improved theory. 5. Love theory improved by Bishop. 6. Theory of Internal Constraints (1st Mode). 7. Elementary theory.

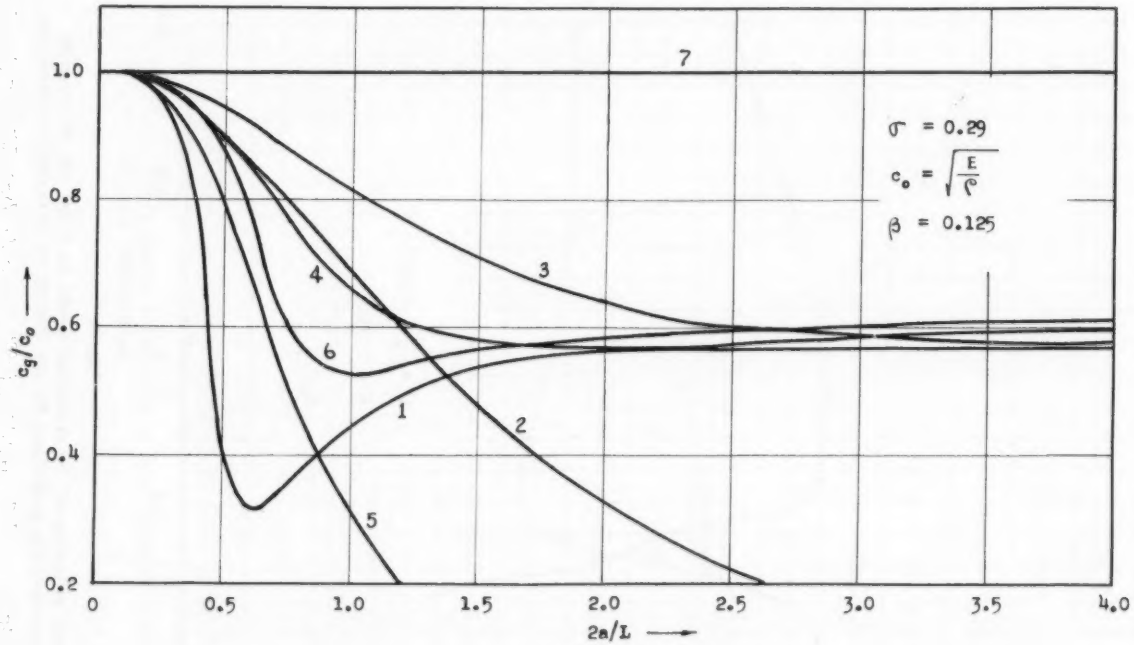

Figure 5

Group velocity of longitudinal waves for a bar of rectangular cross-section.

1. Plain stress. 2. Love theory. 3. Bishop theory. 4. Bishop improved theory.
5. Love theory improved by Bishop. 6. Theory of Internal Constraints (1st Mode).
7. Elementary theory.

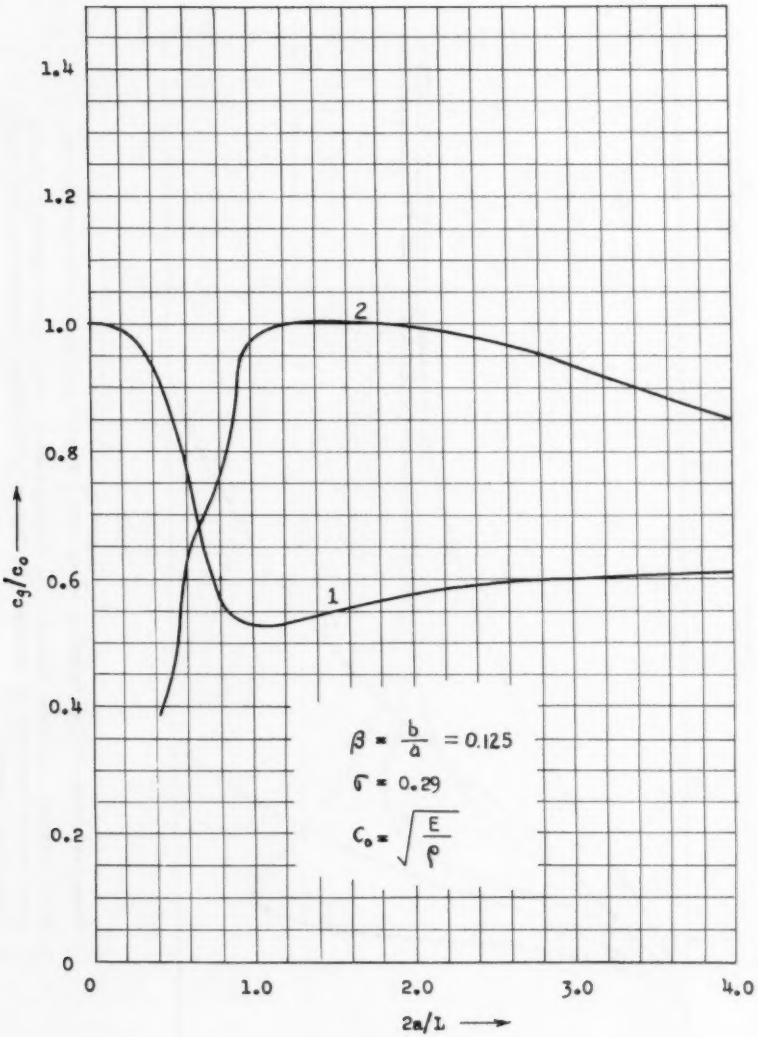

Figure 6

Group velocity of longitudinal waves in a bar of rectangular cross-section according to the Theory of Internal Constraints.

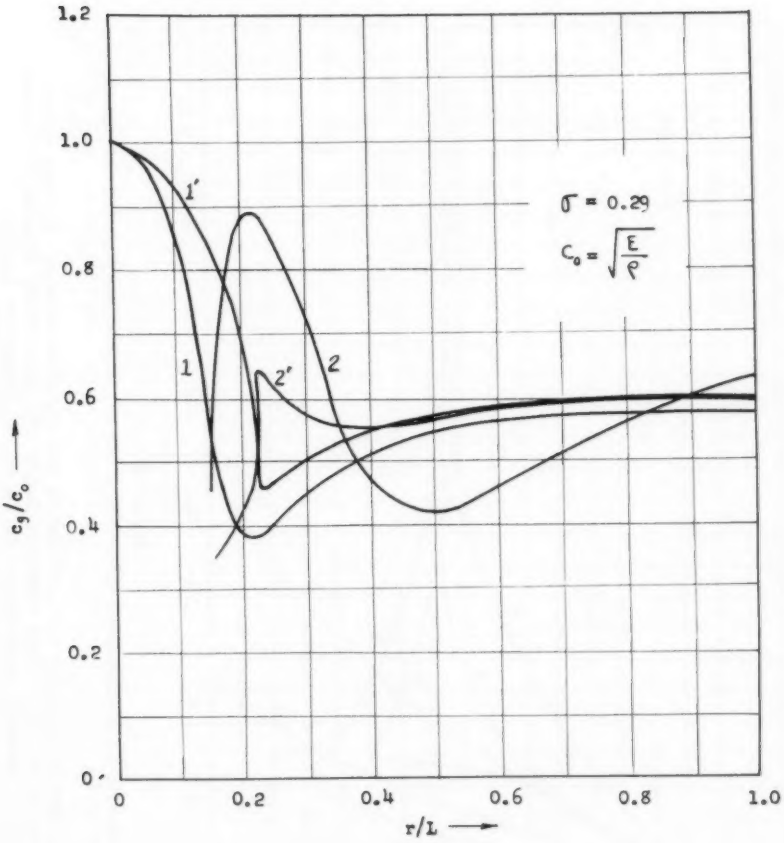

Figure 7

Group velocity, c_g, of longitudinal waves of wave length L, in square cross-section bars of radius of gyration r.

1,2 Exact theory (According to R.M. Davies). 1', 2' Theory of Internal Constraints.

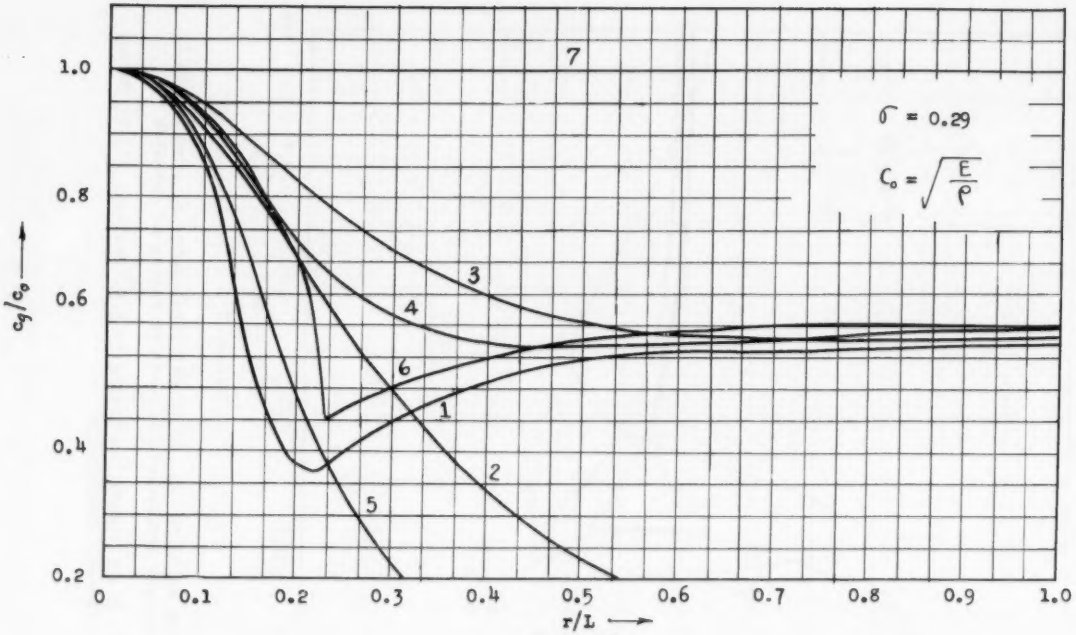

Figure 8

Group velocity of longitudinal waves for a bar of square cross-section of radius of gyration r.

1. Exact theory according to R. M. Davies for cylindrical bars. 2. Love theory. 3. Bishop theory. 4. Bishop improved theory. 5. Love theory improved by Bishop. 6. Theory of Internal Constraints (1st Mode). 7. Elementary theory.

PROCEEDINGS PAPERS

The 16 bound papers published in the past year are identified by number below. Technical division sponsorship is indicated by an abbreviation at the end of each Paper Number, the symbols referring to: Air Transport (AT), City Planning (CP), Construction (CO), Engineering Mechanics (EM), Highway (HW), Hydraulics (HY), Irrigation and Drainage (IR), Pipeline (PL), Power (PO), Sanitary Engineering (SA), Soil Mechanics and Foundations (SM), Structural (ST), Surveying and Mapping (SU), and Waterways and Harbors (WW), divisions. Papers sponsored by the Board of Direction are identified by the symbols (BD). For titles and other coupons, refer to the appropriate issue of "Civil Engineering." Beginning with Volume 4, January 1956, papers were published in Journals of the various Technical Divisions. To locate papers in the Journals, the symbols after the paper numbers are followed by 4 numerals designating the issue of a particular Journal in which the paper appeared. For example: Paper 1113 is identified as 1113 (HY6, which indicates that the paper is contained in the sixth issue of the Journal of the Hydraulics Division during 1956.

VOLUME 82 (1956)

JULY: 1019(ST4), 1020(ST4), 1021(ST4), 1022(ST4), 1023(ST4), 1024(ST4)[C], 1025(SM3), 1026 (SM3), 1027(SM3), 1028(SM3)[C], 1029(EM3), 1030(EM3), 1031(EM3), 1032(EM3), 1033(EM3)[C].

AUGUST: 1034(HY4), 1035(HY4), 1036(HY4), 1037(HY4), 1038(HY4), 1039(HY4), 1040(HY4), 1041(HY4)[C], 1042(PO4), 1043(PO4)[C], 1044(PO4), 1045(PO4), 1046(PO4)[C], 1047(SA4), 1048 (SA4)[C], 1049(SA4), 1050(SA4), 1051(SA4), 1052(HY4), 1053(SA4).

SEPTEMBER: 1054(ST5), 1055(ST5), 1056(ST5), 1057(ST5), 1058(ST5), 1059(WW4), 1060(WW4), 1061(WW4), 1062(WW4), 1063(WW4), 1064(SU2), 1065(SU2), 1066(SU2)[C], 1067(ST5)[C], 1068 (WW4)[C], 1069(WW4).

OCTOBER: 1070(EM4), 1071(EM4), 1072(EM4), 1073(EM4), 1074(HW3), 1075(HW3), 1076(HW3), 1077(HY5), 1078(SA5), 1079(SM4), 1080(SM4), 1081(SA4), 1082(HY5), 1083(SA5), 1084(SA5), 1085(SA5), 1086(PO5), 1087(SA5), 1088(SA5), 1089(SA5), 1090(HW3), 1091(SM4)[C], 1092 (HY5)[C], 1093(HW3)[C], 1094(PO5)[C], 1095(SM4)[C].

NOVEMBER: 1096(ST6), 1097(ST6), 1098(ST6), 1099(ST6), 1100(ST6), 1101(ST6), 1102(IR3), 1103 (IR3), 1104(IR3), 1105(IR3), 1106(ST6), 1107(ST6), 1108(ST6), 1109(AT3), 1110(AT3)[C], 1111(IR3)[C], 1112(ST6)[C].

DECEMBER: 1113(HY6), 1114(HY6), 1115(SA6), 1116(SA4), 1117(SU3), 1118(SU3), 1119(WW5), 1120(WW5), 1121(WW5), 1122(WW5), 1123(WW5), 1124(WW5)[C], 1125(BD1)[C], 1126(SA6), 1127 (SA6), 1128(WW5), 1129(SA6)[C], 1130(PO6)[C], 1131(HY6)[C], 1132(PO6), 1133(PO6), 1134(PO6), 1135(SU3).

VOLUME 83 (1957)

JANUARY: 1136(PP1), 1137(CP1), 1138(SM1), 1139(EM1), 1140(EM1), 1141(EM1), 1142(SM1), 1143(SM1), 1144(SM1), 1145(SM1), 1146(ST1), 1147(ST1), 1148(ST1), 1149(ST1), 1150(ST1), 1151(ST1), 1152(CP1)[C], 1153(HW1), 1154(EM1)[C], 1155(SM1)[C], 1156(ST1)[C], 1157(CM1), 1158 (EM1), 1159(SM1), 1160(SM1), 1161(SM1).

FEBRUARY: 1162(HY1), 1163(HY1), 1164(HY1), 1165(HY1), 1166(HY1), 1167(HY1), 1168(SA1), 1169(SA1), 1170(SA1), 1171(SA1), 1172(SA1), 1173(SA1), 1174(SA1), 1175(SA1), 1176(SA1), 1177(HY1)[C], 1178(SA1), 1179(SA1), 1180(SA1), 1181(SA1), 1182(PO1), 1183(PO1), 1184(PO1), 1185(PO1)[C].

MARCH: 1186(ST2), 1187(ST2), 1188(ST2), 1189(ST2), 1190(ST2), 1191(ST2), 1192(ST2)[C], 1193 (PL1), 1194(PL1), 1195(PL1).

APRIL: 1196(SM2), 1197(HY2), 1198(HY2), 1199(HY2), 1200(HY2), 1201(HY2), 1202(HY2), 1203 (SA2), 1204(SM2), 1205(SM2), 1206(SM2), 1207(SM2), 1208(WW1), 1209(WW1), 1210(WW1), 1211(WW1), 1212(EM2), 1213(EM2), 1214(EM2), 1215(PO2), 1216(PO2), 1217(PO2), 1218 (SA2), 1219(SA2), 1220(SA2), 1221(SA2), 1222(SA2), 1223(SA2), 1224(SA2), 1225(PO2)[C], 1226 (WW1)[C], 1227(SA2)[C], 1228(SM2)[C], 1229(EM2)[C], 1230(HY2)[C].

MAY: 1231(ST3), 1232(ST3), 1233(ST3), 1234(ST3), 1235(HY1), 1236(HY1), 1237(HW2), 1238(HW2), 1239(WW2), 1240(WW2), 1241(WW2), 1242(WW2), 1243(WW2), 1244(HW2), 1245(HW2), 1246 (HW2), 1247(HW2), 1248(WW2), 1249(HW2), 1250(HW2), 1251(WW2), 1252(WW2), 1253(HY1), 1254(ST3), 1255(ST3), 1256(HW2), 1257(HY1)[C], 1258(HW2)[C], 1259(ST3)[C].

JUNE: 1260(HY3), 1261(HY3), 1262(HY2), 1263(HY3), 1264(HY2), 1265(HY2), 1266(HY2), 1267 (PO3), 1268(PO3), 1269(SA2), 1270(SA2), 1271(SA2), 1272(SA2), 1273(SA2), 1274(SA2), 1275 (SA2), 1276(ST3), 1277(HY3), 1278(HY3), 1279(PL2), 1280(PL2), 1281(PL2), 1282(SA2), 1283 (HY3)[C], 1284(HY3), 1285(PO3), 1286(PO3), 1287(PO2)[C], 1288(SA2)[C].

JULY: 1289(SM3), 1290(EM3), 1291(EM3), 1292(EM3), 1293(EM3), 1294(HW3), 1295(HW3), 1296(HW3), 1297(HW3), 1298(HW3), 1299(SM3), 1300(SM3), 1301(SM3), 1302(ST4), 1303 (ST4), 1304(HY4), 1305(SU1), 1306(SU1), 1307(SU1), 1308(ST4), 1309(SM3), 1310(ST4)[C], 1311(EM3)[C], 1312(ST4), 1313(ST4), 1314(ST4), 1315(ST4), 1316(ST4), 1317(ST4), 1318 (ST4), 1319(SM3), 1320(ST4), 1321(ST4), 1322(EM3), 1323(AT1), 1324(AT1), 1325(AT1), 1326(AT1), 1327(AT1), 1328(AT1)[C], 1329(ST4)[C].

[C] Discussion of several papers, grouped by Divisions.